ADVANCED MAGNETIC RESONANCE IMAGING AND METABOLIC STUDIES OF LOW GRADE GLIOMAS IN CHILDHOOD

by

ELENI ORPHANIDOU

A thesis submitted to the
University of Birmingham
for the degree of
DOCTOR OF PHILOSOPHY

School of Cancer Sciences
University of Birmingham
September 2011

DECLARATION

The work presented in the thesis is entirely the work of the author except for the instances which are stated below and the following. The clinical imaging and spectroscopy data were collected by radiographers in the radiology departments of Birmingham Children's Hospital and Queen's Medical Centre, Nottingham. The radiographers also helped in the transfer of this data from the clinical environment. Technical help and advice in protocol setting, data collation, transfer and processing was given by members of the Brain Tumour Research Group, in particular Dr Nigel Davies and Dr Martin Wilson together with other members of the Cancer Imaging Programme. Administrative support for patient recruitment was given by Rachel Grazier.

In Chapter 7, «Preliminary study of in vitro NMR of paediatric pilocytic astrocytoma cell lines», spectral processing and Principle Component Analysis Plots were performed by Dr. Martin Wilson.

Chapter 9, «Texture Analysis of T1- and T2-weighted Magnetic Resonance Images and Probabilistic Neural Network to Discriminate Posterior Fossa Tumours in Children» is a result of collaborative work with Dr. Nikolaos Vlachos. Dr. Vlachos developed the texture analysis methodology used and performed the statistical analysis. I was involved in identifying the regions of interest on the MR images,

performing the texture analysis on some of the patients, collating the results and preparing the manuscript.

The matlab codes (1&2) in Appendix 2 are the result of collaborative work with Dr. Nigel Davies (1&2) and Dr. James Davison (2).

CONFERENCE PAPERS RESULTING FROM THIS WORK

ORAL PRESENTATIONS

1) British Chapter ISMRM 2010; Nottingham; Texture Analysis of T1- and T2-weighted Magnetic Resonance Images and Probabilistic Neural Network Discriminates Medulloblastomas, Pilocytic Astrocytomas and Ependymomas of the Posterior Fossa in Children; N. Vlachos, E. Orphanidou-Vlachou, N.P. Davies, T.N. Arvanitis, R.G. Grundy, A.C. Peet

2) ISPNO 2010 Multicentre prospective classification of childhood brain tumours based on ^{1}H MRS metabolite profiles. N. P. Davies, T. N. Arvanitis, D. Auer, A. French, R. Grazier, R. Grundy, F. A. Howe, D. Hargrave, T. Jaspan, S. Lateef, M. O. Leach, L. MacPherson, K. Natarajan, G. Payne, E. Orphanidou-Vlachou, D. Saunders, Y. Sun, M. Wilson, A. C. Peet
Published in Neuro-oncol 2010;12(6):ii32

3) BSNR 2009 A prospective multi-centre evaluation of paediatric brain tumour classifiers based on metabolite profiles from ^{1}H magnetic resonance spectroscopy at 1.5 Tesla. Davies NP, Orphanidou E, Natarajan K, Sun Y, MacPherson L, Coupland J, Auer D, Jaspan T, Saunders D, Payne G, Arvanitis TN, Grundy R, Peet AC

4) BSNR 2009 Investigation of glycine levels in paediatric brain tumours measured by MRS at 1.5 Tesla: a potential prognostic biomarker. Davies NP, Wilson M, Natarajan K, Orphanidou E, Sun Y, MacPherson L, Brundler MA, Arvanitis TN, Grundy RG, Peet AC

POSTER PRESENTATIONS

1) NCRI 2010. Patterns of relapse in paediatric high grade gliomas treated with radical radiotherapy. Pek Keng Koh, Kal Natarajan, Po Fung, Eleni Orphanidou-Vlachou, David Spooner, Andrew Peet, Daniel Ford

2) British Chapter ISMRM 2010; Nottingham; Characterisation and Classification of Paediatric Low Grade Brain Tumours Using ^{1}H Magnetic Resonance Spectroscopy and Logistic Regression; E. Orphanidou-Vlachou, N.P.Davies, T.Jaspan, Y.Sun, M.Wilson, T.N.Arvanitis, R.G.Grundy, A.C.Peet

3) ISPNO 2010 Glycine as a potential non-invasive prognostic biomarker in childhood brain tumours. : N. P. Davies, M. Wilson, K. Natarajan, E. Orphanidou-Vlachou, Y. Sun, L. MacPherson, M. A. Brundler, T. N. Arvanitis, R. Grundy, A. C. Peet

4) ISPNO 2010 The Children's Cancer and Leukaemia Group (CCLG) Functional Imaging e-repository for clinical trials of childhood brain tumours. T.N. Arvanitis, K. Natarajan, J. Rossiter, J.I.H.Ting, Y. Sun, M. Wilson, N.P.Davies, E. Orphanidou-Vlachou, R. Grazier, J.Crouch, D.P. Auer, C.A. Clark, R. Grundy, D. Hargrave, F. Howe, T. Jaspan, M.O. Leach, L. MacPherson, G.S.Payne, D.E. Saunders, A.C.Peet

5) ISMRM 2009. Honolulu. A Multicentre study of ^{1}H MRS for the Characterisation of Low Grade Brain Tumours of Childhood. E. Orphanidou-Vlachou, D. Auer, J. Coupland, N. P. Davies, T. Jaspan, L. McPherson, K. Natarajan, D. Saunders, Y. Sun, T. N. Arvanitis, R. G. Grundy and A. C. Peet..

6) 18th British Chapter International Society of Magnetic Resonance in Medicine Annual Symposium for PhD Students and Post-Docs 2009. London. 1H Magnetic Resonance Spectroscopy in Paediatric Low Grade Brain Tumours: Comparing Classification between Linear Discriminant Analysis and Artificial Neural Networks. Eleni Orphanidou-Vlachou,

N.P.Davies, N.Vlachos, M.P. Wilson, L. McPherson, K.Natarajan, Y.Sun, T.N. Arvanitis, R. G. Grundy, A.C. Peet.

7) 18th British Chapter International Society of Magnetic Resonance in Medicine Annual Symposium for PhD Students and Post-Docs 2009. London. Discriminating 5 Types of Paediatric Low Grade Brain Tumours using Texture Analysis of T1 and T2 Axial MR Images and Artificial Neural Networks. Nikolaos Vlachos, E. Orphanidou-Vlachou, N.P.Davies, T.N. Arvanitis, R. G. Grundy, A.C. Peet.

8) International Society for Magnetic Resonance in Medicine British Chapter 2008. Newcastle. A Multicentre study of ^{1}H MRS for the Characterisation of Low Grade Gliomas of Childhood (accepted but not presented). Orphanidou-Vlachou E, Auer D, Jaspan T, Coupland J, Payne G, Riches S, Germuska M, Leach M, Vaidya S, Arvanitis TN, Grundy RG and Peet AC.

ABSTRACT

Introduction

Paediatric low grade brain tumours present diagnostic and prognostic challenges, providing a need for better non-invasive imaging characterization. ^{1}H Magnetic Resonance Spectroscopy (MRS) holds important biologic information, and in this work its value in the diagnosis and prognostication of an extensive bi-centre cohort of low-grade gliomas is investigated.

Methods

Single voxel MRS was performed routinely in children with brain tumours as part of the clinical imaging (1.5T or 3.0T) prior to any treatment at the Birmingham Children's Hospital and Queen's Medical Centre (1st September 2003 - 31st March 2009). Clinical, imaging, MRS and histopathological data was collected on this patient cohort, up to 31 May 2010. Histopathological features were semi-quantified and correlated with MRS metabolites. In vitro ^{1}H Nuclear Magnetic Resonance spectroscopy (NMR) of cell extracts and whole cell samples from three pilocytic astrocytoma cell lines was performed. Two cases were studied with Magnetic Resonance Spectroscopic Imaging (MRSI). Texture analysis of T1- and T2-weighted MR images was performed for the diagnosis of paediatric posterior fossa brain tumours.

Results

MRS detects differences between subgroups of low grade brain tumours in children and between tumours of the same histology. High myo-inositol and

glycerophosphocholine and low phosphocholine have been found to be markers of good prognosis. Histological correlates for MRS metabolites have been identified and paediatric pilocytic astrocytoma cell lines (‘typical’, metastatic and recurrence) have been discriminated by in vitro ^{1}H NMR. The value of MRSI in answering specific clinical questions has been demonstrated. Texture analysis of MR images has been used to diagnose paediatric posterior fossa brain tumours with high accuracy.

Conclusion

This is the first study to the best of our knowledge which investigates an extensive cohort of paediatric low grade gliomas with MRS, collecting clinical, imaging and histopathological data from 2 centers and 5 scanners. Promising results have been reported by our group and others in the field, and advanced MR techniques now have a significant role in the study of these tumours.

ACKNOWLEDGMENTS

I would like to first thank my supervisors, Dr. Andrew Peet, Dr. Theodoros Arvanitis and Prof. Richard Grundy, for their guidance, support and advice during this work. Their help has been invaluable and has made this work possible.

I would like to also thank all members of the brain tumour research group for their support, especially Dr. Nigel Davies and Dr. Martin Wilson, for their advice and help with data processing. In addition, I would like to thank the staff at the tumour registry at Birmingham Children's Hospital (BCH) and the clinical research nurses at Queen's Medical Centre (QMC), and staff at the radiology departments of BCH and QMC.

Many thanks are due to the Samantha Dickson Brain Tumour Trust which has funded this project, as well as Cancer Research UK, the Engineering and Physical Sciences Research Council, Medical Research Council, NIHR, Poppy Fields and Birmingham Children's Hospital Charities for funding related parts of this work.

Last, but not least, I would like to thank my husband, Dr. Nikolaos Vlachos, for his support and patience during this time, as well as my parents for their never-ending encouragement.

TABLE OF CONTENTS

LIST OF FIGURES
(Chapter number followed by figure number)

LIST OF TABLES
(Chapter number followed by table number)

LIST OF ABBREVIATIONS

Ace=Acetate
Ala=Alanine
Asp=Aspartate
BCH=Birmingham Children's Hospital
Cho=Choline
Cr=Creatine
CSI= Chemical Shift Imaging
DA=Diffuse astrocytoma
DNET=Dysembryoplastic neuroepithelial tumour
GABA=γ-Aminobutyric acid
Glc=Glucose
Gln=Glutamine
Glu=Glutamate
Glx=Glutamate+Glutamine
GPC=glycerophosphocholine
Lac=Lactate
MetPA=Pilocytic astrocytoma metastatic at presentation
mIns or mI=myo-inositol
MMs=Macromolecules
MRI= Magnetic Resonance Imaging
MRS= 1H Magnetic Resonance Spectroscopy
MRSI=Magnetic Resonance Spectroscopic Imaging
NAA= N-Acetyl aspartate
NAAG= N-Acetylaspartylglutamate
NF1=Neurofibromatosis type I
NMR= Nuclear Magnetic Resonance
OPG=unbiopsied optic pathway glioma
PA=Pilocytic astrocytoma
PCh=Phosphocholine
PMA=Pilomyxoid astrocytoma
ppm=parts per million
QMC=Queen's Medical Centre
Scyllo=Scyllo-inositol
SVS=Single voxel spectroscopy
Tau=Taurine
TE=Echo Time
TPG=Tectal plate glioma

CHAPTER 1

INTRODUCTION

CHAPTER 1

INTRODUCTION

Paediatric low grade brain tumours present diagnostic, prognostic and treatment monitoring challenges, providing a need for better non-invasive imaging techniques. They are relatively uncommon, with approximately 350 cases diagnosed each year in the UK, and less than 60 patients treated in any one of the 22 UK Children's Study Group (UKCCSG) centers per year(1). 1H magnetic resonance spectroscopy (MRS) has shown promise in answering some of the management questions in previous studies of brain tumours in adults and children.

1.1. Paediatric Brain Tumours

Brain and spinal cord tumours are the commonest solid tumours in children (2, 3), representing 20% of all childhood cancers (4). In a study of 147 children <15 years, the annual incidence of central nervous system tumours was 26.5 per million children <15 years (3). However, central nervous system (CNS) tumours comprise many histologic entities with widely varying characteristics. Astrocytomas, medulloblastomas and ependymomas are the three commonest types of tumour, in order of incidence (3, 5). In a study of 340 children with primary CNS tumours up to 17 years of age, pilocytic astrocytomas were the most frequently encountered (23.5%), followed by medulloblastomas (16.3%) and ependymomas (10.1%), with

astrocytomas comprising 47.3% of all tumours (5). In a meta-analysis of Rickert and Paulus' data and data from another 15 worldwide studies on brain tumours in children, astrocytomas comprised 37.6% of all tumours, medulloblastomas 17.7%, ependymomas 9.9%, craniopharyngiomas 7.3% and germ cell tumours 4.4% (5). However, there are differences in the relative frequencies of paediatric brain tumours across ages, with medulloblastomas for example being the most common tumour at 6-11 years of age and high-grade astrocytomas, ependymomas and medulloblastomas being more frequent in the first 3 years of life (5). Differences are detected between Western countries and Japan and between ethnic groups in the US in total incidence and relative frequencies of certain histologic types, suggesting the contribution of genetic predisposition in the aetiology of CNS tumours (4).

Furthermore, there is an obvious difference in relative frequencies of the various tumour types between children and adults, which suggests a different aetiology (4, 6). High grade gliomas are the commonest primary brain tumours in adults, but only comprise 5% of those in children (6). High grade astrocytomas are the most common tumour between 15 and 17 years of age (5). Pilocytic astrocytomas and low-grade fibrillary astrocytomas are more common in children. Ependymomas are significantly more prevalent in children, especially infants and young children, and high grade gliomas originating in the brain stem are detected mainly in children (6).

The prevalence of CNS tumours in boys was found to be higher in all age groups throughout childhood and adolescence (5). There is also a difference in primary location; infratentorial tumours are more common in children, especially >1 year, whereas primary brain tumours in adults are usually supratentorial (3, 6). In children, infratentorial tumours are more prevalent at the ages of 3-11, with initially more supratentorial tumours at ages 0-2, as well as after 11 years of age(5).

Brain tumours also cause the highest number of deaths among paediatric cancer (7) and the combination of the tumour and its treatment commonly causes significant morbidity, in terms of physical deficits, neuropsychological and neuroendocrine effects (8). 75% of brain tumours in children are found in the midline and therefore often cause occlusive hydrocephalus (5). In the study by Stevens et al., survival was reported at 51% at 5 years for all diagnoses, but ranged from 13% in unbiopsied brain stem gliomas to 100% in juvenile astrocytomas (3).

1.2. Paediatric Low Grade Gliomas

Low grade gliomas are a clinically defined group of tumours, used to describe WHO grade I and II tumours of glial origin, excluding ependymomas (9). Some glioneuronal tumours are included in this group and are treated under the same protocol (9). Ependymomas are not included, even though of glial cell origin, as they form a clinically separate entity with a different treatment approach.

Low grade gliomas are the most common brain tumours in children(10). Although commonly grouped together for the purposes of treatment, low grade gliomas are a diverse group in terms of histopathology (11). Most low grade gliomas in children are grade 1 pilocytic astrocytomas (PA), which comprise 23.5% of all brain tumours in children, but some are grade 2 diffuse astrocytomas (5% of all paediatric brain tumours are fibrillary astrocytomas) and many other rarer tumour types are seen (5). Pilocytic astrocytomas are particularly common between 3 and 14 years of age, ranging from 21.8% in 9-11 years of age to 32.8% in 3-5 years of age (5). Furthermore, low grade glioneuronal tumours such as gangliogliomas are often grouped with the pure gliomas in treatment protocols. Low grade gliomas may occur throughout the brain and prognosis depends greatly on the site. Cerebellar PAs have an excellent prognosis and are often curable by complete surgical resection (11, 12). Conversely, optic pathway tumours which account for 2-5% of all brain tumours in childhood are much more challenging to treat (11, 13). Up to 70% of optic pathway tumours are associated with neurofibromatosis type 1 (NF1)(14), and approximately 15% of patients with NF1 can have an optic pathway glioma (6).

Although overall survival (OS) rates are generally high for low grade gliomas in children, progression-free survival (PFS) is much lower. In a study by Fisher et al., 5 and 10 year (from initial surgery) OS for low grade astrocytomas was 87% and 83%, and PFS was 55% and 42% (15). A significant number of children progress after incomplete tumour resection or biopsy, and patients who have not had a

complete surgical resection at diagnosis often receive adjuvant treatment with chemotherapy and/or radiotherapy (9). Response to adjuvant treatment is variable and differs between tumour types, accurate diagnosis and improved tumour characterization is therefore important.

A substantial proportion of low grade gliomas are not biopsied or biopsy is limited with its inherent risks of sampling error (11, 16, 17). Currently, clinical findings together with conventional magnetic resonance imaging (MRI) appearances are used for non-invasive diagnosis, which provides information on the position, size, shape and structure of tumours. However, they present multiple management challenges, as they can have similar clinical presentations, magnetic resonance imaging (MRI) characteristics, and even histopathological features when biopsied, whilst simultaneously having very different responses to treatment. Treatment of low grade gliomas in the UK follows the SIOP-LGG 2004 protocol, and can include surgery, chemotherapy or radiotherapy or a combination of these (9). In addition, the clinical symptoms and signs and the magnetic resonance imaging (MRI) characteristics of these tumours are not always straightforward to interpret. A tumour may appear to be getting smaller on MRI but the patient's vision may be deteriorating and vice versa. Tumour measurements have been the major focus in assessing tumour response, and there have been multiple guidelines, such as World Health Organization (WHO) in 1979, Response Evaluation Criteria in Solid Tumours (RECIST) in 2000, the revised RECIST 1.1 in 2009 (18-20), and the Response Assessment in Neuro-Oncology (RANO) working group criteria (21).

The RANO criteria recognize that contrast enhancement (addressed in the Macdonald Criteria (22)) is non-specific and may not always reflect tumour response, and account for the non-enhancing component of brain tumours (21). These have been applied in diffuse low-grade gliomas (23) and are currently being developed for paediatric brain tumours (24). However, there are significant limitations in measuring tumour size, such as lack of distinct borders and irregular shape tumours (20). Although decreasing tumour volume is considered a sign of response, the tumour may contain dead cells and there may be a delay in volume change during treatment (25). There is therefore increasing interest in using functional imaging to assess tumour response, as this can give information on metabolic, hypoxic, proliferative and receptor status of lesions. However, these modalities need to be validated if they are to be incorporated in future RECIST versions (26).

These tumours therefore present significant challenges for non-invasive diagnosis but also an opportunity for improved non-invasive characterization where novel biomarkers of clinical behavior can be identified. New magnetic resonance techniques are becoming available which can give information on tumour properties providing insight into the biology of these lesions and improving their non-invasive assessment (27, 28). One such technique, ^{1}H Magnetic Resonance Spectroscopy (MRS) provides information on chemical composition and has been shown to be a valuable non-invasive tool for the diagnosis and grading of brain tumours both in adults (29) and children (16, 30, 31). It can easily be combined

with current MR imaging protocols making it an attractive adjunct to current assessments (27).

1.3. Treatment of Paediatric Low Grade Gliomas

In the UK, low grade gliomas (histologically or radiologically confirmed, WHO grade I or II, tumours of glial origin, some mixed glioneuronal tumours) in any part of the central nervous system in children and adolescents up to the age of 16 years are treated with the SIOP-LGG 2004 protocol (9). Ependymomas and diffuse intrinsic tumours of the pons are excluded, although grade 2 pontine gliomas in NF1 patients are eligible for the study (9). This protocol separates patients into groups according to tumour location and NF1 status, and then by the extent of primary resection, presence of severe neurologic symptoms and tumour progression. Different histologic entities are included in different locations, making the treatment recommendation very complex; this is why largely individualized treatment is allowed within the protocol. The protocol suggests the following: patients who have complete tumour resection, or incomplete resection or clinical diagnosis without symptoms or progression should be observed; definite indications for treatment after incomplete resection, non-resectable relapse or progression of an unresectable tumour should be treated with non-surgical therapy; children ≥8 years of age should receive primary radiotherapy and may also receive chemotherapy under specific conditions; interstitial radiotherapy indication in not restricted according to age; younger children should receive primary chemotherapy (duration

of 18 months); children with NF1 should be treated with chemotherapy at all ages; children without NF1 should be randomized to receive standard induction chemotherapy with vincristine and carboplatin or intensified induction with vincristine, carboplatin and etoposide; consolidation therapy is the same for all patients (vincristine and carboplatin). There is a high frequency of carboplatin hypersensitivity reactions (42% in a study of 105 patients from 10 Canadian centers (32)). Alternative chemotherapy in SIOP-LGG 2004 (for patients not affected by NF1) includes alternating Cisplatin/Vincristine and Cyclophosphamide/Vincristine (9). However, cisplatin is nephrotoxic and neurotoxic (9).

Surgery should be considered first at diagnosis or relapse, and complete resection is possible in up to 90% in some locations (9). Chemotherapy has been shown in several large, national studies to be effective against surgically unresectable, progressive or symptomatic low grade gliomas (9). It decreases tumour volume, prolongs progression-free survival and delays radiotherapy. However, the role of chemotherapy in long-term outcome, and its effect on improving the clinical and neurological function need further investigation (9).

1.4. Imaging of Paediatric Brain Tumours

Paediatric brain tumours are routinely imaged with Computed Tomography Imaging (CT) and/or Magnetic Resonance Imaging (MRI) (33). Most children have

an MRI of the brain before surgery, as it is better at determining tumour extent and spread compared to CT (33), but as CT is widely available it is often the first imaging modality used when a child presents with symptoms relating to a possible brain tumour (7). CT can be used to more easily assess the presence of calcifications which helps in the characterization of craniopharyngiomas and teratomas. MR is better at detecting the presence of blood (34). Functional imaging has also been gaining increasing interest and use, including Magnetic Resonance Spectroscopy (MRS) and Magnetic Resonance Spectroscopic Imaging (MRSI), perfusion MR, diffusion weighted imaging (DWI) and diffusion tensor imaging (DTI) and cortical activation mapping (33). Functional imaging modalities have different applications and are at different stages of development and review regarding clinical application in paediatric brain tumours. Imaging is involved in characterization (detection, spatial localization, extent, grading, histology), staging, prognostication, treatment planning and assessment of treatment response, as well as surveillance of patients and evaluation of long-term tumour and treatment effects. (33)

When a mass is detected on imaging, the distinction between intra- and extra-parenchymal lesions needs to be made. If it is intraparenchymal, its nature needs to be defined; infection, large plaques of demyelination and infarction can mimic the appearance of neoplasms (34). Standard sequences used in MR evaluation of paediatric brain tumours include sagittal T1-weighted images, followed by axial T2-weighted spin echo or fast spin echo and fluid attenuated inversion recovery

(FLAIR) images. Additional coronal or axial images can be performed through the tumour, and post-contrast images are performed in the optimal planes based on the pre-contrast images (34).

MRI has excellent sensitivity and specificity in the detection of paediatric brain tumours, and is slightly better than CT in this regard, and can also detect local tumour extent very accurately in non-infiltrative lesions. However, the extent of infiltration is often not determined when lesions are infiltrative or have significant surrounding oedema, which cannot be discriminated from tumour. It is possible to have normal appearing areas on MRI which are infiltrated by tumour. Grading of lesions on MRI features is often possible using their mass effect, presence of peritumoural oedema, sharpness of tumour margins, signal intensity patterns and patterns of enhancement. However, it is possible to have malignant tumours appearing very benign on conventional MRI (33).

Pre-operative diagnosis is often possible with MRI, when tumours have characteristic imaging features, such as infiltrative pontine gliomas and optic pathway gliomas in patients with Neurofibromatosis type I (NF1) (33). However, optic pathway tumours can be very infiltrative and difficult to discriminate from the T2 bright foci of vacuolation within myelin sheaths which are characteristic of NF1(33). Furthermore, cortical lesions such as gangliogliomas, dysembryoplastic neuroepithelial tumours (DNET) and pilocytic astrocytomas can have suggestive imaging features, but also demonstrate overlap with other histologies such as ependymomas, pleomorphic xanthoastrocytomas and oligodendrogliomas (33, 35).

Regarding staging (33), MRI is used to assess the central nervous system and detect dissemination of disease. In most tumour types, subarachnoid metastatic disease is a negative prognostic indicator. Spinal MRI is routinely used with CSF cytology to diagnose leptomeningeal disease, as spinal MRI does not diagnose all patients with leptomeningeal disease and has false positives and false negatives. Subarachnoid metastatic deposits are detected on gadolinium T1 weighted images as enhancing nodules or carpet-like covering of the surface of the brain and spinal cord or in the lumbar thecal sac below the conus. Furthermore, gadolinium-enhanced T1-weighted MR images used to detect subarachnoid metastatic deposits can lack sensitivity when the primary tumour does not enhance, as these deposits may also not enhance. FLAIR images can identify menigneal disease in the cranium that may not be detected by gadolinium-enhanced T1-weighted images, but this also has limitations due to CSF pulsatility and the use anaesthetics and oxygen in some children, and cannot be used for the spine (33).

Tumour volume measurements performed on MRI have various limitations, but are currently the only validated imaging marker which is predictive of outcome. In assessing the response to therapy, MRI also has limitations in discriminating tumour recurrence from post-radiation necrosis (33).

1.4.1. Tumour Location and Typical MR Imaging Characteristics of Paediatric Brain Tumours

The diagnosis of paediatric brain tumours involves several factors which need to be considered in obtaining an accurate differential. These are the patient's age, tumour site, intra-axial versus extra-axial location, lesion cellularity, enhancement pattern, and amount of perilesional oedema (7).

1.4.1.1. Posterior Fossa Tumours

The most common posterior fossa tumours in children are medulloblastomas, pilocytic astrocytomas and ependymomas (7). Although «typical» imaging appearances can be identified for posterior fossa tumours, it is important to note that there is significant overlap in these, and conventional imaging is not always definitive. Medulloblastomas usually arise from the roof of the fourth ventricle and the inferior medullary velum, and have hypointense T2 signal due to their increased cellularity (7). Ependymomas usually arise from the floor of the fourth ventricle and extend through the foramen of Luschka or Magendie, and can have varied T2 signal according to their histological subtype (7). Pilocytic astrocytomas are usually cystic with a mural nodule, the solid part being hyperintense on T2-weighted images, but can also be more solid (7). Ependymomas may present with similar T2 signal intensity to medulloblastomas, and medulloblastomas can have similar growth patterns to ependymomas (7). Also, cystic/necrotic

medulloblastomas may have imaging features overlapping with posterior fossa pilocytic astrocytomas (7).

1.4.1.2. Suprasellar Tumours

The main suprasellar tumours in children are optic pathway/hypothalamic gliomas, craniopharyngiomas and germ cell tumours. These tumours can have characteristic appearances, but can also present as mixed cystic and solid lesions. Craniopharyngiomas are discriminated by their predominantly cystic nature and rim clacification on CT or gradient echo imaging. Germ cell tumours have hypointense solid portions on T2-weighted imaging whereas optic pathway/hypothalamic gliomas (usually pilocytic astrocytomas) have hyperintense solid portions (7).

1.4.1.3. Supratentorial Tumours

Primitive neuroectodermal tumours, pilocytic astrocytomas, ependymomas and atypical teratoid rhabdoid tumours can be found supratentorially. Fibrillary (diffuse) astrocytomas, low-grade astrocytomas, anaplastic astrocytomas and glioblastoma multiformis can present supra- or infratentorially. Pleomorphic astrocytomas and subependymal giant cell astrocytomas usually present only supratentorially. Ganglion cell tumours including gangliogliomas and dysembryoplastic neuroepithelial tumours often present supratentorially (7). Pilocytic astrocytomas are often cystic, appear bright on T2-weighted MRI and enhance after contrast administration (7). Grade 2 and 3 astrocytomas are mostly non-enhancing, and

show significant variation in imaging characteristics within same grade tumours and within the same tumours (7).

1.4.1.4. Brain Stem Tumours

Brain stem tumours encompass significantly varying lesions in terms of appearance, therapy and prognosis; they form at least four separate major categories: medullary tumours, pontine tumours, mesencephalic tumours and tumours associated with NF1. These can be further subclassified into focal and diffuse tumours (7, 34). The most common lesion is diffuse intrinsic brain stem glioma or diffuse pontine gliomas, which can be low-grade at presentation, but is inoperable, resistant to treatment and has the worst prognosis of all tumours in paediatric neuro-oncology (7). Other brainstem lesions have a better prognosis; astroyctomas can be found in the tectum (7).

1.5. Magnetic Resonance Spectroscopy (MRS) Applications

1.5.1. Applications in Various Disorders

MRS is a technique which can be combined with magnetic resonance imaging to measure the concentration of a multitude of metabolites and lipids, and allows the biochemical characterization of tissue in vivo. ^{1}H MRS has been used extensively in recent years to investigate various disorders involving the brain as well as other organs, in adults and children. In the study of malignant lesions, it has been used particularly in brain, prostate and breast tumours. Prostate cancer is often difficult

to detect by routine ultrasound, CT and MRI (36) and biopsy samples only are not accurate for determining the Gleason score (37); Proton Magnetic Resonance Spectroscopic Imaging (MRSI) with MRI can provide information on the location and extent of cancer in the peripheral zone of the prostate, detect changes in citrate, creatine and choline which predict the presence of tumour, and achieve high sensitivity and specificity (36, 38), as well as assess aggressiveness of the tumour (39, 40). Furthermore, MRSI has been used to detect local recurrence after external-beam radiotherapy of the prostate (36, 41, 42). Breast cancer is diagnosed mainly by conventional film-screen mammography, but this method has a low specificity for detection of abnormal breast tissue (36). ^{1}H MRS has shown increased choline in malignant lesions (43, 44), and the addition of MRS to MRI has been shown to improve sensitivity, specificity and accuracy in distinguishing malignant from benign breast lesions (45, 46). Furthermore, MRS has been used to monitor response to treatment after neoadjuvant chemotherapy in locally advanced breast cancer (47, 48). It is worth noting that there is a consistent increase in choline in vivo and in vitro in tumours relative to surrounding healthy tissue, and a consistent decrease in choline in lesions responding to treatment compared to those which are not (36).

In vivo MRS has been used to study many disorders of the CNS system or systemic disorders with CNS involvement. Burtscher et al. reviewed proton MR sepctroscopy in clinical routine, and described that N-acetyl-aspartate (NAA) has been shown to be decreased in temporal lobe epilepsy, cerebral space occupying

lesions, multiple sclerosis (MS), Alzheimer's disease (AD) and other types of dementia and hypoxia (49). Other metabolites vary in these disorders as well, such as early choline (Cho) and lactate (Lac) increases and early transient creatine (Cr) decrease in MS; increased myo-inositol (mIns) in AD and increased Cho in multi-infarct dementia, and accumulation of lactate and increase in glutamate+glutamine (Glx) in hypoxia (from asphyxia, stroke, trauma etc.) (49).

In vivo MRS has been used to study metabolic disorders such as mitochondrial disorders, phenylketonuria and chronic hepatic encephalopathy (49); neuropsychiatric disorders, such as schizophrenia, bipolar disorder and autism (50), and various types of non-CNS tumours, such as musculoskeletal tumours (51) and non-Hodgkin's lymphoma (52). In vivo ^{31}P NMR spectroscopy has been used to provide predictors of treatment response to chemotherapy in human musculoskeletal tumours (51). In non-Hodgkin's lymphoma, pre-treatment ^{31}P MRS characteristics differed between low and high grade lymphoma, and metabolite changes occurred with treatment before changes in tumour size (52).

1.5.2. MRS Applications in Adult Brain Tumours

One of the main disorders studied by 1H MRS is brain tumours, and extensive research has been published on adult patients or cohorts of adults and children together. One such project was INTERPRET (53), a multi-centre project which developed a decision-support system (DSS) to aid radiologists in the diagnosis and

grading of brain tumours. Most tumour spectra had elevated choline relative to creatine, in contrast to normal brain spectra. The DSS classified 89% of the cases in an independent test set of meningiomas, low-grade gliomas and high-grade malignant tumours successfully (53). This project was expanded in the HEALTHAGENTS work, which included a distributed multi-centre agent architecture, an in-vivo classification method with negotiation, a web-based user interface and additional cases (54). eTUMOUR built on INTERPRET and used classifiers developed from previous data at different hospitals with the same acquisition protocol to evaluate predictive models with unseen cases, achieving high discrimination accuracies (55). Other applications of ^{1}H MRS in brain tumours included tumour biopsy guidance (56), tumour grading (lower mIns/Cr ratios in anaplastic astrocytomas and GBMs compared to low-grade astorcytomas at short TE(57), correlation between choline and Ki-67 in homogeneous gliomas at long TE(58)), detection of necrosis, and assessment of treatment (36, 59, 60).

1.5.3. MRS in Paediatric Brain Tumours

1.5.3.1. Diagnosis and Characterization

There have been increasing numbers of studies in the paediatric population, although still limited compared to published work on adult brain tumours. There is now a growing body of literature on specific metabolic changes in paediatric brain tumours, which can be used as a basis for further larger multicentre studies,

needed to increase the numbers of patients, study specific tumour sub-types, and validate the use of ^{1}H MRS clinically.

A preliminary Chemical Shift Imaging (CSI) and haemodynamic MR imaging study of brain tumours in children and young adults (61), suggested that active tumour may be discriminated from normal tissue and necrosis. Normal tissue demonstrated characteristic peaks from N-acetyl-aspartate (NAA), choline-containing compounds (Cho) and total creatine (tCr). Biopsy-proven tumours had prominent Cho, reduced NAA, variable tCr and/or lactate or lipids. Radiation treatment caused lower metabolite peaks. Tissue necrosis had no Cho, NAA, or tCr. Another study of CSI in paediatric brain tumours (10 months-24 years) found significantly higher Cho and lipids and/or lactate (L) and lower tCr and NAA in tumours compared to normal brain in what was termed as «active tumours» (Cho and NAA also significant in «inactive tumours») (62). Similarly, Peet et al. (27) demonstrated significantly lower NAA/Cho and Cr/Cho in all types of tumours studied with short TE SVS compared to normal brain tissue, as well as the presence of lipids and macromolecules in most tumours, which are low in normal brain tissue (27). Furthermore, myoinositol (Inos)/choline was significantly lower in untreated tumours compared to normal brain, was high in diffuse pontine gliomas and low in medulloblastomas and supratentorial primitive neuroectodermal tumours(27). Glutamate/Glutamine (Glut)/ Cho was high in grade 1 astrocytomas and unbiopsied optic gliomas and low in diffuse pontine gliomas(27). Diffuse pontine gliomas also had significant metabolite differences from other gliomas in

the brain stem (27). Panigrahy et al. (63) used short echo time SVS to discriminate between individual tumour types from all other tumours and between pairs of tumours types, and found many significant differences; taurine was significantly higher in medulloblastomas compared to all other tumours, creatine was significantly lower in pilocytic astrocytomas and ependymomas and anaplastic ependymomas demonstrated low NAA compared to all others. Decision support systems with an interactive clinical user interface have also been produced for the characterization of childhood brain tumours with MRS, and provide a flexible method for tumour classification by clinicians (64).

A short echo time SVS study by Peet et al. (65) showed that children with metastatic medulloblastomas had significantly smaller primary tumours, higher choline levels and choline/lipids ratio and lower mobile lipid (at 1.3+0.9 ppm) and lactate levels, than children with localized disease (65). Total choline also had a significant positive correlation with Ki67(65). Tzika et al. (16) has demonstrated a positive correlation between Cho and relative cerebral blood volume (rCBV) and an inverse correlation between Cho and apparent tissue water diffusion coefficient (ADC). Cho and lipids were not correlated, and lipids were positively correlated with ADC. Total creatine was significantly positively correlated with NAA as well as Cho (16). MRSI has also been investigated (28) regarding its relationship to gadolinium diethylenetriaminepentaacetic acid (Gd-DTPA) enhancement in paediatric brain tumours, and choline-containing compounds and lipids did not correlate with percent enhancement. High choline indicating tumour was seen in

tumour regions as well as outside the enhancing tumour beds. Also, contrast-enhancing regions in malignant and inoperable tumours did not always have high choline levels. However, percent enhancement correlated positively with relative cerebral blood volume (rCBV) and negatively with apparent diffusion coefficients (ADC). rCBV, ADC and lipids were found to be significant independent predictors of percent enhancement.

Differences in metabolite profiles have also been detected within a single histologic tumour type, pilocytic astrocytomas, with supratentorial tumours having significantly higher myoinositol and glutamate + glutamine than cerebellar tumours prior to treatment, but no difference on qualitative review of conventional MRI characteristics (66). One of the earlier studies by Lazareff et al. (67) also studied low grade astrocytomas in 7 children with ^{1}H MRSI (TE= 272ms) and demonstrated lower normalized (to value in normal brain) NAA, creatine and choline (except 1 patient) and higher Cho/NAA (significant in 6 patients) in tumours compared to normal brain, with wide variation in Cho/NAA even within the same tumour (67).

1.5.3.1.1. NF1

In a study of brain lesions in children with NF1 by Wilkinson et al. (68), N-acetyl group resonance at 2.02ppm (NA) was found to be significantly lower in typical Neurofibromatosis Bright Objects (NBOs) and non-optic tract/hypothalamic tumour/atypical NBO compared to controls. Cho and mIns were significantly higher

in tumour/atypical NBO compared to typical NBO and control groups. Three of the glutamate+glutamine (Glx) resonances were significantly lower in tumour/atypical NBO compared to controls. Gonen et al.(69) found that focal areas of signal intensity (FASI) in children with NF1 had significantly elevated Cho, reduced creatine, 2>Cho/Cr>1.3 and nearly normal NAA, and differed from tumours which had no NAA and Cho/Cr>2. Castillo et al.(70) studied hamartomas in NF1 patients (5-49 years) and found they had lower NAA/Cr than healthy volunteers, but higher NAA/Cr, Cr/Cho and NAA/Cho than astrocytomas. Cr/Cho and NAA/Cho in hamartomas was similar to healthy volunteers. However, the astrocytomas studied were from patients with no NF1 and included low and high grade tumours.

1.5.3.1.2. Posterior fossa tumours

A study of 17 children with posterior fossa tumours achieved discrimination between medulloblastoma, ependymoma, pilocytic astrocytoma and infiltrating gliomas using a combination of ADC values and MRS metabolites normalized using water (likelihood $<1x10^{-9}$). Medulloblastomas demonstrated increased taurine (Tau) and Cho and reduced ADC, ependymomas had significantly higher glutamate+glutamine (Glx) compared to all other tumours, and infiltrating gliomas had higher mIns compared to pilocytic astrocytomas (71).

In a study of paediatric cerebellar tumours with single voxel long echo time (135 or 270ms), Wang et al. (31) found that benign astrocytomas had lower Cr/Cho and NAA/Cho compared to normal brain. NAA/Cho and Lac/Cho in ependymomas and

astrocytomas were similar, but Cr/Cho was higher in ependymomas. Cr/Cho and NAA/Cho was low in most primitive neuroectodermal tumours, and most did not have highly elevated Lac/Cho, in many lactate being undetectable. Astrocytomas differed significantly on NAA/Cho from ependymomas and primitive neuroectodermal tumours, and ependymomas differed marginally significantly from primitive neuroectodermal tumours. Astrocytomas and primitive neuroectodermal tumours differed significantly on Cr/Cho from ependymomas. Primitive neuroectodermal tumours differed significantly from ependymomas and astrocytomas on Lac/Cho. Discriminant analysis on ependymomas, astrocytomas and primitive neuroectodermal tumours using NAA/Cho and Cr/Cho yielded classification sensitivities of 75-91% and specificities of 84-92% (no cross-validation). Arle et al.(72) also studied 33 children with primitive neuroectodermal tumours, astrocytomas and ependymomas/other tumours of the posterior fossa (30 patients same as in study by Wang et al. (31)) with long TE SVS. Cr/NAA, NAA/Cho and Cr/Cho, 10 MR imaging tumour characteristics, tumour size, patient's age and sex were used in a neural network and compared to predictions made by a neuroradiologist blind to the MRS and histopathology results. The neuroradiologist predicted the tumour type with 73% accuracy, and neural networks with different data combinations as inputs achieved accuracies of 58-95%. The neural network with MRS data alone achieved a prediction accuracy of 58.5%, with MR imaging characteristics + age + sex + tumour size 71.7%, with MRS + age + sex + tumour size 87.8% and with all data 94.6%.

1.5.3.2. Grading

Peet et al. showed absolute mobile lipid levels detected by short TE single-voxel MRS in children with brain tumours to be significantly lower in non-involved brain compared with low-grade gliomas. They were also significantly lower in low grade gliomas compared with malignant brain tumours. Cho/Cr was not found to be significantly different between low-grade and malignant tumours (73). Choline and lipids discriminated between low– and high-grade paediatric brain tumours, being significantly higher in histologic category I than in II and III (CCG) (16), and in a larger study (74) Cho and lipids and/or lactate (L) were elevated in high grade (WHO grade III and IV) vs. low grade tumours (WHO grade I and II) and were found to be independent predictors of tumour grade. Normalized values of Cho+ 0.49L maximized diagnostic accuracy (74). Furthermore, the region of the MRSI spectrum with the highest Cho has been shown to strongly correlate with the most malignant areas in the biopsy specimens (74).

Glycine, a metabolite often not included in metabolite profile studies due to strong overlap with myoinositol and a low concentration in normal brain, has been shown in a study of paediatric brain tumours in vivo at short and long TE to be significantly higher in high-grade compared to low-grade tumours. This was also the case on HRMAS data, and normalized glycine concentrations from HRMAS spectra correlated significantly with the corresponding normalized glycine concentrations from short TE in vivo MRS(75). Bluml et al. (76) have also reported mean citrate to

be significantly higher in aggressive WHO grade II paediatric astrocytomas compared to indolent grade II astrocytomas (stable disease for >2 years). However, anaplastic astrocytomas and glioblastomas did not show a consistent pattern of citrate in their spectra.

1.5.3.3. Prognosis and Response to treatment

Peet et al.(27) demonstrated myoinositol (Inos)/Cho to be significantly lower in untreated compared to treated brain tumours. Harris et al. showed that children with supratentorial pilocytic astrocytomas who progressed had a significantly lower value of myoinositol at pre-treatment short TE SVS compared to those with stable disease. Furthermore, the patients who progressed had a significant decrease in myoinositol between the pre-treatment and first on-treatment MRS (66). These changes in myoinositol were detected before clinical and radiological progression (66). Long TE single-voxel ^{1}H MRS in 14 young people with hemisphere tumours showed NAA/Cho and Cr/Cho to be significantly lower in patients who died compared to those who were alive after follow-up (77). Mobile lipids have been shown to be highest (short TE SVS) in children with low-grade gliomas having rapid clinical progression (73). In a study of 11 patients with low grade gliomas by Lazareff et al., normalized choline detected by ^{1}H MRSI pre-treatment was significantly higher in tumours that progressed compared to those which had stable disease (78).

MRSI has been used to predict progression in paediatric brain tumours, with the percent change in Cho/NAA being significantly higher in patients with progressive compared to stable outcomes, and being the most important prognostic indicator of tumour progression (TE=65ms). Relative tumour blood volume was also higher in progressing compared to stable outcomes. Normalized choline and relative tumour blood volume (rTBV) were significantly positively correlated and Cho/NAA and rTBV interacted to predict the probability of a progressing clinical outcome, both being independent multivariate predictors of outcome (79). Warren et al. studied recurrent primary brain tumours with ^{1}H MRSI and found that patients with a maximum Choline/NAA ratio equal to or below the median had a significantly greater survival than those with ratios above the median (80). Cho and lipids and/or lactate have been shown to be significantly higher and total creatine (tCr) lower in «active tumours» (recurrent or untreated) compared to «inactive tumours» (treated with no signs of recurrence). tCr was shown to be the only significant independent multivariate predictor of tumour growth (62). Tumour spectral patterns (high choline) in paediatric malignant and inoperable brain tumours have been demonstrated outside the enhancing tumour beds in patients who had recurrence at these sites subsequently (4 patients) (28).

In an MRSI study of 76 children with brain tumours at TE of 65ms, choline-containing compounds (Cho), lipids and/or lactate (L), Cho/NAA, Cho+0.1L and grade were significantly lower in survivors compared to non-survivors, and Cho+0.1L was the only independent predictor of survival (81). A study of ^{1}H MRSI

(TE=272ms) in paediatric gliomas (82) showed tumour-to-brain choline decreased significantly after treatment in patients who had a decrease or stable tumour volume and excellent clinical condition, and this decrease remained significant during follow-up, whereas in the patients who progressed this ratio increased after treatment. The post-treatment choline was significantly higher in the non-responders. However, pre-treatment values of normalized choline did not differ significantly between non-responders and responders to therapy (82).

In diffuse intrinsic pontine gliomas (DIPG), which have a very poor prognosis, high Cho/NAA on the initial study and increase in Cho/NAA between time points, as well as increases in the variance in Cho/NAA in different magnetic resonance spectroscopic imaging (MRSI) voxels in a tumour have been shown to be predictive of poorer survival (83). Another study of DIPGs by Hipp et al. (84), also found increased Cho/NAA at baseline imaging to be predictive of poorer survival, in addition to increased perfusion on DSC-MRI. At subsequent time points increased maximum Cho/NAA on MRSI and increased Cho/NAA on single voxel spectroscopy, increased perfusion and the presence of enhancement predicted shorter survival (84). Yamasaki et al.(85) reported high Cho/NAA and lactate expression to be associated with shorter overall survival (5 of 19 patients >20).

MRS studies have been performed at various echo times (TE) (28, 74, 86, 87) and these are usually referred to as short and long echo time. Long echo time studies were initially preferred, as they are easier to perform and collect good quality data

from, however this limits the number of metabolites that can be detected, in particular myo-inositol and glutamate/glutamine (86). Myo-inositol has been shown to be a prognostic indicator in pilocytic astrocytomas (66) and glutamate/glutamine have been shown to be useful in distinguishing tumours from controls in patients with NF1 (68). Therefore, short echo time MRS is becoming standard practice.

MRS is a challenging technique in children with brain tumours as many of the tumours are small and close to bone or blood such as near the base of the skull, and it is difficult to get homogeneous magnetic fields (86). This can result in poor quality data, which is a major problem with MRS. In addition, most studies have been performed at single centers (86), as it is very difficult to get multicentre data which follow the same acquisition protocols, and are collected consistently, and collecting clinical data from multiple centers is also challenging. However, this is very important as it is the only way to increase the number of patients in studies and get more reliable and statistically meaningful results.

1.6. Aims & Objectives

The project described in this thesis aims to assess the ability of ^{1}H MRS to contribute additional biochemical information to the non-invasive characterization of paediatric low grade gliomas. Diagnosis and prognostication of low-grade gliomas using ^{1}H MRS will be investigated, and metabolic correlates of routinely assessed brain tumour histopathological features examined. In vitro ^{1}H NMR

spectroscopy of different pilocytic astrocytoma cells lines will aim to detect subtle differences between them, investigate the origin of N-acetyl-aspartate (NAA) in pilocytic astrocytomas in vivo, and provide a high resolution metabolic fingerprint. The clinical application of Magnetic Resonance Spectroscopic Imaging (MRSI) will also be demonstrated using case studies. Finally, we will test another quantitative technique, texture analysis of MR images, for the diagnosis of posterior fossa paediatric brain tumours, which can serve as a test-bed for the methodology.

1.7. Thesis Outline

As discussed above, paediatric low grade brain tumours present diagnostic, prognostic and treatment monitoring challenges, providing a need for better non-invasive imaging techniques. Furthermore, childhood brain tumours are relatively uncommon, with approximately 350 cases diagnosed each year in the UK, and less than 60 patients treated in any one of the 22 UK Children's Study Group (UKCCSG) centers per year (1). MRS has shown promise in answering some of the management questions in previous studies of brain tumours in adults and children.

Therefore, this thesis discusses paediatric brain tumours, their treatment and imaging and the applications of magnetic resonance spectroscopy in various disorders, particularly paediatric brain tumours (Chapter 1). The technique of ^{1}H Magnetic Resonance Spectroscopy (MRS) will be described in Chapter 2. The

common methods employed in the collection of the in vivo ^{1}H single voxel MRS data, as well as the patient cohort, will be given in Chapter 3. The investigation of the use of MRS in the diagnosis and prognosis of an extensive bi-centre cohort of low grade brain tumours will be presented in Chapters 4 and 5 respectively. Chapter 6 will discuss the investigation of histopathological correlates of metabolites detected by MRS in paediatric brain tumours. Chapter 7 describes some pilot work with pilocytic astrocytoma cell line in vitro NMR. 2 case studies of patients with magnetic resonance spectroscopic imaging (MRSI) will be discussed in Chapter 8, demonstrating the ability of this technique to answer specific clinical questions. Chapter 9 will describe collaborative work on texture analysis of magnetic resonance images for the diagnosis of paediatric posterior fossa tumours, demonstrating another quantitative characterization technique, which can be potentially combined with MRS. Finally, Chapter 10 will conclude the work and discuss future work.

CHAPTER 2

MAGNETIC RESONANCE SPECTROSCOPY

CHAPTER 2 MAGNETIC RESONANCE SPECTROSCOPY

2.1. Theory

MRS allows the biochemical characterization of tissue in vivo. It measures the concentration of a multitude of molecules by detecting the radiowave resonance frequency of certain atomic nuclei (proton being the most widely measured in vivo, but also ^{13}C, ^{31}P, ^{19}F and others) when placed in a strong magnetic field. Nuclei resonate at a specific frequency, f, determined by the equation below:

$f= \gamma B_0$, where γ is the gyromagnetic ratio for the nucleus and B_0 is the strength of the external magnetic field (88). However, each nucleus in a molecule has a slightly different resonance frequency due to shielding from its surrounding electronic cloud in the structure, or its chemical environment, which alters the actual B_0. This small change in resonance frequency is called chemical shift, and it enables detection of specific molecules, which can be seen as peaks at different positions (88). Chemical shift is measured in parts per million (ppm) relative to a standard because it scales with the B_0 field strength; it is therefore independent of the magnetic field at which the acquisition takes place, and is the same in all human MR scanners (89). Thus, it is used instead of absolute frequency to enable comparisons. The peaks are seen on a graphical representation of relative frequency on the x-axis and intensity on the y-axis (spectrum), and the area under each peak is proportional to the concentration of the molecule (concentration of protons) (88). The signal detected by the MR spectrometer is called Free Induction

Decay (FID), which represents the time evolution of the signal. A spectrum shows the components of the signal as a function of frequency, and is produced from the FID by Fourier transform (FT) (90).

2.2. Acquisition

As with conventional MR imaging the patient lies on a bed in a space with an external magnetic field and additional electromagnetic fields which are repeatedly switched on and off. The signals from resonating protons are mapped to produce an image. ^{1}H MRS is most commonly used in vivo, as protons have a high abundance and gyromagnetic ratio and thus provide a stronger signal in a reasonable time frame than MRS based on other nuclei. Three additional steps are needed in performing MRS. A volume of interest or voxel needs to be selected based on the reference images acquired, the magnetic field within this voxel needs to be refined (uniform) by shimming, and for ^{1}H MRS the protons of water within the voxel need to be suppressed (particular frequency band suppressed) (91). Shimming is very important (usually done automatically) as it affects resolution and lineshape which have a significant impact on quantitation. A water unsuppressed spectrum is acquired after the water suppressed one, and is used as a concentration reference and for eddy current correction. ^{1}H MRS of the brain can be performed with a standard volume head coil, but to increase the signal surface coils or an assembly of surface coils called phased-array (most commonly used) can also be used (91).

MRS can be performed in vitro and in vivo. In in vivo MRS, data is collected from voxels, which are pre-defined volumes of interest, such as the site of a tumour. One problem with voxel location by the PRESS method is chemical shift artifacts, which means that the excited volume (i.e. voxel position) can depend on the chemical shift of individual resonances. When a volume with metabolites of different chemical shifts is subjected to a section-selective gradient, there is a displacement of the sensitive volume for each resonance (92, 93). Volumes in this work are usually defined on the 2ppm resonance (not consistent for all scanners), the advantages being that this resonance is approximately the centre of the most interesting signals for tumours and also minimizes the effect of contamination from NAA in normal brain outside the target volume.

The severity of the chemical shift artifact effect depends on the excitation bandwidth per unit distance and the field strength of the magnet (94). For the same voxel size, a stronger gradient and broader excitation bandwidth reduces chemical shift displacement, which can be negligible at lower field strength (1.5T). Furthermore, it is easier to reduce the chemical shift displacement for single voxel spectroscopy (SVS) than magnetic resonance spectroscopic imaging (MRSI), since smaller excitation volumes are used and a lower demand on the excitation bandwidth is placed (93). PRESS sequence also results in larger chemical shift displacement artifact than STEAM, although lately the characteristics of the 180° pulses in PRESS have been greatly improved, reducing this issue (93).

When a single voxel is used (single voxel spectroscopy (SVS)), MR signal from one region of interest is measured and signals outside this area are excluded. The localization techniques used can select cubes, rhomboid shapes, «slices», or multiple boxes by applying certain sequences. The most commonly used sequences in ^{1}H MRS include stimulated echo acquisition mode (STEAM) and point-resolved spectroscopy (PRESS). Each has certain advantages, but more important is consistency (91). They both aim to excite the volume of interest with a minimum excitation of the rest of the sample. Three slice-selective pulses along x, y, and z are applied in a single pulse sequence (89). STEAM uses three 90° pulses for the excitation, whereas PRESS uses one 90° pulse and two 180° pulses. PRESS (which is used for all spectra in this thesis) uses the first 90° pulse to excite all the magnetization in one slice; the second pulse (180°) is applied in a slice perpendicular to the previous slice and generates a first spin echo from a row or column of intersection between the two slices; the third pulse (180°) is perpendicular to the previous two excited slices and generates a second spin echo of magnetization form the intersection of all three slices (89). Additional crusher gradients are applied between radiofrequency (RF) pulses and before the data readout, in order to suppress unwanted echo signals not arising from the final 180° pulse and to dephase any FID from imperfect 180° pulses (89). PRESS has the advantage of faster acquisition time or acquisition from smaller voxels in the same time with comparable signal-to-noise (S/N) ratio. This is due to the inherent loss of 50% of the signal in each STEAM acquisition (89). It is therefore preferred in brain tumour applications where S/N ratio and voxel size are important (89). However,

STEAM allows shorter echo times (TE), as the time between the second and third RF pusle (TM) does not affect the TE (89).

Magnetic resonance spectroscopic imaging (MRSI) or chemical shift imaging (CSI) involves a grid of voxels in a plane (2D) or a volume (3D), which investigate specific areas of interest. Chemical shift imaging involves the simultaneous acquisition of multiple spectra from a slice (Fig.1) or volume in the brain and combines MRI and MRS features. Images of specific metabolites can be formed and co-registered on MR images (89, 91). Spatial localization is done by phase encoding in two or three directions. CSI has the obvious advantage of acquiring multiple spectra efficiently, covering a large area of the brain, and also allows the adjustment of any voxel position after the measurement is finished (grid shifting). However, it is more difficult to achieve a good shim and uniform water suppression over a large volume. Furthermore, lipid signals from the skull due to incomplete localization can interfere. The acquisition time is longer and patients may move and the data sets are bulky and difficult to analyze (89, 91).

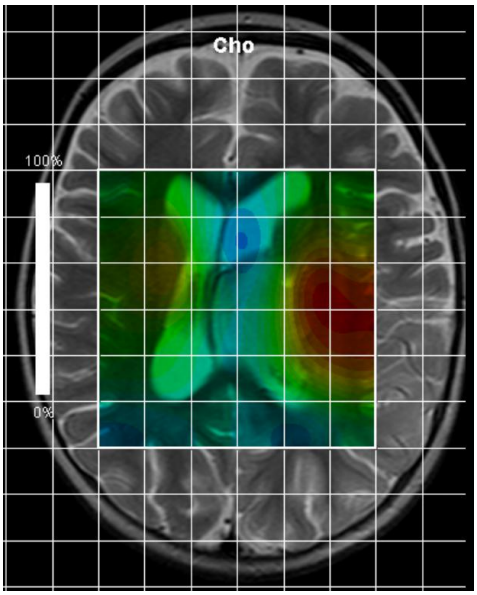

Fig. 1 CSI grid and choline map co-registered on MR image in a child with a diffuse fibrillary astrocytoma grade II. The choline map shows a red area (blue-red=low-high) adjacent to the main bulk of the tumour, indicating that this may represent an area of higher malignancy.

Echo time (TE) is the time interval in which the magnetization is on the transverse plane and undergoes T2 decay. It is an important parameter in MRS which affects the metabolites which can be detected and the baseline, which is much flatter at long TE. ^{1}H MRS can be performed at short echo time (TE) (<135ms, usually 20-40ms,) or long echo time (>135ms, usually 135 or 270ms) (Fig.2). At long TE, lipid signals and signals from metabolites with a complex spectral pattern like glutamate and glutamine decay due to J-coupling and T2 relaxation effects. J-coupling is the splitting of resonances into multiplet components, due to an internal indirect interaction of two spins via the intervening electron structure of the molecule. Eddy

current problems are also less severe at long TE (although shielded gradients and post-processing address this). Long TE spectra are therefore easier to analyze, as good estimates of metabolite concentrations can be obtained at lower resolutions and signal-to-noise (S/N) ratios. Short TE enables more metabolite information to be obtained and gives the smallest T2 losses thus producing the best S/N ratio. It is therefore becoming common practice to acquire short TE spectra. However, short TE spectra are more complex to analyze and assign peaks, due to the increased and often overlapping signals (metabolites detected described under analysis). Another parameter which is reported in MRS sequences is the repetition time (TR). This is the time between each initial excitation of the magnetization in the multiple single scans which are acquired and averaged to improve the S/N ratio (89, 91, 95).

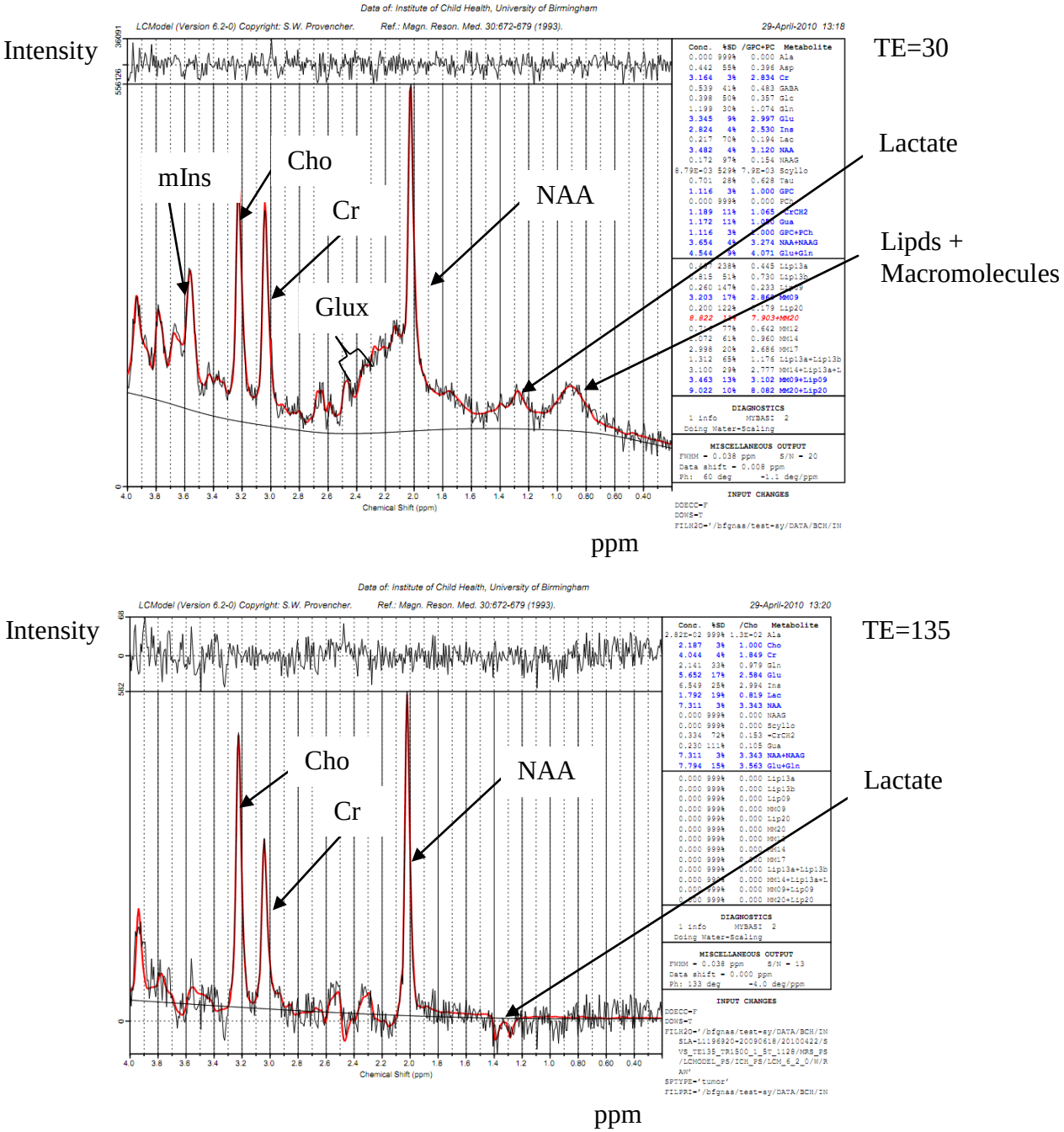

Fig.2 Short (TE=30) and long (TE=135) TE spectra of normal white matter. Myo-inositol, Glutamine+Glutamate and Lipids+Macromolecules are not seen in the long TE spectrum, and the lactate doublet is inverted. NAA=N-acetyl-aspartate, Cr=Creatine, Cho=Choline, mIns=myo-inositol, Glux=glutamine+glutamate, ppm=parts per million

2.3. Post-processing

Post-processing encompasses a multitude of techniques which aim to enhance the measured signal in MRS after acquisition. This is necessary as the quality of the data obtained by in vivo MRS has certain limitations, such as low S/N ratio due to low concentration of metabolites and limited acquisition time, poor uniformity of the magnetic fields which would result in unreliable quantitation of the signals and residual water. These techniques are usually integrated in quantification software and therefore done automatically (90).

2.3.1. Eddy Current Correction

Switching gradients on and off during a sequence causes respective current changes in the conductive parts of the MR scanner, called eddy currents. These in turn cause additional magnetic fields which add to the gradient field used for slice selection and interact with the signal. The lineshapes of peaks can be distorted as a result (time dependent phase shifts in the FID), impairing accurate quantitation of the signal. Eddy current correction involves the elimination of the time dependent phase shifts from the FID, usually by acquiring a water unsuppressed reference FID (for ^{1}H MRS), using the same protocol so that it is subject to approximately the same eddy currents (90).

2.3.2. Water Removal

Water suppression is performed during acquisition, as water concentration in the brain is several orders of magnitude higher than the concentration of other metabolites, and small distortions of the water peak's tail can disturb the lower intensity signals. However, a residual water signal remains in the spectrum, due to magnetic field inhomogeneities and water's multi-compartment nature. This can be removed by post-processing techniques (90).

2.3.3. Signal filtering in the time domain

Filters or windows are special functions used to enhance or suppress different parts of the FID to improve the quality of the signal (multiplied by the FID or other mathematical operations). Noise corrupts the FID and small resonances can be lost in it; it is caused by thermal motion of charged particles in the sample and by thermal motion of electrons in the coil and reception paths (major source of noise). The S/N ratio is used to describe the quality of the signal. Post-processing to reduce the noise by signal filtering is called sensitivity enhancement. Another use of post-acquisition filtering is resolution enhancement, which refers to the artificial narrowing of linewidths in the spectrum. When the acquisition finishes before the signal decays to the noise level because the acquisition time is too short, the signal is truncated, and typical oscillatory signal tails or 'ripples' are seen in the spectrum (when zero filling is performed). A third use of post-acquisition filtering is apodization, which refers to removal of the discontinuity at the end of the FID which

suppresses the ripple from the spectrum. Only one filter is applied to the data in practice (90).

2.3.4. Zero Filling

The signal of the FID is sampled point by point during acquisition, using an analogue to digital converter. If the number of points is insufficient, the signal is misrepresented. The number of points is dictated by the measurement parameters, but they can be increased artificially after acquisition. This is done by zero filling, which appends zeros after the last measured point in the FID. The spectrum produced by Fourier transform is therefore interpolated to the total number of points (including the zeros). This improves digital resolution (not true resolution) when a longer acquisition time is not possible (e.g. acquisition of just noise if longer acquisition time applied), and is useful in FFT which needs the number of points to be a power of 2 (90).

2.3.5. Phase Correction

The initial phase of the different components of the FID is usually non-zero. Phase correction therefore needs to be applied to restore pure absorption and dispersion lineshapes. This is done by multiplying the complex spectrum by the complex phase factor equal to the initial phase of the FID (90).

2.3.6. Baseline Correction

The baseline is the unknown background in the spectra, which causes peaks not to lie on a flat line with zero intensity. A distorted baseline is due to hardware imperfections and signal originating from the sample. Background signals are usually broad signals with very short T2* values, such as macromolecules and lipids. Baseline correction removes this signal after acquisition. The function which describes the course of the background signal can be subtracted, or the portion of the FID with broad signals can be removed (all signals influenced), or baseline signals are incorporated into the model function used for signal fitting.

2.4. Analysis/ Signal Fitting & LCModel Software

The signal acquired needs to undergo processing and the processed signal needs to be fitted to individual metabolites and the metabolite concentrations calculated. The software used in this work for processing, signal fitting and metabolite quantitation is LCModel (96), which is widely used and determines metabolite concentrations by fitting the data to a linear combination of basis functions formed from individual metabolite spectra (Fig.3). LCModel is automatic with no subjective input necessary, although default settings can be adjusted via the control file or additional post-processing modules incorporated. The uncertainties of the metabolite concentration estimates, the Cramér-Rao lower bounds, are also calculated by LCModel (95).

The software automatically accounts for the baseline (including residual water signal, susceptibility artifacts and macromolecule or lipid signals) and lineshape (eddy currents and field inhomogeneities). Parameters for zero order and first order phase corrections and overall referencing shift are included in the model. For the data presented in this thesis, the LCModel analysis steps included zero-filling, Fourier transform, eddy current correction using the water reference, automatic zero and first-order phasing (with some constraints for GE data), frequency referencing and quantitation. It can be applied to all field strength and sequences, by selecting the appropriate model spectra (95). The concentrations obtained by LCModel analysis can be used individually, in ratios, or as part of pattern recognition methods, to provide information about the biological characteristics of the tumours, and answer specific clinical questions. Older studies tended to report ratios of metabolites, but more recently the concentrations of single metabolites are estimated by normalization to the area of the water peak (referencing to the water unsuppressed spectrum), with correction factors for assumed differences in T2 and the assumption of constant tissue water content (that of white matter).

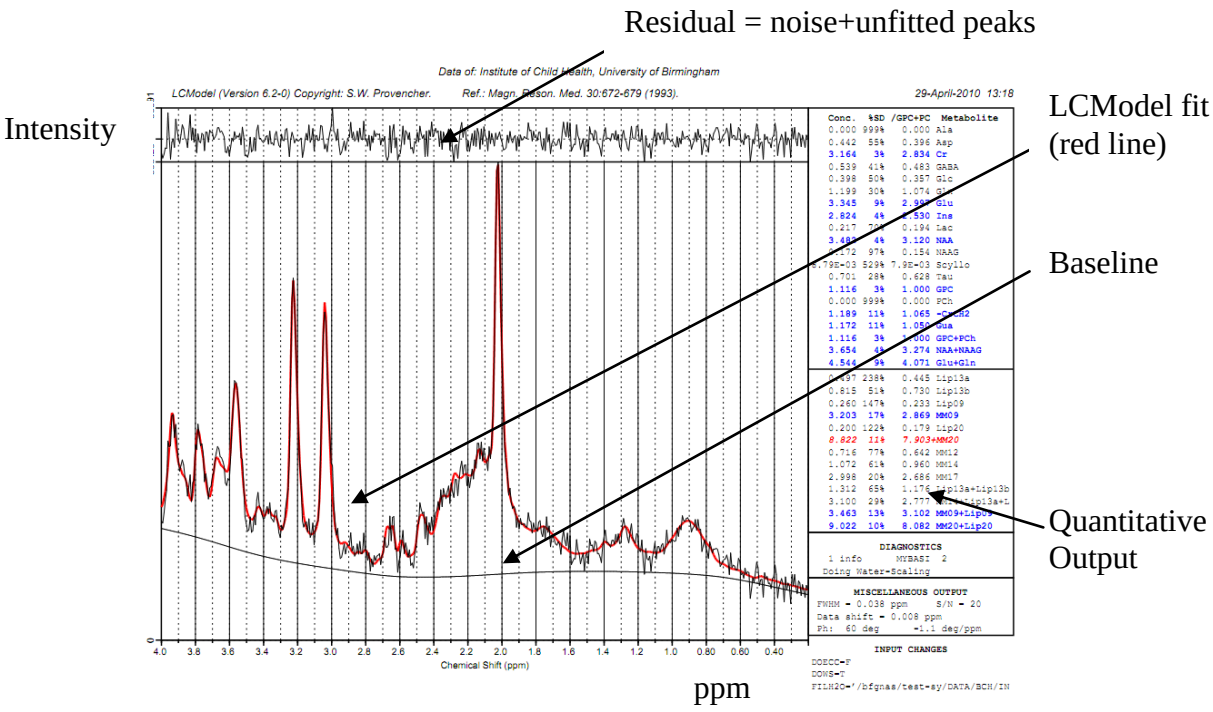

Fig.3 LCModel fitted spectrum

The main metabolites detected by short TE ^{1}H MRS are:

1) choline and choline-containing compounds (mainly phosphocholine (PCh) and glycerophosphocholine (GPC)) at 3.2ppm, which is a cell membrane and myelin marker

2) total creatine and phosphocreatine at 3.0 ppm, which is a marker of brain energy metabolism

3) N-acetyl aspartate (NAA) at 2.02ppm, which is a neuronal marker although there is much controversy about its function

4) myoinositol (mIns) at 3.6ppm, an astrocyte marker and osmolyte

5) glutamate (Glu), a neurotransmitter, redox marker and when at pathologically increased concentration a neurotoxin, and glutamine (Gln), an astrocyte marker, summarized as a multiplet, Glx, at 2.2-2.4ppm

6) glycine at 3.55ppm, an inhibitory neurotransmitter (75)

7) lactate (Lac) at 1.3ppm, which is not seen in the healthy human brain but results from glycolysis

8) and lipids/macromolecules (mainly at 0.9, 1.3 and 2.0 ppm).

Some of these metabolites are illustrated in Fig.2. Long TE metabolites include total choline, creatine, NAA, lactate (seen as an inverted doublet at 135ms), glycine, and some lipids and macromolecules (decrease with increasing TE). (1, 49, 88)

CHAPTER 3

PATIENTS AND METHODS-

SINGLE VOXEL MRS FOR

DIAGNOSIS AND PROGNOSIS

OF PAEDIATRIC LOW GRADE

BRAIN TUMOURS

CHAPTER 3 PATIENTS AND METHODS- SINGLE VOXEL MRS FOR DIAGNOSIS AND PROGNOSIS OF PAEDIATRIC LOW GRADE BRAIN TUMOURS

3.1. MRS Acquisition

MRS was performed routinely in children with brain tumours as part of the clinical imaging, at 1.5T (Siemens Symphony, GE Excite) or 3.0T (Philips Achieva), prior to any treatment (except stereotactic biopsy) at the Birmingham Children's Hospital (BCH) and Queen's Medical Centre (QMC), from 1st September 2003 to 31st March 2009. This cohort of patients was followed-up and clinical, imaging, MRS and histopathological data collected, up to 31 May 2010 or the day of last clinical contact for the patient before this. All clinical data collected was stored in a Microsoft Access database designed for this purpose (Appendix 1), which enabled advanced queries to be created and facilitated the analysis of this complex set of data. The MRS acquisition protocol involved using point-resolved spectroscopy (PRESS) localization for a single voxel. The voxel volume was either 3.375cm^3 or 8cm^3 according to the size of the tumour. A TE of 30ms was used for most patients, with all spectra acquired at TEs of 23-41ms. Repetition time was 1500-2000ms and 128 repetitions were used for 8cm^3 voxels while 248 repetitions were used for 3.375 cm^3 voxels. A water unsuppressed MR spectrum was acquired for eddy current correction and as a concentration reference. The concentrations of single metabolites were estimated by normalization to the area of the water peak

(referencing to the water unsuppressed spectrum), with correction factors for assumed differences in T2 and the assumption of constant tissue water content (that of white matter). However, this does not give an accurate absolute concentration in millimolar units, as the water concentration can be significantly increased in pathological conditions such as brain tumours (92). Therefore the concentrations calculated are inaccurate by an unknown factor, and are obtained in “institutional units”, differing from mM by up to 20% (97).

3.2. Spectral processing

Raw MRS signal data and voxel position images were transferred to a dedicated computer network. The signal was processed using LCModel software (version 6.2.0) (96) which determines metabolite concentrations by fitting the data to a linear combination of basis functions formed from individual metabolite spectra. 1.5T and 3.0 T basis sets were used for the respective data. Cramer-Rao Lower Bounds (CRLB) were also determined by LCModel, and these indicate the accuracy with which the metabolite concentrations have been estimated.

3.3. Quality Control

The spectra were reviewed individually to assess quality, and the ones failing the criteria set were excluded from the analysis. These criteria included signal-to-noise ratio (S/N) ≥ 4 and full-width half-maximum (FWHM) ≤ 0.15ppm. Baseline stability,

good phasing, adequate water suppression and absence of artifacts were assessed by inspection. The voxel positioning was also reviewed to ensure the voxel was positioned over tumour and did not include large amounts of normal brain or cyst and was at least 3mm away from lipid-containing bone and scalp. The Crammer-Rao Lower Bounds (CRLB) were also reviewed and only metabolites where at least 2 patients had a CRLB < 30 were included (aspartate (Asp) and γ-Aminobutyric acid (GABA) were excluded from all analyses). The metabolite concentrations and CRLBs were automatically retrieved from the filing system using the Matlab code (1) in Appendix 2. Mean spectra were automatically produced using the Matlab code (2) in Appendix 2.

As this is a multicentre study, Quality Control (QC) is also important in ensuring results from different scanners and centers can be combined. Work by Dr. Nigel Davies (98) has addressed this issue; protocols for QC have been implemented across six hospitals and nine MRI scanners. These protocols utilise phantoms of two different designs (Flood Phantom and Localisation Phantom) and volunteer scans to assess basic localisation efficiency, signal-to-noise ratio (SNR), water linewidth for shimming efficiency, water line-shape for eddy current distortions, effectiveness of eddy current (B_0) correction and scalp lipid suppression. The Localisation Phantom is used to assess localisation efficiency and is scanned at least once on each scanner at the start of the study and after major scanner upgrades and has been performed on 7 scanners at 5 hospitals so far. The results from 4 scanners showed considerable variation in efficiency and contamination for

different scanner manufacturers, and this information can be used to calibrate the "true" voxel sizes indicated by the "nominal" voxel size for each scanner. The Flood Phantom consists of a polypropylene sphere containing metabolites to simulate a brain like spectrum. Each centre scans one of these phantoms at regular intervals using standard protocols (SVS and CSI). A preliminary analysis indicated variations of less than 10% in metabolite concentration measurements between scanners. Normal adult volunteers have been scanned at 3 hospitals on 4 scanners so far, with short and long TE SVS acquired with consistent voxel placement in the basal ganglia and parietal white matter. Analysis of this data is pending.

3.4. Statistics

Statistical analysis was carried out in SPSS statistics software v. 17.0 and p-values of <0.05 were considered statistically significant. Various statistical methods have been employed to analyze and assess spectroscopy results for diagnosis, prognosis and follow-up of paediatric low grade gliomas. These include simple comparisons of group means (independent samples t-test, paired samples t-test, ANOVA)(99), Receiver Operating Characteristic (ROC) curves, and logistic regression, as well as survival analyses (Kaplan-Meier curves, Cox regression).

T-tests calculate Student's t to compare sample means and display the probability of the difference between the means. Independent samples t-tests are used when

the same variable is compared for two groups of patients, and paired samples t-tests when a different variable is compared for the same group of patients (e.g. first and second MRS) (99). One-way ANOVA gives a one-way analysis of variance for a quantitative dependent variable (e.g. metabolite) by an independent variable (e.g. type of tumour), and tests the hypothesis that several means are equal (99).

ROC curves are used for binary classifications from a numerical variable, and can assess the performance of different cut-off values. A ROC curve is a plot of sensitivity against 1-specificity, for different cut-offs (100). ROC curves were used to define the best classification cut-offs to be used in binary logistic regression, and to dichotomise variables for survival analyses. Binary logistic regression uses predictor variables to predict a dichotomous outcome, such as the probability of a tumour being glial or glioneuronal. Multinomial logistic regression is similar, but the outcome variable can have more than two categories (99).

Kaplan-Meier survival analysis estimates time-to-event models, when censored cases are present (censored cases are cases where the event has not occurred, e.g. patients who did not progress), using one independent variable. Variables found to have a significant effect on progression-free survival in Kaplan-Meier analysis were then used in a Cox regression to determine independent predictors or progression-free survival. Cox regression also looks at time-to-event data; it builds a model which produces a survival function predicting the probability that the

event (e.g. progression) has taken place at a given time for given values of predictor variables (metabolites) (99).

Ethical approval was given for all parts of the study presented in this thesis and written parental informed consent obtained.

CHAPTER 4

^{1}H MAGNETIC RESONANCE SPECTROSCOPY IN THE DIAGNOSIS OF PAEDIATRIC LOW GRADE BRAIN TUMOUR

CHAPTER 4

^{1}H MAGNETIC RESONANCE SPECTROSCOPY IN THE DIAGNOSIS OF PAEDIATRIC LOW GRADE BRAIN TUMOURS

4.1. INTRODUCTION

Low grade brain tumours include various histological entities of grade 1 and 2 lesions, which although treated under the same protocol, have very different clinical courses and outcomes (9). The diagnoses range from cerebellar pilocytic astrocytomas (PA) which are usually resected surgically and do not progress (11, 12), to complex optic pathway gliomas (OPG) with NF1 hamartomas, which are difficult to manage due to their site and multiple progressions (11, 13), and diffuse and pilomyxoid astrocytomas which are more aggressive (11). Glioneuronal tumours (gangliogliomas, dysembryoplastic neuroepithelial tumours (DNETs)), are also included in this group, as well as tectal plate gliomas (TPG) which are not biopsied and are usually observed without progression (11). Although clinical and MRI information give some indication as to the type of tumour, it is often difficult to discriminate between these very similar or even histologically identical tumours. ^{1}H Magnetic Resonance Spectroscopy can detect tumour metabolites and lipids/macromolecules, and add unique information regarding the biology of the tumours, aiding clinical management in terms of the need to biopsy lesions and selection of appropriate treatment. It has shown promise in discriminating between different brain tumours in adults and children (27, 53-55, 63), although most

studies include various tumour types. This study includes an extensive bi-centre cohort of low grade brain tumours, and uses MRS to discriminate between them.

Numbers of paediatric patients in previous studies is limited and those which have included children invariably include data from a single center. In a study by Astrakas et al. which included 66 patients, with tumours of various histologies, choline and lipids and/or lactate have been shown to be higher in high grade tumours vs. low grade tumours (74). A study by Peet et al, which included 59 patients, established differences between various tumour types (27) and a study by Panigraphy et al. found significant differences between the common childhood brain tumour types in pre-treatment MRS. Studies of specific tumour types are rarer but Harris et al. established differences in the MRS of pilocytic astrocytomas depending on location and produced pilot data showing that mIns could provide an important prognostic marker; Hwang et al. found elevated lactate and Cho/NAA of 3.40 (66, 87). Multicentre studies are required to accrue sufficient cases to study specific tumour groups and also to demonstrate that consistent results can be obtained across various centers. Multi-centre studies have been published in adults from projects such as INTERPRET (101, 102) but such data is only just emerging in children (103).

The aim of this study is to investigate a sufficiently large cohort of low grade brain tumours with MRS to allow differences between the subgroups of tumours to be established. Data is collected from several scanners from more than one centre

following common acquisition protocols, thereby establishing the credibility of the technique in a clinical environment.

4.2. METHODS

The methods for this study and the patients included are discussed in Chapter 2. The statistical analysis was carried out in SPSS statistics software v.17.0 and p-values of <0.05 were considered statistically significant. The tests included two-tailed independent samples T-Tests, ANOVA (Hochberg and Games-Howell), ROC curves and binary and multinomial logistic regression. The metabolites used as input for all T-Tests and ANOVA were: alanine (Ala), creatine (Cr), glucose (Glc), glutamine (Gln), glutamate (Glu), myo-inositol (mIns), lactate (Lac), scyllo-inositol (Scyllo), taurine (Tau), glycerophosphocholine (GPC), phosphocholine (PCh), guanidinoacetate (Gua), total choline (GPC+PCh), total NAA (NAA+NAAG), Glu+Gln, total lipids and macromolecules at 1.3 ppm (MM14+Lip13a+Lip13b), at 0.9 ppm (MM09+Lip09) and 2.0 ppm (MM20+Lip20). The metabolites found to be significantly different in the T-tests and ANOVA were then used to build corresponding logistic regression classifiers. For each binary logistic regression classifier the best cutoff value (giving the highest sensitivity+specificity) for classifying a tumour in the reference category was determined using a ROC curve.

4.3. RESULTS

108 patients had pre-treatment MRS (81 from BCH, 27 from QMC). 32 patients were excluded on quality control criteria (23 BCH, 9 QMC) and 7 patients were excluded due to missing data (1 BCH, 6 QMC). This left a cohort of 69 patients (57 BCH, 12 QMC) who had pre-treatment MRS which passed quality control and were included in the analysis. The patient ages at the time of MRS ranged from 2-195 months, mean 104 months, and there were 36 male and 33 female patients. 49 of the 69 patients had a biopsy (and 30 of the 39 patients excluded), all cases had their diagnosis reviewed by the local multidisciplinary team and central pathology review was undertaken in 43% of cases in the final cohort in the analysis (n=21). The diagnosis was altered after central pathology review in only 2 patients, and both were minor changes (1 from diffuse astrocytoma with extensive gemistocytic differentiation to diffuse astrocytoma fibrillary, and the other from low grade astrocytoma to pilocytic astrocytoma). The breakdown by diagnosis (summarized in Table 1) was: 19 posterior fossa biopsied Pilocytic Astrocytomas (PF PA), 9 supratentorial PA and unbiopsied optic pathway gliomas (STPA+OPG) without NF1, 7 STPA+OPG with NF1, 7 gangliogliomas, 6 diffuse astrocytomas (including fibrillary), 6 tectal plate gliomas (TPG) which includes a rosette forming glioneuronal tumour of the 4^{th} ventricle (RFGNT), 5 dysembryoplastic neuroepithelial tumours (DNET) (biopsied and unbiopsied), 4 pilomyxoid astrocytomas (including 1 pilocytic/pilomyxoid tumour grade 1-2), 4 neurofibromatosis bright objects (NBO), and 2 metastatic Pilocytic Astrocytomas

(MetPA) at presentation. NBOs were diagnosed on clinical and radiological features (they were all under observation only and did not progress). The biopsied tumours were categorized according to the World Health Organization (WHO) classification system 2007 (104). The term optic pathway glioma (OPG) is used in this paper to refer exclusively to tumours of the optic pathway which have not been biopsied. Since OPGs in children, particularly those with NF1, are invariably pilocytic astrocytomas, in the analysis, OPG have been combined with biopsy-proven pilocytic astrocytomas. This combined group is referred to as PA+OPG (i.e. biopsied pilocytic astrocytomas + unbiopsied optic pathway gliomas) but is also subdivided according to NF1 status and site in the analysis (105). Excluding metastatic PA, PA+OPG make up 51% of the tumour cohort.

Table 1. Summary of tumour types and patient numbers

Tumour type	**Number of patients**
Posterior fossa pilocytic astrocytoma	19
Supratentorial pilocytic astrocytoma + unbiopsied optic pathway glioma without NF1	9
Supratentorial pilocytic astrocytoma + unbiopsied optic pathway glioma with NF1	7
Ganglioglioma	7
Diffuse astrocytoma	6
Tectal plate glioma (includes a rosette forming glioneuronal tumour of the 4th ventricle)	6
Dysembryoplastic neuroepithelial tumour	5
Pilomyxoid astrocytoma	4
Neurofibromatosis bright object	4
Pilocytic astrocytoma metastatic at presentation	2

An example of voxel positioning in a tumour is shown in Fig. 1. Mean spectra of different brain tumours are shown in Fig.2. Groups of tumours, represented in the tree structure in Fig. 3, were compared using T-Tests and ANOVA for the metabolite means (significant metabolite differences also shown in the figure). Logistic regression was also performed between the groups to provide classifiers which allow cases to be allocated to their most likely tumour type according to their MRS using the tree structure. The results are summarized in Table 3. It should be noted, however, that the number of patients in some groups is small (<10) and this may have biased the logistic regression coefficients and significantly influenced the validity of the models (106), which need to be tested on larger datasets.

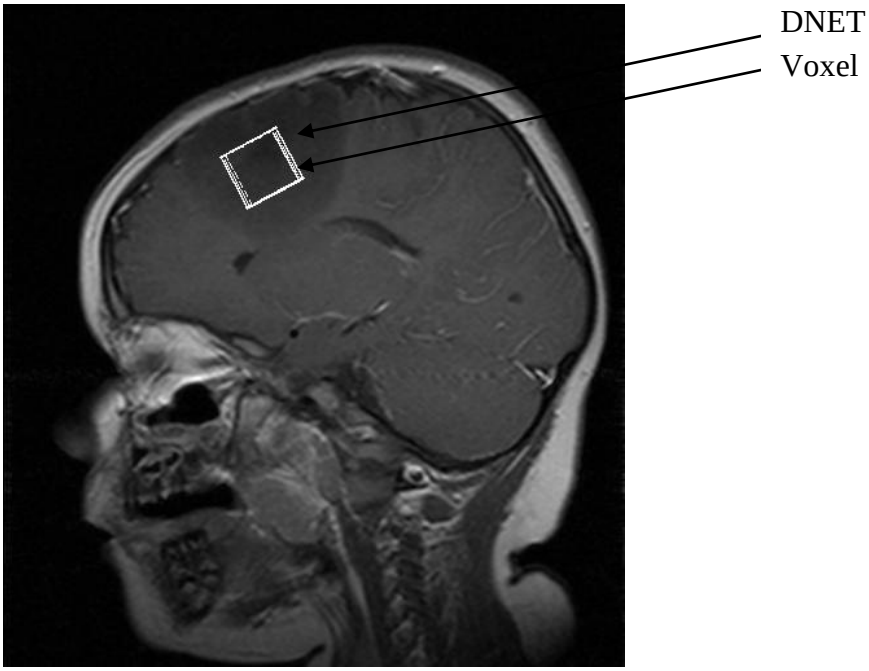

Fig. 1 Voxel placement over a frontal Dysembryoplastic Neuroepithelial Tumour (DNET)

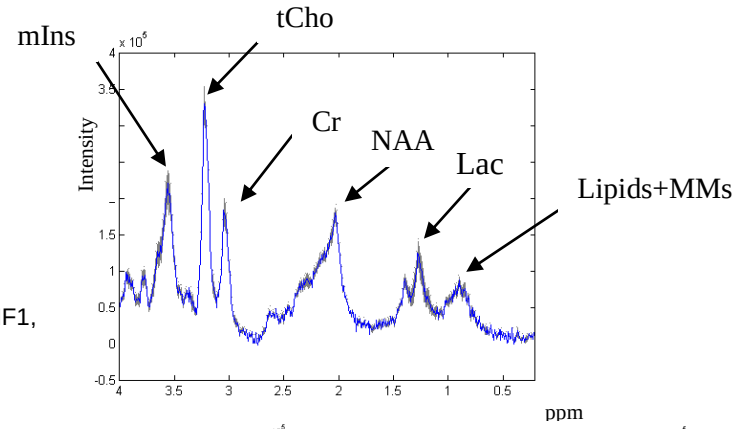

Supratentorial PA+OPG with NF1, n=7

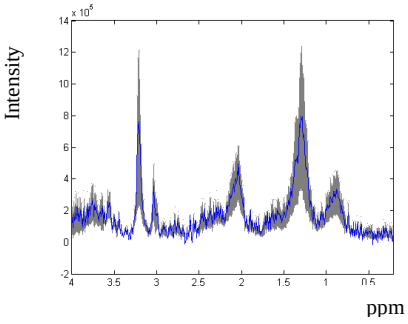

Supratentorial PA+OPG, no NF1, n=9

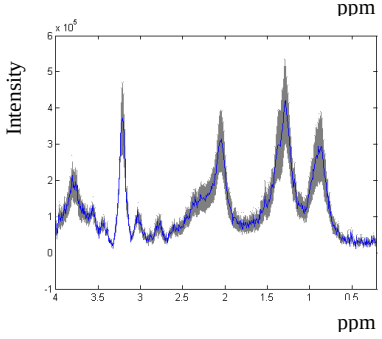

Posterior Fossa PA, n=19

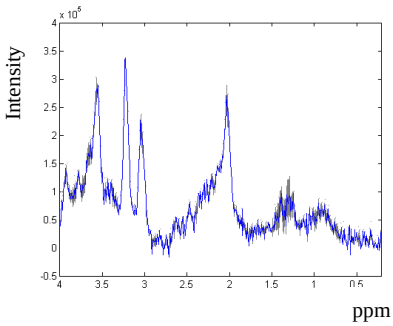

NBO, n=4

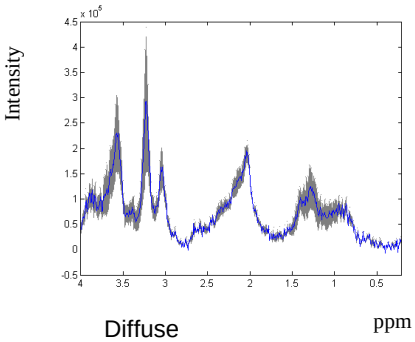

Diffuse Astrocytoma,n=6

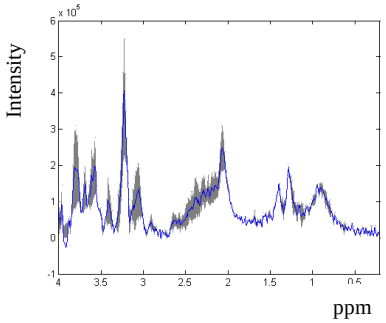

Metastatic PA, n=2

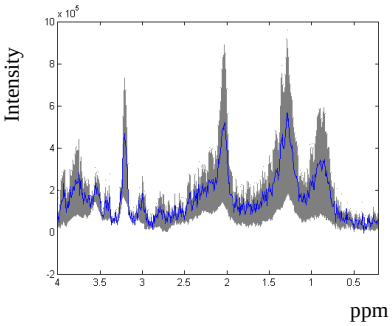

PMA, n=4

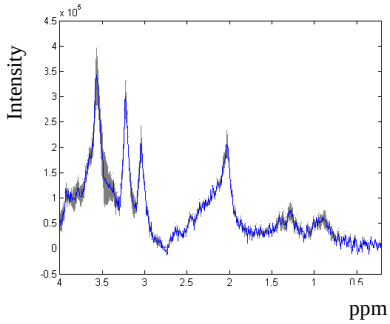

TPG, n=6

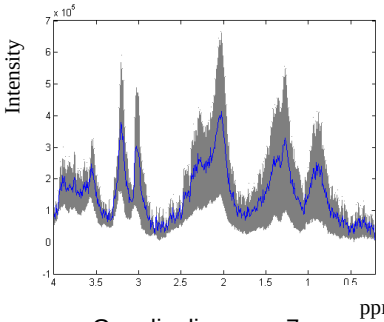

Ganglioglioma, n=7

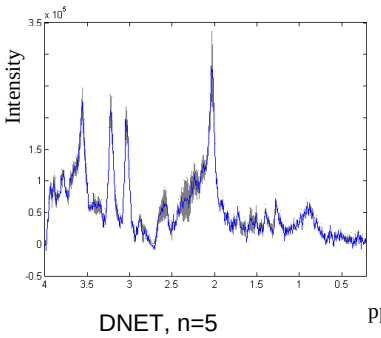

DNET, n=5

Fig.2 Mean spectra of low grade glioma subgroups +/- 1 standard error. mIns= myo-inositol, tCho= total choline, Cr= creatine, NAA= N-acetyl-aspartate, Lac= lactate, Lipids+MMs= lipids and macromolecules, PA= pilocytic astrocytoma, OPG= optic pathway glioma, NBO= neurofibromatosis bright object, PMA= pilomyxoid astrocytoma, TPG= tectal plate glioma, DNET= dysembryoplastic neuroepithelial tumour

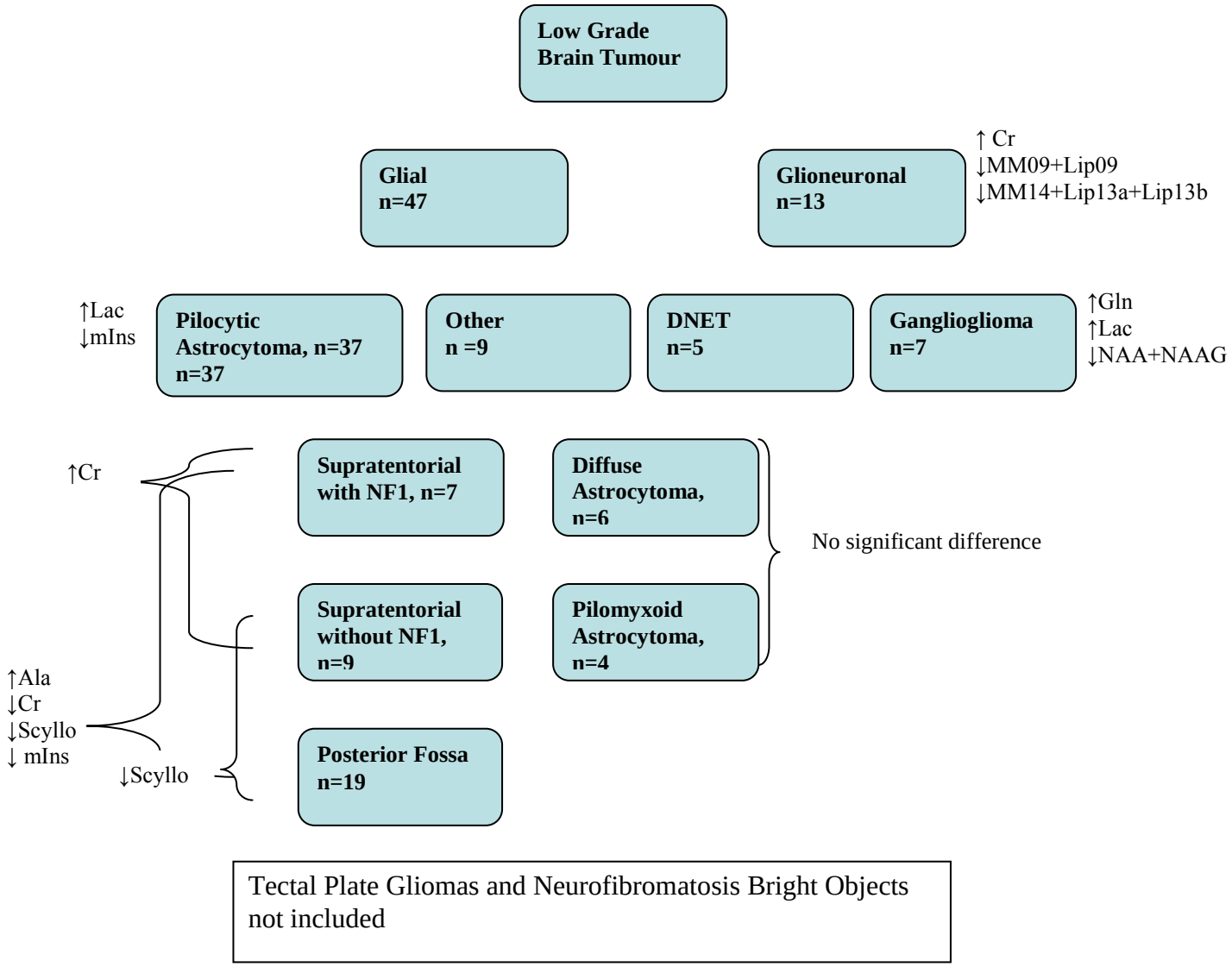

Fig.3 Classification scheme for low grade brain tumours. Statistically significant metabolite differences given by the side of the boxes and refer to the tumour group closer to them e.g. glioneuronal tumours have significantly higher Cr and lower MM09+Lip09 and MM14+Lip13a+Lip13b compared to glial tumours. Cr=creatine, MM09+Lip09=lipids and macromolecules at 0.9ppm, MM14+Lip13a+Lip13b=lipids and macromolecules at 1.3ppm, Gln=glutamine, Lac=lactate, NAA+NAAG= total N-acetyl aspartate, Scyllo=scyllo-inositol, mIns=myo-inositol, Ala=alanine

Mean concentration values for all groups included in the comparisons and for all metabolites are shown in Table 2. Concentration values and means are in “institutional units” (referenced to water unsuppressed spectrum- described in Chapter 3). The logistic regression equations giving the probability of a tumour belonging to a certain group, the probability cutoff values, the area under the ROC curve and the ROC curve significances are given in Table 3.

All glial tumours (N=47) were compared to all glioneuronal tumours (N=13), using an independent samples T-Test (4 NBOs and 5 TPGs excluded, RFGNT included). Cr ($p<0.001$) was found to be significantly higher and MM09+Lip09 ($p=0.005$) and MM14+Lip13a+Lip13b ($p=0.032$) significantly lower in glioneuronal tumours. Binary logistic regression to classify these tumours (using Cr, MM09+Lip09 and MM14+Lip13a+Lip13b) resulted in a sensitivity of 1 and a specificity of 0.745 (reference category=glioneuronal).

Within the glioneuronal group, gangliogliomas (N=7) were compared to DNETs (N=5) using an independent samples T-Test. Gln ($p=0.017$) and Lac ($p=0.032$) were significantly higher and NAA+NAAG ($p=0.045$) lower in gangliogliomas. PCh ($p=0.051$) approached significance and was higher in gangliogliomas. The binary logistic regression classifier included only NAA+NAAG. The sensitivity was 0.8 and the specificity 0.857 (DNET is considered to be the positive result).

4.3.1. Comparison of Pilocytic Astrocytomas with Other Glial Tumours

PA+OPG+MetPA (N=37) were compared to other glial tumours (PMA, Diffuse) (N=9) using a t-test and Lac was found to be significantly higher and mIns significantly lower in PA+OPG+MetPA (p=0.017 and 0.008 respectively). The logistic regression model (variables: Lac and mIns) gave a sensitivity of 0.889 and a specificity of 0.676 (positive result=other glial).

PA+OPGs (N=35) were compared to diffuse astrocytomas (N=6) (grade 2) using an independent samples T-Test. Cr (p=0.007), NAA (p=0.040) and mIns (p=0.005) were found to be significantly higher in diffuse astrocytomas and Lac (p=0.040) significantly lower. The logistic regression model (variables: Cr, NAA, mIns and Lac) gave a sensitivity of 1 and a specificity of 0.771 (positive result=diffuse astrocytoma).

Supratentorial PA+OPG without NF1 (n=9) were compared to PMA (n=4) using an independent samples T-Test and no significant differences were found. Posterior fossa PAs (n=19) were compared to MetPAs (n=2) using an independent samples T-Test, and MetPAs were found to have significantly higher GPC+PCh (p=0.044) and Glu+Gln (0.050). All PA+OPG were compared with MetPA+PMA and no significant differences were found. Diffuse astrocytomas were compared to PMA (t-test) and no significant differences were found.

4.3.2. Pilocytic Astrocytomas and Optic Pathway Gliomas

The differences within the PA+OPG group were further investigated, as this is the biggest cohort and previous work has shown that MRS can detect differences by site of tumour (66). In addition, the differences by neurofibromatosis type 1 (NF1) status were investigated, as optic pathway tumours are prevalent in patients with NF1(8). An independent sample t-test comparing all supratentorial PA+OPG (n=16) with posterior fossa PA (n=19) showed Cr ($p=0.002$), Scyllo ($p<0.001$), Tau ($p=0.042$) and mIns ($p=0.001$) to be significantly higher in the supratentorial tumours.

Using ANOVA to compare the three groups, STPA+OPG in patients with NF1, without NF1 and posterior fossa PAs showed posterior fossa PAs to have significantly higher Ala ($p=0.050$) and lower Cr ($p=0.001$), Scyllo ($p=0.008$) and mIns ($p=0.011$) than STPA+OPG with NF1; posterior fossa PAs to have significantly lower Scyllo ($p= 0.028$) than STPA+OPG without NF1; STPA+OPG with NF1 to have significantly higher Cr ($p=0.043$) than those without NF1. A T-Test comparing STPA+OPG with and without NF1 also shows Cr ($p=0.022$) to be significantly higher in STPA+OPG with NF1, in addition to mIns ($p=0.041$), and Ala to be lower in STPA+OPG with NF1 ($p=0.014$). Multinomial logistic regression to classify the 3 groups of pilocytic astrocytomas (variables: Ala, Cr, mIns, Scyllo) yielded a classification accuracy of 95% for posterior fossa PA (N=19), 86% for STPA+OPG with NF1 (N=7) and 78% for STPA+OPG without NF1 (N=9). The

equations giving the probability of a tumour being a member of one of these groups are given in Table 3.

Comparing STPA+OPG in patients with NF1 with NBOs, yielded many significant differences; NBOs have significantly higher Cr ($p=0.017$), Glu ($p<0.001$), Glu+Gln ($p=0.044$) and NAA+NAAG ($p<0.001$) and significantly lower MM09+Lip09 ($p=0.047$) and MM20+Lip20 ($p=0.049$).

Posterior fossa PAs were compared to TPGs using an independent samples T-Test. Many significant differences were found, including significantly higher Cr ($p=0.004$), GPC ($p=0.029$), GPC+PCh ($p=0.002$), Glu+Gln ($p=0.047$), NAA+NAAG ($p=0.001$), Scyllo ($p=0.014$) and mIns ($p=0.006$) in TPG and significantly lower Lac ($p=0.012$), MM09+Lip09 ($p=0.042$) and MM13+Lip13a+Lip13b ($p=0.002$) in TPG.

Table 2. Mean concentration values for all metabolites analysed for all low grade glioma subgroups/comparisons in text. Mean= mean concentration value, GN=glioneuronal, PA+OPG=biopsied pilocytic astrocytomas and unbiopsied optic pathway gliomas, ST PA=supratentorial pilocytic astrocytoma, Post. Fossa PA=posterior fossa pilocytic astrocytoma, MetPA=metastatic pilocytic astrocytoma, PMA=pilomyxoid astrocytoma, DA=diffuse astrocytoma, DNET=dysembryoplastic neuroepithelial tumour, GG=ganglioglioma, NBO=neurofibromatosis bright object, TPG=tectal plate glioma

	Glial (N=47)	GN (N=13)	All PA+ OPG (N=35)	ST PA+ OPG with NF1 (N=7)	ST PA+ OPG no NF1 (N=9)	All ST PA (n=16)	Post. Fossa PA (N=19)	PA+ OPG+ MetPA (N=37)	MetPA (N=2)	PMA (N=4)	Other Glial (DA+ PMA) (N=9)	DA (N=6)	PMA+ MetPA (N=6)	DNET (N=5)	GG (N=7)	NBO (N=4)	TPG (N=6)
	Mean	Mean	Mean	Mean	Mean	Mean	Mean	Mean	Mean	Mean	Mean	Mean	Mean	Mean	Mean	Mean	Mean
Ala	0.80	0.78	0.84	0.23	0.98	0.65	1.00	0.82	0.51	1.23	0.55	0.36	0.99	0.46	1.03	0.08	0.47
Cr	1.15	2.35	1.00	2.32	1.02	1.58	0.51	1.02	1.32	0.61	1.74	2.29	0.85	2.26	2.47	3.55	3.24
GPC	0.78	0.73	0.75	0.97	0.70	0.82	0.69	0.74	0.64	0.45	0.90	1.24	0.51	0.89	0.58	1.20	1.17
GPC+ PCh	1.22	1.09	1.20	1.64	1.25	1.42	1.03	1.22	1.54	0.92	1.23	1.42	1.13	0.89	1.24	1.61	1.54
Glc	0.85	0.80	0.88	0.84	0.71	0.77	0.98	0.86	0.40	0.99	0.70	0.69	0.79	0.99	0.57	1.10	1.10
Gln	2.52	2.79	2.55	2.57	3.34	3.00	2.17	2.58	3.07	2.37	2.26	2.25	2.61	1.62	3.86	2.31	2.42
Glu	1.54	2.48	1.40	1.42	1.40	1.41	1.40	1.46	2.39	2.18	1.77	1.63	2.25	2.27	2.77	3.25	2.36
Glu+Gln	4.06	5.28	3.95	3.99	4.74	4.41	3.56	4.03	5.46	4.56	4.03	3.88	4.86	3.89	6.63	5.56	4.78
Gua	1.08	1.42	1.03	0.64	1.10	0.90	1.14	1.12	2.63	1.02	0.93	0.91	1.56	1.10	1.63	0.80	1.14
Lac	2.36	1.48	2.67	1.46	3.14	2.40	2.90	2.64	2.08	2.03	0.94	0.85	2.05	0.67	2.20	0.54	0.75
MM09+ Lip09	6.40	3.94	6.66	5.02	7.04	6.16	7.09	6.67	6.72	6.21	4.63	4.89	6.38	2.82	4.71	2.91	3.48
MM14+ Lip13a+ Lip13b	10.76	5.22	10.68	7.99	12.42	10.48	10.85	10.56	8.43	13.60	10.68	10.15	11.88	2.29	7.37	3.40	4.31
MM20+ Lip20	7.81	7.28	7.73	8.81	8.44	8.60	6.99	7.71	7.49	6.99	7.81	8.93	7.16	5.50	8.37	6.30	6.58
NAA+ NAAG	1.13	1.88	1.01	1.09	1.27	1.19	0.86	1.04	1.41	1.37	1.28	1.52	1.38	2.81	1.20	2.96	2.07
PCh	0.44	0.35	0.46	0.67	0.55	0.60	0.34	0.48	0.90	0.48	0.33	0.18	0.62	0.00	0.66	0.40	0.36
Scyllo	0.07	0.12	0.05	0.13	0.07	0.10	0.01	0.06	0.23	0.07	0.15	0.17	0.12	0.14	0.09	0.17	0.26
Tau	0.14	0.18	0.15	0.41	0.21	0.30	0.02	0.14	0.02	0.21	0.18	0.13	0.15	0.15	0.23	0.42	0.61
mI	2.22	3.31	1.81	4.24	2.13	3.06	0.76	1.86	2.72	2.37	3.88	4.36	2.49	3.82	2.86	5.58	7.42

Table 3. Logistic Regression analysis equations, probability cutoff values, areas under the ROC curve and ROC curve significances. DNET=dysembryoplastic neuroepithelial tumour, PA=pilocytic astrocytoma, OPG=unbiopsied optic pathway glioma, MetPA= metastatic pilocytic astrocytoma, NF1=Neurofibromatosis type 1, Cr=creatine, Lip09+MM09=lipids and macromolecules at 0.9ppm, MM14+Lip13a+Lip13b= lipids and macromolecules at 1.3ppm, NAA=N-Acetylaspartate, NAAG=N-Acetylaspartylglutamate, Lac=lactate, mIns=myo-inositol, Ala=alanine, Scyllo=scyllo-inositol

	Binary Logistic Regression Equations	**Probability cutoff value**	**Area under ROC curve**	**ROC curve significance**
Glial vs Glioneuronal	Prob(glioneuronal)= 1/(1+e^-z) z= -1.3 + (0.871*Cr) + (-0.240*Lip09MM09) + (-0.044*MM14Lip13aLip13b)	0.18	0.867	p<0.0001
DNET vs Ganglioglioma	Prob(DNET)=1/(1+e^-z) z= -2.368 + (1.072*NAANAAG)	0.34	0.857	p=0.042
PA+OPG+Met PA vs Other Glial Tumours	Prob(other glial)= 1/(1+e^-z) z= -0.479 + (-1.054*Lac) + (0.263*mIns)	0.12	0.868	p=0.001
PA+OPG vs Diffuse Astrocytoma	Prob(Diffuse)= 1/(1+e^-z) z= -3.113 + (-1.047*Lac) + (0.235*mIns) + (0.149*Cr) + (1.867*NAA)	0.09	0.919	p=0.001
	Multinomial Logistic Regression Equations			
Supratentorial PA+OPG with NF1 vs Supratentorial PA+OPG without NF1	Prob(ST_with_NF1)=1/(1+e^-z) z= -1.819 + (-5.559*Ala) + (1.212*Cr) + (0.912*mIns) + (-4.821*Scyllo)			
Posterior Fossa PA vs Supratentorial PA+OPG without NF1	Prob(PF PA)= 1/(1+e^-z) z= 5.651 + (-0.057*Ala) + (-0.359*Cr) +(-3.039*mIns) + (-33.871*Scyllo)			

4.4. DISCUSSION

This study shows that MRS has the ability to discriminate between the different tumour groups of paediatric low grade brain tumours, many of which are very similar radiologically and histologically. The main differences can be readily identified on visual inspection of the spectra and mean spectra have been presented to aid this. Quantitative analysis of the spectra to yield metabolite concentrations can further aid the identification of specific subgroups by comparison with mean values and logistic regression equations can be used to give a more formal classification in cases where the tumour type is difficult to discern by visual inspection of the spectra. The collection of data from more than one centre has allowed rarer tumour types to be investigated and also established that MRS can be applied across centers with success in this challenging tumour group.

Previous work on a small cohort, showed differences between STPA+OPG and cerebellar PA , with supratentorial tumours having significantly higher Ins and Glu+Gln (66). In our study, a comparison of all supratentorial PA+OPG with posterior fossa PAs confirmed that mIns is significantly higher in supratentorial tumours, but also found Cr, Scyllo, and Tau to be significantly higher. A comparison of supratentorial PA+OPG with and without NF1 and posterior fossa PAs revealed significant differences between these three groups and multinomial logistic regression showed that the group of PA+OPG can be subdivided according

to site and NF1 status. A review of the MR images did not reveal any obvious correlation with conventional MR characteristics according to NF1 status. This is a promising finding as MRS can detect differences in a group of tumours which is histologically identical and more importantly could hold prognostic information as patients with NF1 usually have more indolent disease. A proportion of brain gliomas in patients with NF1 remain stable and may spontaneously regress (68) and the MRS profile of these tumours may be representative of tumours which have a better clinical course.

An abnormality found in 43-93% of children with NF1 are neurofibromatosis bright objects (NBOs), which are seen as areas of increased T2 signal on MRI (107). It can be difficult to detect differences radiologically between NBO, which are benign and often resolve spontaneously in the second decade, and brain gliomas (68). There can be multiple NBOs throughout the brain, and a non-invasive method of discriminating these from PAs would aid clinical decision making. MRS is showing promise at being able to solve this question. In a study of brain lesions in children with NF1 by Wilkinson et al. (68), Cho and mIns were significantly higher in tumour/atypical NBO compared to typical NBO and control groups. Gonen et al.(69) found that focal areas of signal intensity (FASI) in children with NF1 had significantly elevated Cho, reduced creatine, 2>Cho/Cr>1.3 and nearly normal NAA, and differed from tumours which had no NAA and Cho/Cr>2. Barbier et al. (108) found lower NAA/Cr, NAA/mIns, NAA/Cho and higher mIns/Cho in the right lateral thalamus of children with NF1 who had unidentified bright objects (UBO)

compared to those without UBO. Interestingly, the site of the metabolic differences was not the site of the T2 hyperintensities. Our comparison of ST PA+OPG with NF1 and NBOs showed that NBOs have significantly higher Cr, Glu, Glu+Gln, total NAA, and significantly lower MM09+Lip09 and MM20+Lip20. Although the number of NBOs is small, this is a promising result as there seem to be multiple differences, some of which may be expected from previous work. For example NAA may have been expected to be higher in NBOs as they are more diffuse and perhaps have more normal brain entrapped, which would increase NAA, a neuronal marker (74). NAA is mainly a component of healthy neurons, and the origins and functions of NAA which is seen in tumours are still under debate. For diffuse tumours, it may simply indicate the presence of neurons in brain which has been infiltrated by tumour. However, NAA may also be present in immature oligodendroglia and could be seen in neoplastic changes (74, 109). NAA was also higher in TPG and diffuse astrocytomas compared to PAs and these are more diffuse tumours with more entrapped normal brain. In addition, lipids and/or lactate have been shown to be increased in higher grade tumours (74), and in our results lipids were higher in PA than NBOs as expected.

Due to their location and the surgical challenge they present, as well as the indolent course they usually follow, tectal plate gliomas are often not biopsied to obtain a definitive histological diagnosis (11). Following imaging, they are commonly observed without treatment (11), making a firm non-invasive diagnosis a key component of their management. Different types of pathology have been

described in this region of the brain in adults and children, including pilocytic astrocytoma and high grade astrocytoma (110, 111). Improved non-invasive characterization of tumours in this region is therefore important. Comparing these TPG with posterior fossa PAs shows that MRS can detect many significant differences and shows that TPGs are biologically distinct from pilocytic astrocytomas.

Although the numbers in some groups are small, the results of this study are in agreement with those predicted based on the literature and known clinical and biological behavior of the tumours. For example, choline has been linked to cell proliferation (58, 112), malignancy and higher grade tumours (74), and our results show a higher total choline in metastatic PAs than focal PAs. Furthermore, mIns is high and lipids low in TPG, which generally have a more indolent course compared to PAs, and both of these metabolites have been similarly associated with lower grade tumours (57, 74).

4.5. CONCLUSION

This study shows that MRS can detect differences between subgroups of low grade brain tumours in children. The main differences can be readily identified on visual inspection of the spectra and quantitative analysis can aid the process of interpretation, making MRS a valuable aid to non-invasive diagnosis. The detection of metabolite differences between tumours of the same histology emphasizes the

potential for metabolite profiles to improve the characterization of these tumours and its combination with emerging molecular genetic biomarkers should improve the assessment of these tumours. Some of the most discriminatory metabolites are known to be important prognostic markers in other tumour groups, and future work is needed to determine whether they can predict progression-free survival in low grade gliomas in children.

CHAPTER 5

MAGNETIC RESONANCE SPECTROSCOPY IN THE PROGNOSIS AND FOLLOW-UP OF LOW GRADE BRAIN TUMOURS

CHAPTER 5

MAGNETIC RESONANCE SPECTROSCOPY IN PROGNOSIS AND TREATMENT- MONITORING OF LOW GRADE BRAIN TUMOURS

5.1. INTRODUCTION

Low grade gliomas and their treatment may cause significant morbidity, in terms of physical deficits, neuropsychological and neuroendocrine effects (8). Although overall survival (OS) rates are very high, progression-free survival (PFS) is much lower. In a study by Fisher et al. 5 and 10 year (from initial surgery) OS for low grade astrocytomas was 87% and 83%, and PFS was 55% and 42% (10, 15). A significant number of children have recurrences after surgical resection or progress after incomplete tumour resection or biopsy (9), which means that a non-invasive method for predicting prognosis and thus modifying initial treatment is extremely important. In addition, the clinical symptoms and signs and the magnetic resonance imaging (MRI) characteristics of these tumours are not always straightforward to interpret. A tumour may appear to be getting smaller on MRI but the patient's vision may be deteriorating and vice versa.

Low grade tumours present multiple management challenges, as they can have similar clinical presentations, magnetic resonance imaging (MRI) characteristics,

and even histopathological features when biopsied, whilst simultaneously having very different responses to treatment.

The aim of this study is to use ^{1}H MRS to predict progression-free survival in an extensive cohort of low grade brain tumours specifically, by short echo time MRS pre-treatment, and to combine results from 2 centers. This is very important as getting multicentre data which follow the same acquisition protocols, are collected consistently, and have accurate clinical data over a long period of time and in patients with complicated clinical courses is very challenging, but the only way to increase the number of patients in these studies and get more reliable and statistically meaningful results. Another part of this study investigates metabolite changes in sequential MRS studies and correlates this with clinical data.

5.2. PATIENTS AND METHODS

The patients and methods are described in Chapter 3. Progression is difficult to define in low grade brain tumours, as there are often discrepancies between imaging, clinical and histopathological data. Progression was therefore defined by the decision by the neuro-oncology multi-disciplinary team to change treatment, therefore taking into account all available information and being directly relevant to clinical practice.

5.3. RESULTS

5.3.1. Prognosis

The tumour cohort in this study is the same as in the study on diagnosis of low grade brain tumours with ^{1}H MRS (except for one patient who was removed as progression occurred before the pre-treatment MRS). The cohort therefore consisted of 68 patients. The ages at pre-treatment MRS ranged from 2-195 months, with a mean age of 103 months.

Tumour diagnoses in accordance to the WHO classification, split by progression status are shown in Table 1.Treatments received in the first episode (i.e. from presentation to progression or end of follow-up), split by progression status are shown in Table 2.

Further analysis excluded patients with a complete or near complete resection and diffuse astrocytomas, leaving a cohort of 49 patients. 15 patients progressed (2 died) in the duration of the study. Mean spectra of progressors and non-progressors are shown in Fig.1.

Table 1 Diagnoses (according to WHO), split by progression status. ST=supratentorial, PA = pilocytic astrocytoma, OPG=unbiopsied optic pathway glioma, NF1=neurofibromatosis type 1, NBO=neurofibromatosis bright object, DNET=dysembryoplastic neuroepithelial tumour, RFGT= rosette forming glioneuronal tumour of the 4th ventricle

	Progressed	Not progressed	Total number of patients
ST PA+OPG with NF1	3	4	7
ST PA+OPG without NF1	2	6	8
Posterior fossa PA	1	18	19
Pilomyxoid astrocytomas (1 pilocytic/pilomyxoid)	2	2	4
NBO	0	4	4
PA metastatic at presentation	1	1	2
Diffuse astrocytomas (including fibrillary)	4	2	6
Tectal plate gliomas (includes a rosette forming glioneuronal tumour of the 4th ventricle)	1 (RFGT)	5	6
Gangliogliomas	3	4	7
DNET (biopsied and unbiopsied)	2 (biopsied)	3	5
	Total=19	Total=49	Total=68

Table 2 First episode treatments, split by progression status. Surgical resection is judged on MR imaging. Surgery R1+R2= complete or near complete resection, Surgery R3+R4=incomplete resection or open biopsy or stereotactic biopsy

	Progressed	Not progressed	Total number of patients
Observation only	5	17	22
Surgery R1+R2	0	13	13
Surgery R3+R4	6	13	19
Chemotherapy	1	1	2
Surgery R3+R4+Chemotherapy	5	4	9
Surgery R3+R4+Radiotherapy	2	1	3
	Total=19	Total=49	Total=68

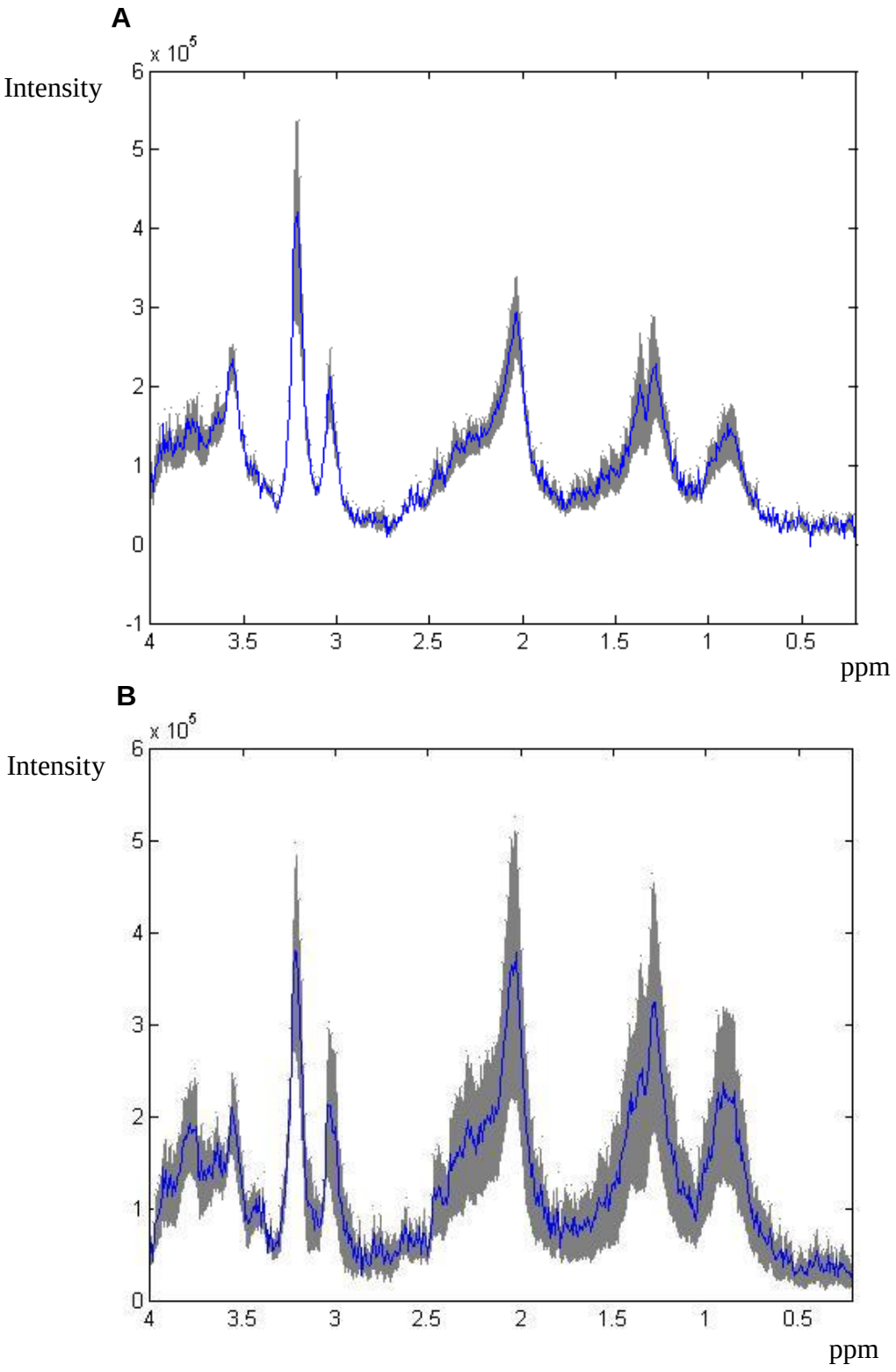

Fig.1 A. Mean spectrum of patients who did not progress +/- standard error
B.Mean spectrum of patients who progressed +/- standard error

mIns was dichotomised using a ROC curve where the positive result was ‘not progressed’, and using the value giving the highest sensitivity + specificity, which was 4.1095. 31 patients had low mIns, and 14 of these progressed, whereas 18 patients had high mIns and only 1 progressed. Patients with high mIns had significantly better progression-free survival (PFS) than those with low mIns (log-rank significance=0.005). The survival curve (time in months) is shown in Fig. 2.

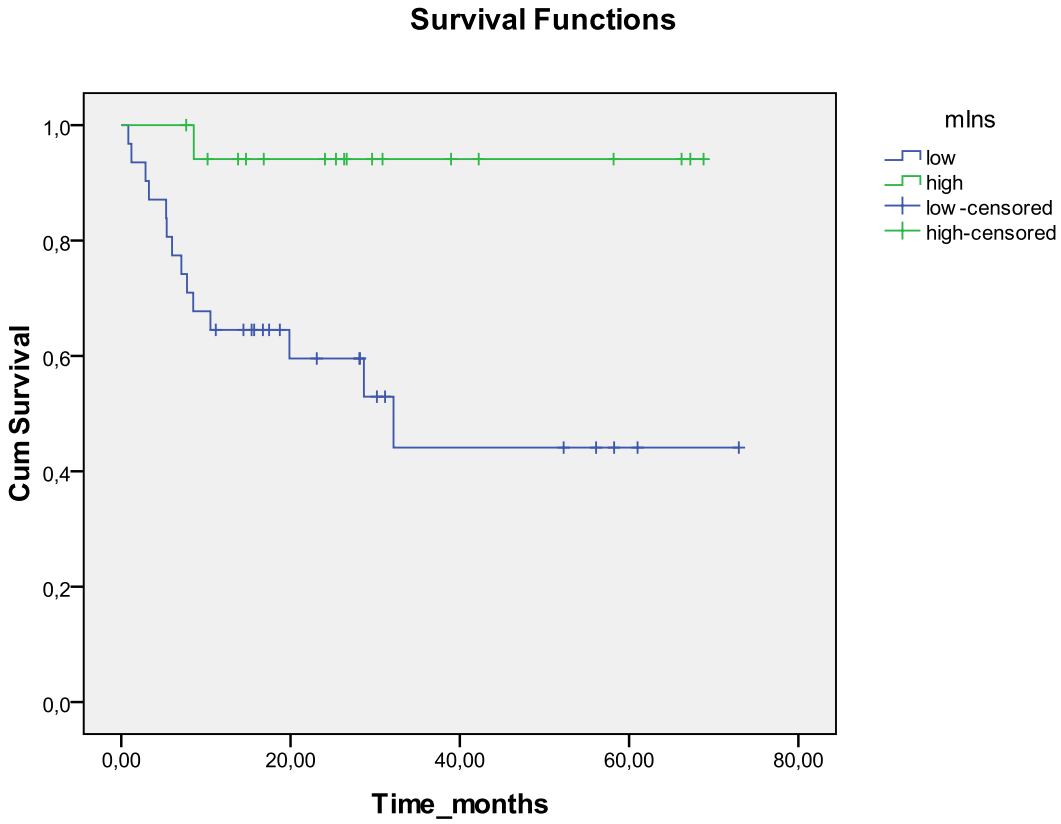

Fig.2. Kaplan-Meier survival curve based on mIns concentrations.

GPC was dichotomised using a ROC curve where the positive result was ‘not progressed’, and using the value giving the highest sensitivity+specificity, which was 1.171. 32 patients had low GPC, and 13 of those progressed, whereas 17 patients had high GPC and 2 of those progressed. Results approached significance, with patients having high GPC showing better progression-free survival (PFS) than those with low GPC (log-rank significance=0.057). The survival curve (time in months) is shown in Fig. 3.

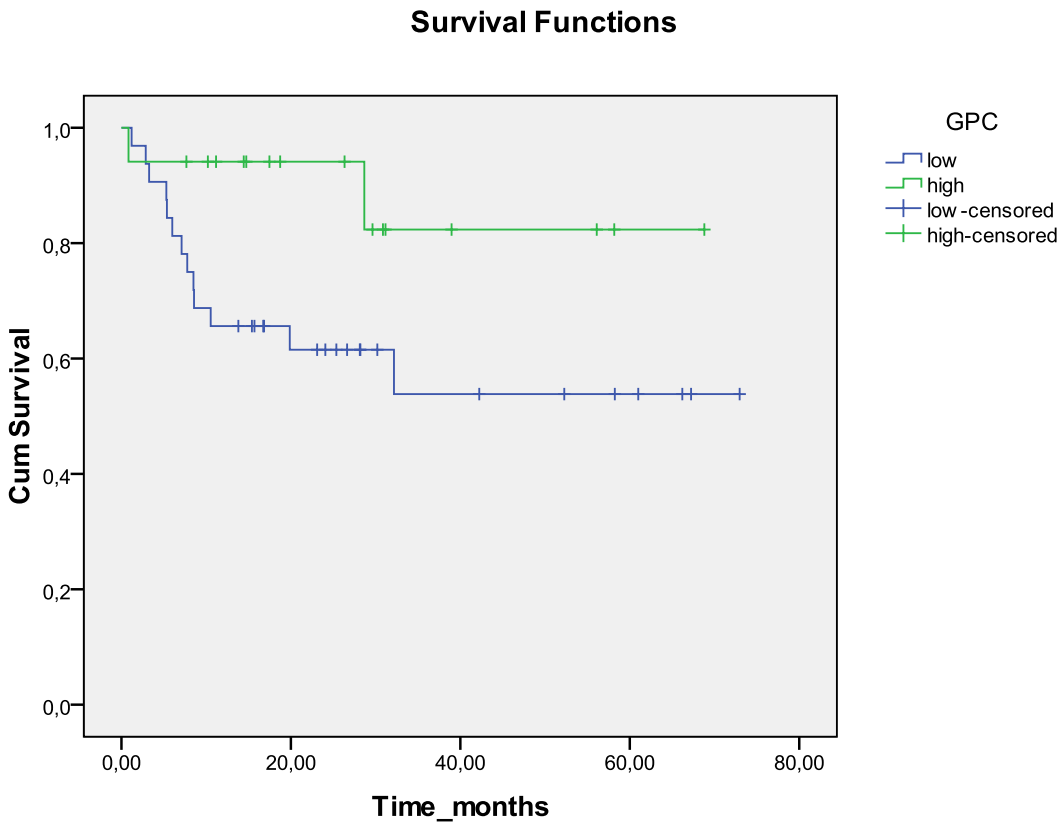

Fig.3. Kaplan-Meier survival curve based on GPC concentrations.

PCh was dichotomised using a ROC curve where the positive result was ‘progressed’, and using the value giving the highest sensitivity + specificity, which was 1.696. 46 patients had low PCh, and 13 of those progressed, whereas 3 patients had high PCh and 2 of those progressed. Patients with high PCh had worse progression-free survival (PFS) than those with low PCh (log-rank significance= 0.047), although it should be noted that there are only 3 patients in the ‘high’ category.

Cox regression included 15 patients who progressed and 34 who did not. A stepwise forward likelihood ratio (LR) method was used. Variables included in Cox regression are the ones found to have a significant or near significant effect on survival in Kaplan-Meier analysis. Reference categories are always the ‘high’ group. mIns and PCh are included in the final model as significant predictors of survival. Patients with low PCh (<1.696) have 0.153 times the risk of progression compared to those with high PCh (p=0.026). Patients with low mIns (<4.1095) have 11.980 time the risk of progressing compared to those with high mIns (p=0.018). The -2 log likelihood of the model has a significance of 0.005 at step 1 and 0.002 at step 2, which means the model is significantly better than the null model. Survival functions are shown in Fig. 4.

A

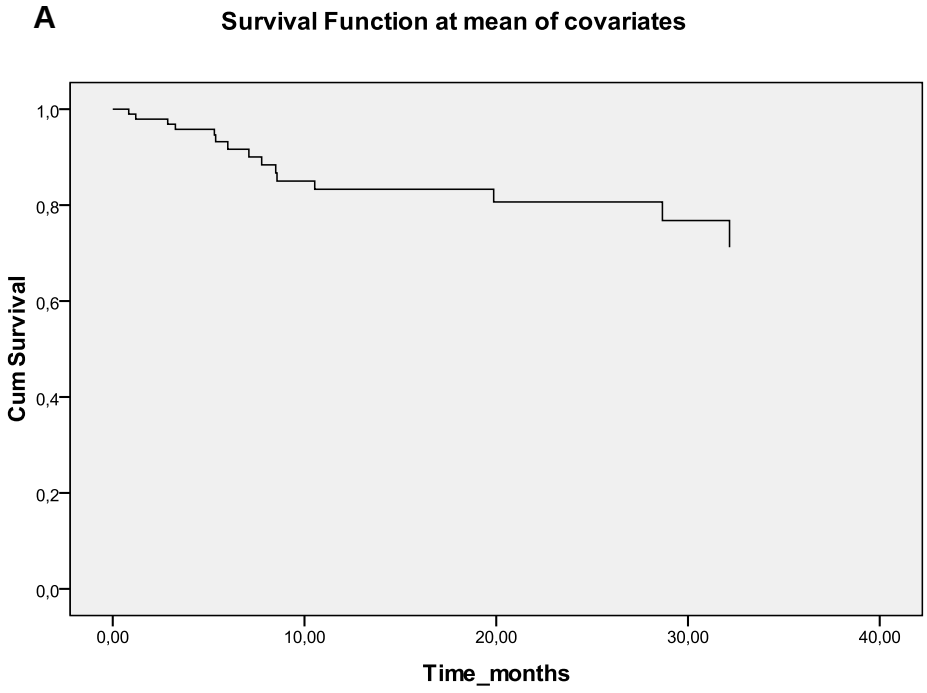
Survival Function at mean of covariates
Cum Survival
1,0
0,8
0,6
0,4
0,2
0,0
0,00
10,00
20,00
30,00
40,00
Time_months

B

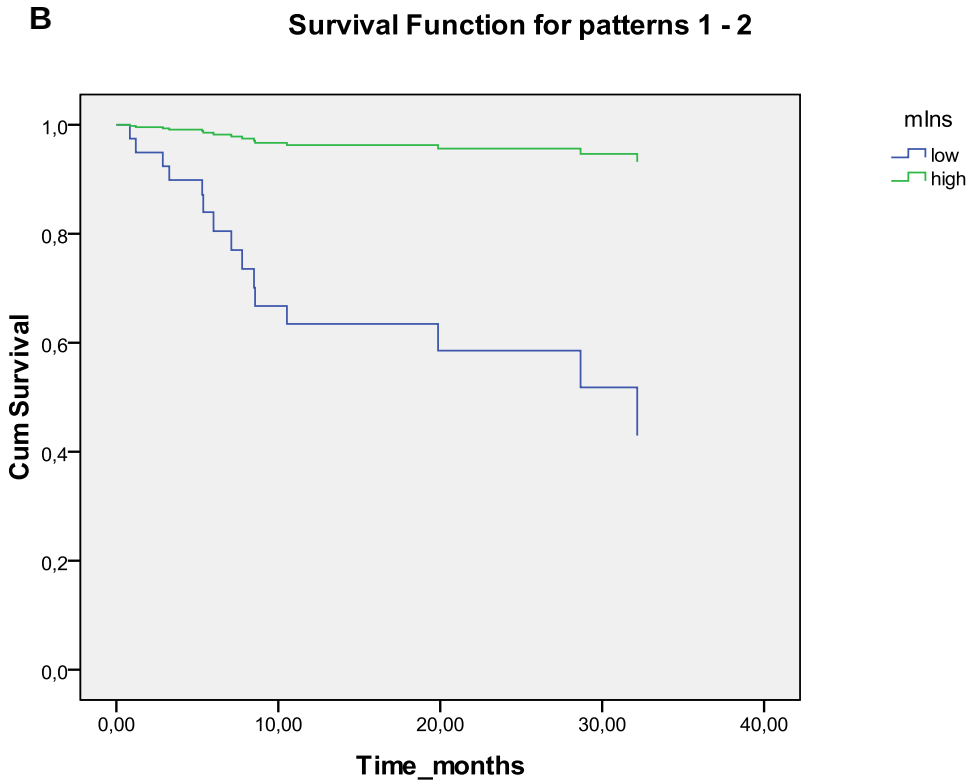
Survival Function for patterns 1 - 2
Cum Survival
1,0
0,8
0,6
0,4
0,2
0,0
0,00
10,00
20,00
30,00
40,00
Time_months
mlns
low
high

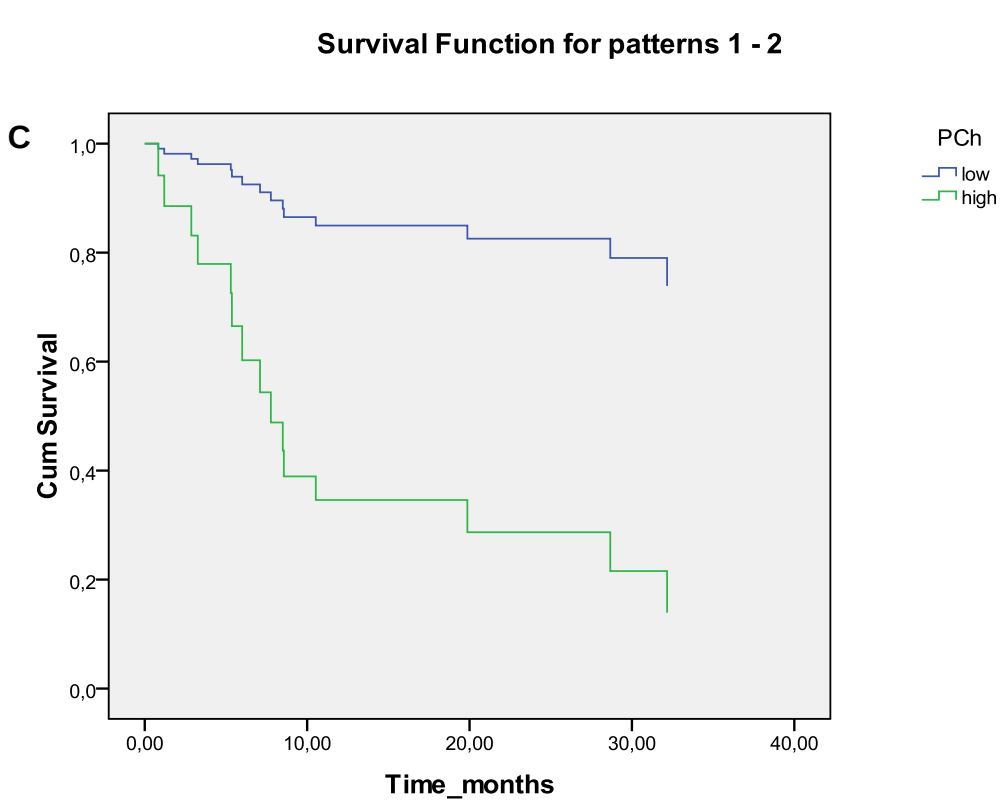

Fig. 4. Survival functions produced by Cox regression analysis. A- survival function at mean of covariates, B- survival function for mIns, C-survival function for PCh. mIns=myo-inositol, PCh=Phosphocholine

5.3.2. Follow-up

A summary of the follow-up results is given in Table 3. Patients who did not progress and were only observed were investigated (n=10), and their first two good-quality MRS studies compared. The diagnoses of these patients included 3 NBOs, 3 TPGs, 2 DNETs, 1 ganglioglioma and 1 ST PA with NF1. Paired samples t-test showed a statistically significant difference between the first and second MRS in Lip13b (p=0.043), MM20 (p=0.025), MM20+Lip20 (0.030) and PCh (p=0.045). All metabolites had lower concentrations in the second MRS.

Patients who did not progress and had MRS pre-treatment and after incomplete resection (surgery R3+R4) or observation followed by incomplete resection (surgery R3+R4) were investigated (n=3). The diagnoses of these patients included 1 diffuse astrocytoma, 1 ST PA without NF1 and 1 posterior fossa PA. Paired-samples t-test did not show any significant differences between the two MRS studies.

Patients who did not progress and had MRS pre-treatment and during or after chemotherapy or radiotherapy or surgery R3+R4 or a combination of treatments were investigated (n=6). The diagnoses included 1 ST PA with NF1, 1 ST PA without NF1, 1 PA metastatic at presentation, 2 PMA and 1 diffuse astrocytoma. One patient had radiotherapy and the second MRS used in the analysis was performed approximately 3 months after radiotherapy. Paired samples t-test

showed a statistically significant difference between the first and second MRS in Ala ($p=0.021$) and MM12 ($p=0.016$); both metabolites had lower concentrations in the second MRS.

Patients who progressed (looking at first progression) and had MRS pre-treatment and before progression were investigated (n=11), choosing the MRS which was closest to but before progression. Patients had varying treatments including observation, surgery, chemotherapy, radiotherapy or a combination. Diagnoses included 2 ST PA without NF1, 1 ST PA with NF1, 1 PF PA, 1 PA metastatic at presentation, 1 PMA, 1 DNET, 1 ganglioglioma, 1 RFGT, and 2 diffuse astrocytomas. 2 patients had radiotherapy and their second MRS in the analysis was right after and approximately 8 months after radiotherapy respectively. Paired samples t-test showed a statistically significant difference between the first and second MRS in Gln ($p=0.041$), with this metabolite having a higher concentration in the second MRS study.

Table 3. Summary of results from MRS follow-up. The first and second good quality MRS studies were compared, the first being pre-treatment and the second during or after the treatment in column 1. For the patients who progressed, the second MRS was before progression.
Chemo= chemotherapy, Radio=radiotherapy, Obs=observation, Surg=surgery, NBO=neurofibromatosis bright object, TPG=tectal plate glioma, DNET=dysembryoplastic neuroepithelial tumour, Ganglio=ganglioglioma, STPA=supratentorial pilocytic astrocytoma, DA=diffuse astrocytoma, PF PA=posterior fossa pilocytic astrocytoma, PA met at pres=pilocytic astrocytoma metastatic at presentation, PMA=pilomyxoid astrocytoma, RFGT=rosette forming glioneuronal tumour of the 4th ventricle

Treatment category	**Progression**	**Diagnoses**	**Statistically significant differences between 1st and 2nd MRS**		
Observation only	No	NBO n=3 TPG n=3 DNET n=2 Ganglio n=1 STPA with NF1 n=1	Lip13b	p=0.043	Lower in 2nd MRS
			MM20	p=0.025	
			MM20+Lip20	p=0.030	
			PCh	p=0.045	
Incomplete resection	No	DA n=1 STPA no NF1 n=1 PF PA n=1	none		
Chemo/ Radio/ incomplete resection/ combination	No	STPA with NF1 n=1 STPA no NF1 n=1 PA met at pres n=1 PMA n=2 DA n=1	Ala	p=0.021	Lower in 2nd MRS
			MM12	p=0.016	
Obs/ Chemo/ Radio/ Surg/ Combination	Yes	STPA no NF1 n=2 STPA with NF1 n=1 PF PA n=1 PA met at pres n=1 PMA n=1 DNET n=1 Ganglio n=1 RFGT n=1 DA n=2	Gln	p=0.041	Higher in 2nd MRS study

5.4. DISCUSSION

This study has investigated a large cohort of patients with low grade brain tumours over a long time period with respect to progression-free survival (PFS) and sequential spectral profile changes. Short echo time MRS pre-treatment was used to predict prognosis, and follow-up MRS studies were used to monitor changes in tumours. Although this is the largest cohort of low grade brain tumours for which this kind of data is reported in the literature, the number of patients and progression events is still low and therefore limits the power of the results. However, significant results have been demonstrated, data from 2 centers combined, and a detailed method of following-up patients with low-grade brain tumours and collecting MRS data alongside clinical, imaging and histopathological information established.

In the investigation of PFS, tumours which were completely resected and diffuse astrocytomas were removed from the analysis, and the rest were grouped together. Gross total resection is the most consistent good prognostic factor (11, 12). Non-pilocytic gliomas, particularly diffuse fibrillary gliomas, are more highly associated with progression, and tumour histology may be independent predictor of progression (11, 12). Whilst other prognostic factors such as age and metastatic disease are emerging as important prognostic factors, the relatively small numbers of patients in the study prevented any further subcategorisation.

Pre-treatment MRS was shown to be predictive of progression-free survival using Kaplan-Meier survival analysis and Cox regression analysis, with high mIns, high GPC and low PCh being indicators of good prognosis. mIns was also shown by Harris et al. (66) to be significantly lower at pre-treatment short TE SVS in children with supratentorial pilocytic astrocytomas who progressed compared to those with stable disease. Peet et al.(27) demonstrated myoinositol (Inos)/Cho to be significantly lower in untreated compared to treated brain tumours. NAA/Cho and Cr/Cho have been shown by Girard et al. (77) to be lower in patients who died, and the percent change in Cho/NAA and normalised choline was significantly higher in patients with progressive compared to stable outcomes in a study by Tzika et al.(79). Warren et al. found that patients with Cho/NAA equal to or below the median had greater survival (80). Other studies have also shown high choline or Cho/NAA to be linked to poor prognosis (progression or death) (62, 78, 81). However, none of these studies reported PCh and GPC separately. This is because it is difficult to separate these two metabolites in vivo at 1.5T, although a study by Wilson et al. (113) found a significant correlation between PCh from in vivo MRS and ex vivo HR-MAS, especially in medulloblastomas which have high PCh and excellent SNR (due to their high cellular density). This also allows the PCh peaks downfield from the PCh and GPC singlets at 3.2ppm to be detected. Furthermore, in a study of paediatric cerebellar tumours by Davies et al. (114), PCh was found to be an important discriminator of medulloblastomas. The LCModel basis set included GPC and PCh, and although the small chemical shift difference between their singlets is not considered enough to distinguish them in

vivo at 1.5T, it is suggested that the relative differences in concentrations of choline-containing metabolites lead to subtle but detectable changes in the total choline peak in the spectra. This was further supported by the narrower choline peak relative to the corresponding water peak width in medulloblastomas, which are known to have a predominant contribution from PCh.

Lipids have also been implicated in progression and poor survival (62, 73, 81); in this study lipids at pre-treatment MRS were not identified as prognostic indicators, but follow-up MRS showed that patients with stable disease had a significant decrease (between pre-treatment and subsequent MRS) in lipids, macromolecules, PCh and Ala or no change in spectral profile, depending on the treatment group. This shows that patients with stable disease show a decrease in metabolites associated with more aggressive tumours, although this depends on the specific group of patients being investigated. Lazareff et al. (82) also found the ratio of tumour/brain choline to decrease significantly after treatment in patients with a decrease or stable tumour volume. However, they did not find normalised choline pre-treatment to be different between responders and non-responders to therapy, although post-treatment choline was significantly higher in then non-responders. Harris et al. showed that children with supratentorial pilocytic astrocytomas who progressed had a significant decrease in myoinositol between the pre-treatment and first on-treatment MRS (66), which we did not find in this study. Alanine, also shown to decrease between MRS studies in patients with stable disease, increases in hypoxic tissues due to increased glycolysis and has been observed in various

brain tumours(115), although its detection is difficult due to the low concentrations seen. Mirbahai et al.(116) showed alanine in nutrient starved and cisplatin treated BT4C cells to decrease, suggesting it may be a biomarker of cell stress and cell death.

.

Patients who progressed were found to have a significantly higher Gln on the second MRS (prior to prognosis) compared to the pre-treatment MRS, suggesting that Gln may be an earlier indicator of disease status than conventional imaging and clinical characteristics. Harris et al. (66) found that patients with supratentorial pilocytic astrocytomas who progressed had a tendency to lower glutamate+glutamine, although this did not reach significance; as glutamate and glutamine were combined in that study, it is difficult to compare the results.

Although it is difficult to directly compare the results of the reported studies, as they use different methodologies (single voxel vs. spectroscopic imaging, ratios vs. single metabolites, different echo times, combined metabolites vs. individual), certain metabolites are emerging as important prognostic indicators in paediatric brain tumours, especially choline, lipids and myo-inositol. Larger studies are needed with consistent protocols, to investigate the relationships currently in the literature, and provide stronger evidence as to the value of these spectral biomarkers. Absolute quantitation using a water reference spectrum, short echo time spectroscopy and robust quantitation software which allows the determination of individual metabolite concentrations (such as GPC, PCh, Glu, Gln) will aid this

investigation. Furthermore, ^{1}H MRS at 3T would enable better distinction between Glu and Gln (117), and ^{31}P MRS can be used to distinguish between GPC and PCh (118).

5.5. CONCLUSION

This study has investigated a large cohort of patients with low grade brain tumours over a long time period with respect to progression-free survival (PFS) and sequential spectral profile changes. High mIns and GPC and low PCh were found to be indicators of good prognosis. Follow-up MRS showed that patients with stable disease had a significant decrease (between pre-treatment and subsequent MRS) in lipids, macromolecules, PCh and Ala or no change in spectral profile, depending on the treatment group. Patients who progressed were found to have a significantly higher Gln on the second MRS (prior to prognosis) compared to the pre-treatment MRS, suggesting that Gln may be an earlier indicator of disease status than conventional imaging and clinical characteristics. This study therefore provides further evidence for the ability of certain metabolites to predict prognosis, focusing on low-grade gliomas.

CHAPTER 6

CORRELATION BETWEEN HISTOLOGICAL FEATURES AND METABOLITE CONCENTRATIONS FROM IN VIVO ^{1}H MRS IN PAEDIATRIC BRAIN TUMOURS

CHAPTER 6

CORRELATION BETWEEN HISTOLOGICAL FEATURES AND METABOLITE CONCENTRATIONS FROM IN VIVO ^{1}H MRS IN PAEDIATRIC BRAIN TUMOURS

6.1. INTRODUCTION

Advances in Magnetic Resonance Imaging (MRI) and functional imaging including Magnetic Resonance Spectroscopy (MRS) in recent years mean there is a wide range of information available from non-invasive techniques. Thus, there is a need to determine how biomarkers obtained using these techniques relate to established tumour markers.

The advent of new treatment protocols including agents directed against neoangiogenesis and gene therapy has increased the urgency for new methodologies of non-invasive characterization of tumours. The ability to develop non-invasive techniques, however, depends heavily on understanding the biology of the tumours and the correlation of this to the imaging tools we use. Magnetic resonance spectroscopy has been used increasingly for the characterization of brain tumours and provides valuable information which aids diagnosis, prognosis and treatment monitoring. Therefore, understanding the effects of features like

proliferation and vascularity and events like apoptosis and necrosis on the MRS spectra is imperative.

This study was designed to test several hypotheses, based on current evidence in the literature on the role of specific metabolites and previous correlation studies, aiming to establish new metabolic correlates or confirm correlations from other small studies. A number of metabolites have already been studied with ^{1}H MRS and their clinical and biological significance and relationship to important cell processes investigated to variable degrees. However, most studies have been performed using long echo time spectroscopy, which does not allow the quantitation of some metabolites which have biological and clinical importance, and there is very limited data from paediatric patients.

The metabolites which have been investigated in previous research include choline (Cho), lipids, taurine (Tau), lactate (Lac) and N-acetyl-aspartate (NAA). The hypotheses we aim to test include the relationship between choline-containing compounds and Ki67 proliferation index, cellular atypia and mitosis. Choline has been linked to nuclear density (119), Ki67 proliferation index (58, 112) and nuclear shape (119, 120), and suggested as a marker of rapid cellular proliferation and tumour aggressiveness (65). Furthermore, the relationship between lipids+macromolecules and apoptosis, necrosis, cellular atypia, and mitosis will be investigated in this work. Lipids have been linked to apoptosis (121, 122) and necrosis (28, 123), as well as Ki67 (119). Tzika et al. suggested that choline and

lipid mapping have value in tumour grading of glial tumours (123). Astrakas et al. showed normalized choline and lipids and/or lactate at 1.3ppm to be independent predictors of tumour grade (higher in high-grade tumours) (74). Furthermore, the importance of lipids and choline in the assessment of paediatric brain tumours is emphasized in the work by Marcus et al., which showed that choline, lipids and/or lactate (L), choline/NAA and choline+0.1L were significantly higher in non-survivors compared to survivors, and Cho+0.1L was the only independent predictor of survival(81).

The correlation between taurine and apoptosis will be investigated, as Moran et al.(124) and Lang et al (125) have shown taurine to possibly be involved in the process of cell shrinkage in apoptosis. Several metabolites detected by ^{1}H MRS in paediatric brain tumours in vivo are involved in energy metabolism, and interest in these has been increasing. One of the cellular metabolism alterations that features prominently in current research is increased aerobic glycolysis or the «Warburg effect» (126, 127). During glycolysis, pyruvate is converted to lactate and alanine (in different ratios depending on organ type). Lactate has been suggested as an indicator of tumour metabolic activity in rat gliomas (128), but others do not agree (65, 129). Terpstra et al. (128) found a putative perfusion threshold above which tumour lactate was independent of haemodynamic and histologic factors (tumour blood flow, necrosis, inflammatory cell infiltrate). This supported the hypothesis that high lactate in most tumours is related to high glycolytic activity of viable neoplastic cells with adequate perfusion. Furthermore, lactate can be produced by anaerobic

glycolysis in degenerating/necrotic cells. Peet et al. (65) found higher lactate in localized compared to metastatic (high proportion of metabolically active cells) paediatric medulloblastomas and suggested this was due to anaerobic stress in the localized tumours. Kugel et al. did not find a correlation between lactate level and histologic tumour grade (129). Lactate is also present in cysts (130). In this study lactate and its relationship to necrosis, tumour architecture and vascularity will be investigated.

Other metabolites of interest that are present in brain tumours and have been studied regarding diagnostic or prognostic value include myo-inositol and glycine. mIns, which can be detected reliably at short echo times, is a cerebral osmolyte and an astrocyte 'marker' (91). Glycine has been ignored in a lot of models that use MRS to discriminate between brain tumours, as it overlaps with myo-inositol and has a low concentration in normal brain (75). However, glycine has been reliably detected in paediatric brain tumours by Davies et al. (75) and shown to be significantly higher in high grade vs low grade tumours. Myo-inositol has been found to be higher in paediatric supratentorial pilocytic astrocytomas compared to cerebellar PAs, and optic pathway and thalamic tumours that progressed had significantly lower mIns at initial MRS compared to those with stable disease (66). Furthermore, tumour cells in astrocytic neoplasms stain intensely with antibodies to GFAP (131). mIns and glycine will therefore be tested for their correlation with neoplastic and reactive glial elements and GFAP staining.

A metabolite that has been used extensively in clinical studies as a putative neuronal marker (132) but has also caused most controversy regarding its origins is N-acetyl-aspartate (NAA). NAA is rarely seen in brain tumours, but significant amounts are seen in paediatric pilocytic astrocytomas, and it is still unclear whether it arises from tumour cells or infiltrating normal brain. This study aims to address this issue at a preliminary level, by testing its relationship with lesional and entrapped neuronal elements, as well as neoplastic and reactive glial elements and synaptophysin staining. Synaptophysin is a reliable marker of neuronal differentiation (133).

Research on the specific relationships between metabolites detected with magnetic resonance spectroscopic techniques and histopathological features is still limited. Furthermore, work in this field is not always in agreement between different research groups, and results also need to be verified in vivo in paediatric patients. This study therefore aims at providing further evidence of the correlations of metabolites detected at short echo time with histopathological features in paediatric brain tumours. This is a small study to establish the existence of important relationships and the need for a larger, more detailed study.

6.2. MATERIALS & METHODS

6.2.1. MRS

MRS was performed routinely in children with brain tumours as part of the clinical imaging, at 1.5T, prior to any treatment (except stereotactic biopsy) at the Birmingham Children's Hospital (BCH) from 2003 to 2009, and analysed retrospectively. The acquisition protocol involved using point-resolved spectroscopy (PRESS) localization for a single voxel. The voxel volume was either 3.375cm^3 or 8cm^3 according to the size of the tumour. A TE of 30ms was used for all patients. Some patients also had long echo time (TE=135) MRS (n=8). Repetition time was 1500-2000ms and 128 repetitions were used for 8cm^3 voxels while 248 repetitions were used for 3.375 cm^3 voxels. A water MRS was acquired for eddy current correction and as a concentration reference. Raw MRS signal data and voxel position images were transferred to a dedicated computer network. The signal was processed using LCModel software (version 6.2.0) (96), which determines metabolite concentrations by fitting the data to a linear combination of basis functions formed from individual metabolite spectra. Crammel-Rao Lower Bounds (CRLB) are also determined by LCModel, and these indicate the accuracy with which the metabolite concentrations have been estimated. Ethical approval was given for the study and written parental informed consent obtained.

The spectra were reviewed individually to assess quality, and the ones failing the criteria set were excluded from the analysis. These criteria included signal-to-noise

ratio (S/N) ≥ 4 and full-width half-maximum (FWHM) ≤ 0.15ppm. Baseline stability, good phasing, adequate water suppression and absence of artifacts were assessed by inspection. The voxel positioning was also reviewed to ensure the voxel was positioned over tumour and did not include large amounts of normal brain or cyst. In addition, voxels needed to be at least 3mm away from lipid-containing bone and scalp. Statistical analysis was carried out using SPSS statistics software v.17.0 and p-values of <0.05 were considered statistically significant. The tests included two-tailed independent samples T-Tests and Two-tailed Spearman-rank correlation tests.

6.2.2. Segmentation

For patients with significant amounts of cyst or ventricle in the voxel, segmentation of the MR images was performed and the metabolite concentrations adjusted accordingly (corrected metabolite concentration= concentration in voxel/active tumour fraction in voxel). The concentration of lactate was not altered in the three patients with cyst in the voxel (the tumour cysts contain lactate), but was altered for the patient with ventricle in the voxel.

6.2.3. Histological review

Histological review of H&E stained sections obtained at the time of biopsy or tumour resection for each patient was undertaken jointly with Dr. Brundler,

consultant histopathologist at BCH, blind to the MRS results. The assessment was semi-quantitative, with each feature assigned a category. The H&E stained slides were assessed (as detailed in Table 1) for architecture and cellularity, presence of cellular atypia, mitosis, apoptosis and necrosis. Also recorded was the presence of neoplastic glial elements, reactive glial elements, entrapped neuronal elements, lesional neuronal elements, and vascularity. Ki67, GFAP and synaptophysin immunohistochemical stains were also reviewed were available.

6.3. RESULTS

27 children with low and high grade brain tumours were included in the study. The breakdown by tumour type (according to WHO 2007(104)) was: 9 medulloblastomas, 5 pilocytic astrocytomas, 3 ependymomas, 2 atypical teratoid/rhabdoid tumours, 2 glioblastomas, 2 diffuse astrocytomas, 2 dysembryoplastic neuroepithelial tumours, 1 pineoblastoma, 1 gliomatosis cerebri.

The categories of all histopathological variables and the respective number of patients are shown in Table 1. Fig.1 shows some of the pathological parameters assessed in representative microphotographs. A summary of the statistically significant correlations described below is given in Table 2. Ki67 proliferation index was tested for correlation with choline-containing compounds and there was a significant positive correlation between Ki67 and PCh ($p= 0.031$ c.c. = 0.442) and Ki67 and GPC+PCh ($p= 0.006$ c.c. = 0.544) but not GPC. A scatter plot of

GPC+PCh against Ki67 is shown in Fig.2C. Apoptosis was also assessed and correlation with lipids/macromolecules and taurine investigated. Apoptosis was assessed through the identification of characteristic nuclear changes, condensation, clumping and fragmentation of nuclei. This has been previously observed in medulloblastomas to correlate well with cleaved (activated) caspase 3, an immunohistochemical marker of apoptosis (65). There was a significant positive correlation with lipids/macromolecules at 0.9ppm ($p=0.001$ c.c.= 0.581), 1.3ppm ($p=0.003$ c.c. = 0.550), and 2.0ppm ($p=0.005$ c.c. = 0.520) and with Tau ($p=0.014$ c.c. =0.466). In addition, there was a significant correlation between lipids+macromolecules at 1.3 divided by those at 0.9ppm ($p=0.001$ c.c.= 0.584). Scatter plots of lipid at 0.9ppm and Tau vs. apoptosis are shown in Fig.2 (A, B respectively). Splitting cases by necrosis (present N=9, absent N=18) showed statistically significant positive correlations between apoptosis and lipids/macromolecules at 0.9 ($p=0.004$ c.c.=0.645), 1.3 ($p=0.003$ c.c.=0.656), 2.0 ($p=0.001$ c.c.=0.718) and 1.3/0.9 ($p=0.002$ c.c.=0.667) ppm and Tau ($p=0.002$ c.c.= 0.668) for the group with no necrosis present.

Necrosis was present in 9 patients as mentioned above but in 1 it was very localized and this patient was removed from the analysis of necrosis and lipids+macromolecules and lactate. A comparison (t-test) of the 2 groups of no necrosis (N=18) and necrosis present (N=8) with respect to the amount of lipids+macromolecules at 0.9, 1.3 and 2.0ppm and lactate found no statistically significant differences. However, long TE lipids+macromolecules at 0.9 ($p=0.002$),

1.3 (p=0.002) and 2.0 (p=0.004) ppm were found to be significantly higher in the group with necrosis (n=2) compared to without necrosis (n=6) (t-test). Lipids at 1.3/0.9 did not show any significant difference. Apoptosis was not found to correlate with lipids/macromolecules at long TE using the Spearman-rank correlation test.

Furthermore, the correlation between cellular atypia and choline compounds and lipids+macromolecules was investigated. There was a significant positive correlation between atypia and PCh (p=0.013 c.c. =0.472), GPC+PCh (p=0.014 c.c. =0.468), lipids+macromolecules at 0.9ppm (p=0.023 c.c. =0.437), 1.3ppm (p=0.016 c.c. = 0.458), and 2.0ppm (p=0.002 c.c. = 0.561). A scatter plot of atypia vs. lipids+macromolecules at 2.0ppm is shown in Fig.2 D. Spearman-rank correlation showed statistically significant positive correlations between mitosis and PCh (p=0.004, c.c.= 0.543), lipids+macromolecules at 0.9 (p=0.006, c.c.= 0.520), 1.3 (p=0.012, c.c.= 0.487), and 2.0ppm (p=0.001, c.c.= 0.602) but not with GPC or GPC+PCh.

Lesional neuronal elements were assessed and tested for correlation with NAA and NAA+NAAG and found to have a statistically significant negative correlation with both ($p<0.0001$, c.c. = -0.708 for both). No significant difference in NAA or NAA+NAAG between patients with and without entrapped neuronal elements was found.

There was a significant positive correlation between neoplastic glial elements and mIns ($p=0.024$ c.c. $=0.432$) and a significant negative correlation with Gly ($p=0.001$ c.c.$= -0.584$), Fig. 2 E and F respectively. mIns+Gly did not have a significant correlation. There was also a significant positive correlation between neoplastic glial elements and NAA and NNA+NAAG ($p<0.0001$ c.c.$=0.719$ for both). mIns, Gly, mIns+Gly, NAA or NAA+NAAG were not singificantly different (t-test) between groups where reactive glial elements were present or absent. There was a significant negative correlation between GFAP staining and Gly ($p=0.003$, c.c. $= -0.576$) but no significant correlation with mIns.

Vascularity and architecture of the tumours were tested for correlation with lactate but no significance was detected. Synaptophysin staining was also tested for correlation with NAA and NAA+NAAG but no significance was detected. It should be noted however that synaptophysin staining was not performed on 16 patients (could be assumed to be negative as not performed when not expected e.g. in glial tumours).

Table 1 Histopathological categories and respective number of patients (short TE studies)

Histopathological feature	Categories	Number of patients
Ki67	<1%	7
	1-2%	2
	4-10%	1
	>10%	14
	Not performed	3
Apoptosis	None	4
	Very low or low	10
	Moderate	7
	Moderate to high or high	6
Necrosis	Present	9 (1 very localised)
	Absent	18
Cellular Atypia	None	3
	Very low or low	8
	Low to moderate or low focally moderate or moderate	8
	High	8
Mitosis	None	7
	Very low or low	7
	Moderate	7
	High	5
	Indeterminate	1 (removed from analysis)
Lesional Neuronal Elements	None	13
	Focally PNET-like	3
	Neuronal Rosettes	4
	PNET-type	7
Entrapped Neuronal Elements	Present	3
	Absent	24
Neoplastic Glial Elements	None	10
	Focally or entrapped	2
	Predominantly neoplastic glial	15
Reactive Glial Elements	Present	15
	Absent	12
GFAP staining	Negative	2
	Very focal or reactive glial	6
	<10%	2
	10-50%	4
	>50%	11
	Not performed	2
Vascularity	Low	8
	Moderate	14
	High	3
	Indeterminate	2
Architecture	Solid	15
	Solid diffuse	6
	Solid occasionally microcystic or microcystic	3
	Half solid half cystic	3
Synaptophysin staining	Negative	1
	Scattered positive synapthophysin cells	1
	Focally positive	3
	Positive	6
	Not performed	16

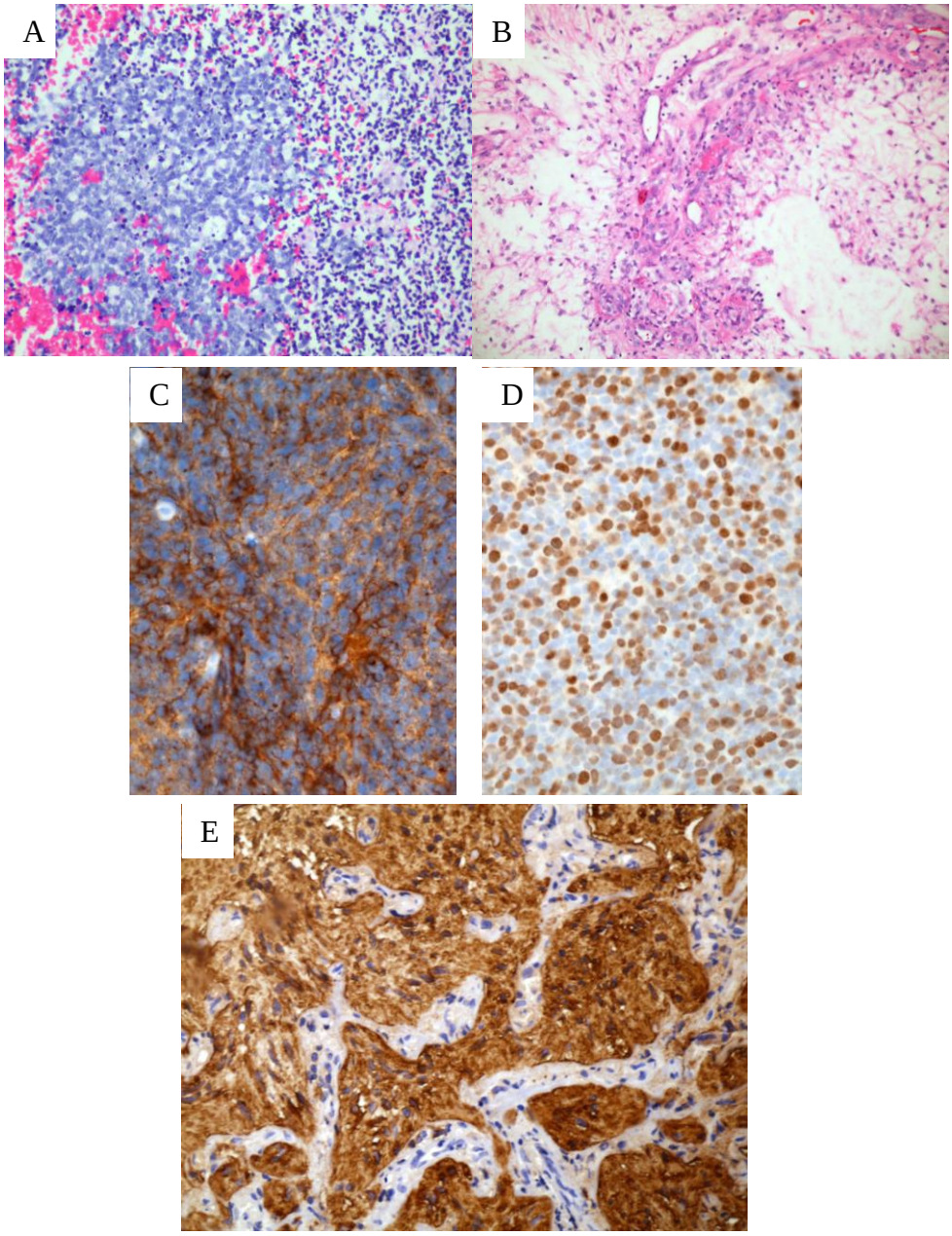

Fig.1 Representative microphotographs illustrating pathological parameters assessed semiquantitatively. A= Classical medulloblastoma (H&E, x40 original magnification) showing a high cellularity and high levels of apoptosis (*), B= Pilocytic astrocytoma (H&E, original magnification x20) showing a low cellularity, and a partly solid, partly cystic (*) architecture, C= Classical medulloblastoma with synaptophysin widely and strongly expressed in tumour cells D= Classical medulloblastoma with high Ki67 labeling (>50% positive), E= Pilocytic astrocytoma showing strong staining with GFAP

Table 2. Summary of statistically significant correlations between histopathological features and metabolites detected by ^{1}H MRS

Feature	Metabolite	Correlation/t-test	p-value
Ki67	PCh	+ve	0.031
Ki67	GPC+PCh	+ve	0.006
Apoptosis	Lip+MM at 0.9, 1.3, 2.0, 1.3/0.9 ppm	+ve	0.001, 0.003, 0.005, 0.001
Apoptosis	Tau	+ve	0.014
Necrosis	Long TE Lip+MM at 0.9, 1.3, 2.0 ppm	Higher - group with necrosis	0.002, 0.002, 0.004
Cellular atypia	PCh	+ve	0.013
Cellular atypia	GPC+PCh	+ve	0.014
Cellular atypia	Lip+MM at 0.9, 1.3, 2.0 ppm	+ve	0.023, 0.016, 0.002
Mitosis	PCh	+ve	0.004
Mitosis	Lip+MM at 0.9, 1.3, 2.0 ppm	+ve	0.006, 0.012, 0.001
Lesional neuronal elements	NAA, NAA+NAAG	-ve	<0.0001
Neoplastic glial elements	mIns	+ve	0.024
Neoplastic glial elements	Gly	-ve	0.001
Neoplastic glial elements	NAA, NAA+NAAG	+ve	<0.0001
GFAP	Gly	-ve	0.003

A

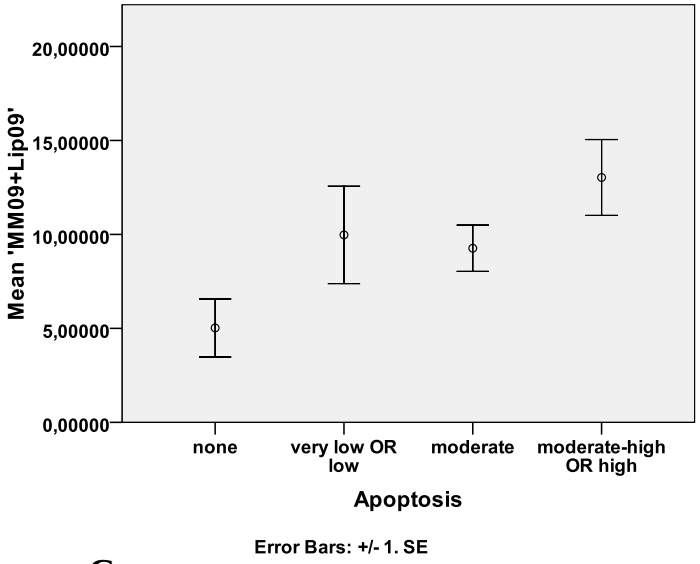
Mean 'MM09+Lip09'
20,00000
15,00000
10,00000
5,00000
0,00000
none
very low OR low
moderate
moderate-high OR high
Apoptosis
Error Bars: +/- 1. SE

B

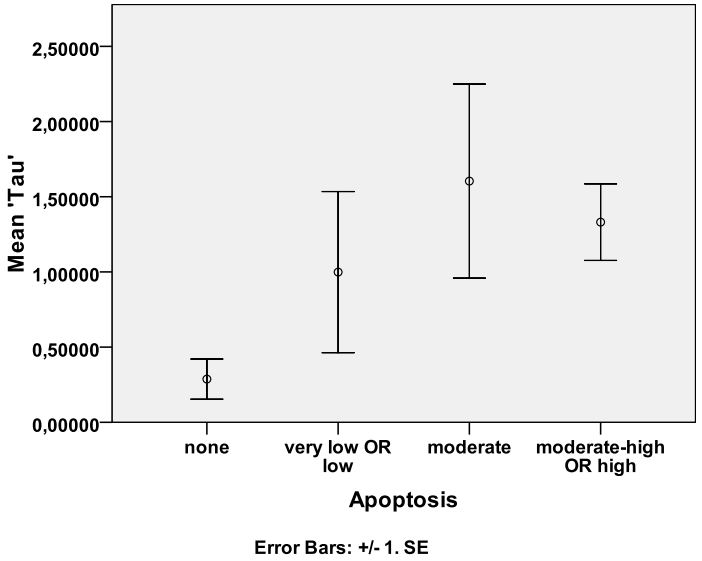
Mean 'Tau'
2,50000
2,00000
1,50000
1,00000
0,50000
0,00000
none
very low OR low
moderate
moderate-high OR high
Apoptosis
Error Bars: +/- 1. SE

C

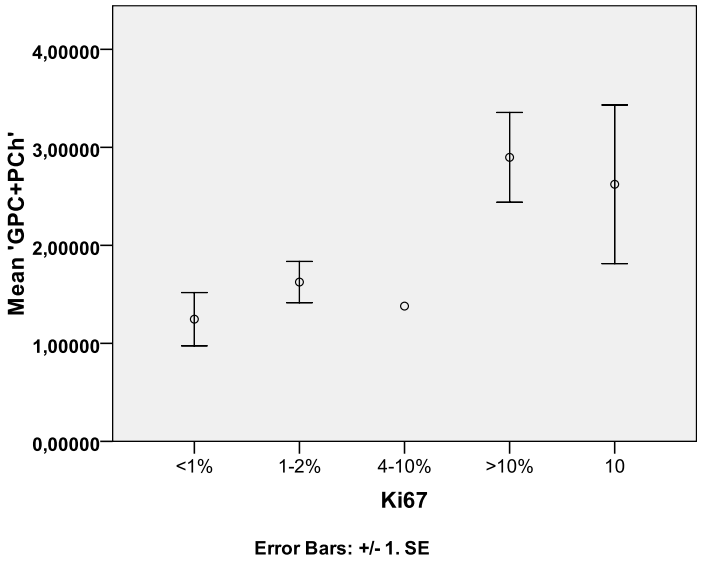
Mean 'GPC+PCh'
4,00000
3,00000
2,00000
1,00000
0,00000
<1%
1-2%
4-10%
>10%
10
Ki67
Error Bars: +/- 1. SE

D

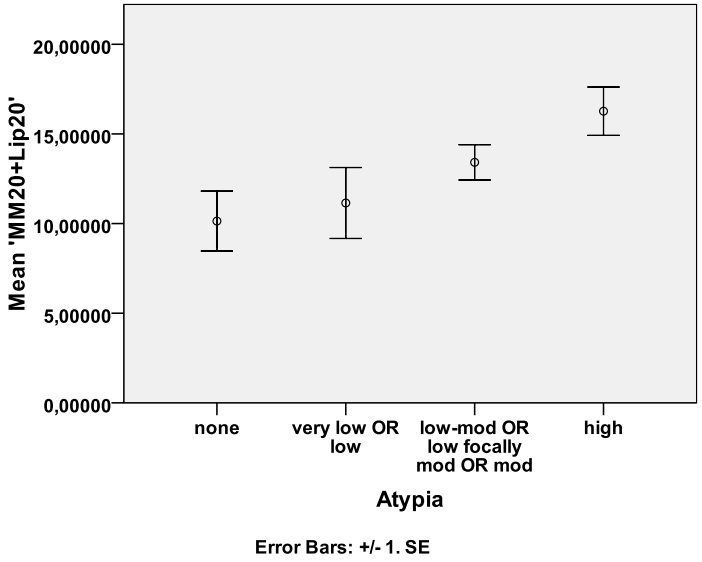
Mean 'MM20+Lip20'
20,00000
15,00000
10,00000
5,00000
0,00000
none
very low OR low
low-mod OR low focally mod OR mod
high
Atypia
Error Bars: +/- 1. SE

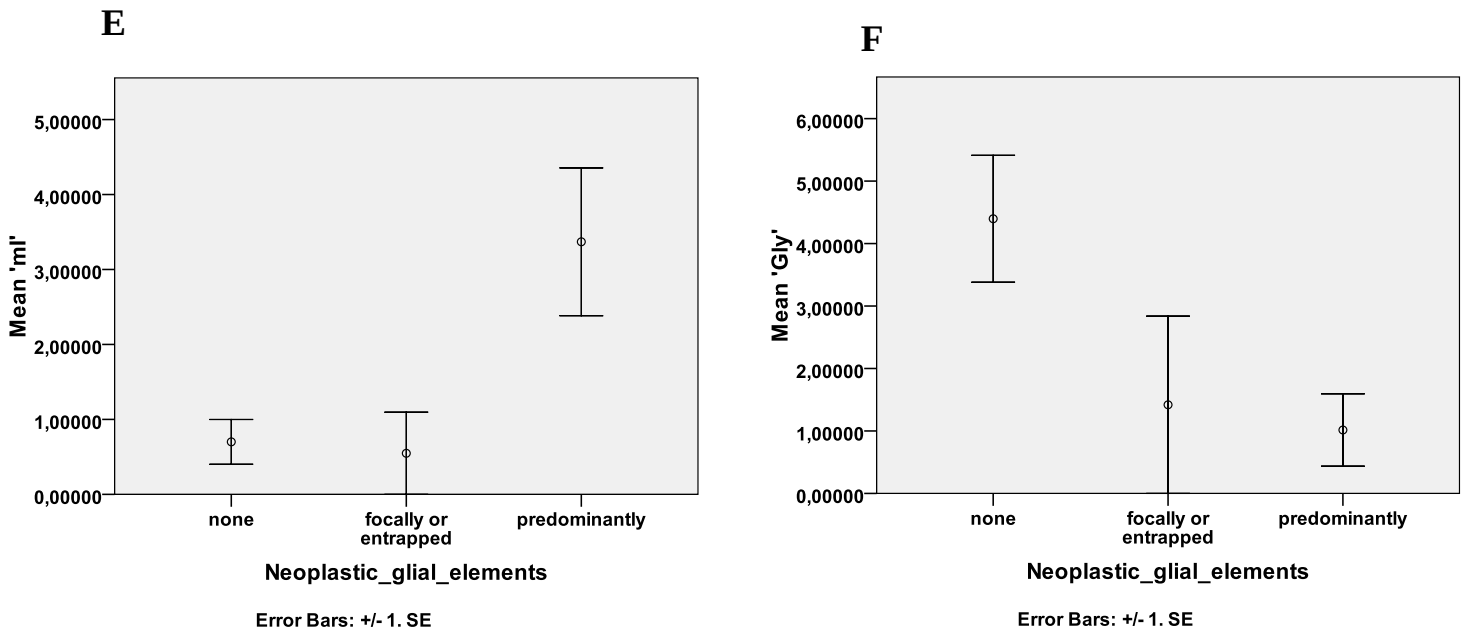

Fig.2 Scatter plots of A) Mean concentration value for MM09+Lip09 vs Apoptosis, B) Mean concentration value for Tau vs apoptosis, C) Mean concentration value for GPC+PCh vs Ki67, D) Mean concentration value for MM20+Lip20 vs Atypia, E) Mean concentration value for mI vs Neoplastic glial elements, F) Mean concentration value for Gly vs Neoplastic glial elements. Error bars represent +/- 1 standard error

Mean= mean concentration value, MM09+Lip09=lipids and macromolecules at 0.9ppm, Tau=taurine, GPC=glycerophosphocholine, PCh=phosphocholine, MM20+Lip20= lipids and macromolecules at 2.0ppm, mI=myo-inositol, Gly=glycine

Mean concentration values are in “institutional units” (referenced to water unsuppressed spectrum - described in Chapter 3).

6.4. DISCUSSION

^{1}H MRS has seen increasing use over the last years as a non-invasive tool for the characterization and monitoring of brain tumours. Although many studies have reported the relationship between metabolites and diagnostic groups, tumour aggressiveness and prognosis, few have addressed the relationship with histopathological features routinely assessed after biopsy or resection. This study has investigated the correlations between metabolites detected by in vivo ^{1}H MRS and histological features such as apoptosis, necrosis, mitosis, atypia, glial and neuronal components and found important relationships. It should be noted, however, that there was no confirmation that the region biopsied corresponded to the exact location of the ^{1}H MRS voxel. Ki67 positively correlates with choline, as does atypia and mitosis. Apoptosis correlates with lipids detected at short echo time, whereas necrosis correlates with lipids at long echo time. Furthermore, relationships relating to glial and neuronal tumour components have been established, such as the inverse correlation of neuronal components with NAA, a quite surprising result, and the positive correlation of mIns with glial elements.

Choline is involved in membrane synthesis and reflects membrane turnover, and Cho elevation has been attributed to rapid cellular proliferation, as a result of increased mitosis, leading to an abnormal increase in metabolism and the destruction of cells (112, 119, 120, 134). In a study by Nafe et al., nuclear density of grade II-IV gliomas was found to correlate positively with total choline at long TE,

and the proliferation index Ki-67 correlated positively with the lipid peak at 0.9ppm (119). Ki-67 did not correlate with the total choline peak in that study, as well as in the study by Gupta et al. (long TE MRSI of adult glioma patients measuring normalized choline)(135), but other studies found a positive correlation, which agrees with the results of this study (positive correlation between PCh and Ki67 and GPC+PCh and Ki67); Tamiya et al.(112) found a positive correlation between total choline/Cr ratio and Ki67 and a negative correlation between NAA/Cho and Ki67 (15-68 years old, grade II-IV astrocytomas); Shimizu et al.(58) found a positive correlation between total choline measured semiquantitatively at long echo time MRS and Ki-67 in the homogeneous adult gliomas but not the heterogeneous ones; and Peet et al. found a positive correlation between total choline at short TE and Ki67 in medulloblastomas (65).

A significant positive correlation was also found between Tau, lipids at 0.9, 1.3, 2.0, 1.3/0.9ppm and apoptosis. Apoptosis is an active process of programmed cell death (124). Some characteristics of apoptosis include cell shrinkage, fragmentation and condensation of nuclear material and cytoplasm vacuolization (124, 136). MAS and histopathological analysis performed by Opstad et al. found taurine to significantly correlate with apoptotic cell density in necrotic and non-necrotic biopsies (137). In a study by Moran et al. a model of apoptotic death in cultured cerebellar granule neurons was used, and the basal release of [3H] taurine from cells started to increase after 3 days up to a maximum at 5 days. At 5 days, the cell morphology of the neurons displayed characteristics of apoptosis,

including marked soma shrinkage (124). This was preceded by caspase induction and chromatin condensation, which are apoptotic death markers (124). However, the nuclear pool of taurine could also be contributing to the decrease in cell volume (124). Lang et al (125) loaded Jurkat human T-lymphocytes with [3H]taurine and induced apoptotic cell death by triggering the Fas(CD95) receptor with monoclonal crosslinking antibody. This led to a release of taurine of 60% of cellular taurine in 90 min. The release coincided and presumably contributed to the cell shrinkage typical of apoptotic death, and preceded DNA fragmentation.

Lipids detected by MR spectroscopy have been linked to necrosis or apoptosis (28, 123). Tzika et al. showed microscopic necrosis in 11 paediatric patients with low total choline and high lipid and/or lactate signal with MRSI at an echo time (TE) of 65ms, and the spectra were assumed to correspond to areas of high neoplastic potential (28). Tzika et al. suggested that choline and lipid mapping have value in tumour grading of glial tumours (123). In another study, paediatric high-grade tumours were distinguished from low-grade ones using normalized choline and lipids from MRSI, with high-grade tumours having significantly higher choline and lipids. Also, lipid peaks positively correlated to percent necrosis (16). Astrakas et al. showed normalized choline and lipids and/or lactate at 1.3ppm to be independent predictors of tumour grade (higher in high-grade tumours) (74). Furthermore, the importance of lipids and choline in the assessment of paediatric brain tumours is emphasized in the work by Marcus et al., which showed that choline, lipids and/or lactate (L), choline/NAA and choline+0.1L were significantly

higher in non-survivors compared to survivors, and cho+0.1L was the only independent predictor of survival(81).

Blankenberg et al. found a directly proportional relationship between the ratio of the methylene (CH2) resonance at 1.3ppm to the methyl (CH3) resonance at 0.9ppm and the percentage of apoptotic lymphoblasts in doxorubicin-treated Jurkat T-cell acute lymphoblastic leukaemia cultures in vitro (122). Hakumaki et al have investigated early biochemical and biophysical events taking place during GCV-induced apoptosis of experimental gliomas (BT4C gliomas in rats), and found an association with accumulation of polyunsaturated fatty acids (PUFAs) detected by ^{1}H MRS in vivo at an echo time of 20ms (121).

In vivo ^{1}H MRS detected lipids are associated with tumour aggression and Opstad et al.(138) studied adult human astrocytoma biopsy samples with magic angle spinning ^{1}H MRS at TE=50ms and suggested that the ~1.3ppm lipid signal correlated strongly with the number of Nile Red-stained lipid droplets and the formation of lipid droplets precedes necrosis. In a study by Zoula et al. of C6 rat glioma, the mobile lipid signal at 1.3ppm at TE=136ms was suggested to arise mainly from lipid droplets in necrosis (139). In humans, this mobile lipid signal has been observed mainly on NMR spectra of necrotic brain tumour biopsies(139, 140) and in metastasis (129) and high grade gliomas (141). However, our results did not show a significant difference between lipids or lactate in necrotic and non-necrotic

tumours, possibly due to the small numbers especially in the necrotic group (n=8). Another explanation is that lipids detected at short echo times relate to apoptosis and those detected at long echo times to necrosis. To investigate this, the long TE spectra of the patients in the study were analysed where available (N=8). Interestingly, lipids at 0.9, 1.3 and 2.0 ppm were significantly higher in patients where necrosis was present. Apoptosis did not correlate with long TE lipids.

Other histological features studied included atypia and mitosis, and both were found to have significant correlations with PCh and lipids at 0.9, 1.3 and 2.0ppm (atypia also correlated with total choline). This may have been expected as choline and lipids are known to be higher in more aggressive tumours (16, 81), and a high degree of atypia and mitosis are also features of aggressiveness.

There are several metabolites detected by ^{1}H MRS in paediatric brain tumours in vivo which are involved in energy metabolism, and interest in these has been increasing. Molecular imaging has seen great advances in recent years (18F-FDG PET, SPECT, MRS) and research into the activation of certain oncogenes and alterations of cellular metabolism has been expanding (126). One of the cellular metabolism alterations that features prominently in current research is increased aerobic glycolysis or the «Warburg effect» (126, 127). During glycolysis, pyruvate is converted to lactate and alanine (in different ratios depending on organ type). Golman et al. showed significantly higher lactate in implanted P22 tumours in rats compared to normal tissue, after injection of hyperpolarized 13C-pyruvate (127).

Spectroscopic studies have shown elevated lactate in the brain in conditions such as ischaemia (142) and brain tumours (129). Lactate has been suggested as an indicator of tumour metabolic activity in rat gliomas (128), but others do not agree (65, 129). Our results did not find a correlation between lactate and necrosis or vascularity. It should also be noted that lactate is found in cysts, and Chang et al. showed that lactate is observed in a variety of intracranial cysts and there tends to be a higher lactate peak in high-grade gliomas (130). In this study, tumour architecture did not correlate with lactate.

Another question we attempted to address at a preliminary level in this work has been the origin of NAA, a matter of much controversy which has been studied extensively so far. It is especially pertinent when looking at pilocytic astrocytomas, as they normally show relatively high levels of NAA, even when no normal brain is contained within the voxel and there is a debate as to whether it arises from the tumour itself or from surrounding entrapped normal brain. Looking at the histology slides, we found a significant positive correlation between NAA and neoplastic glial elements and a significant negative correlation between NAA and lesional neuronal elements. This result suggests that the NAA seen in pilocytic astrocytomas may actually arise from the tumour itself, and previous observations in our lab also suggest that the NAA seen cannot be explained by voxel contamination. Lazareff et al. (67) also observed NAA in paediatric low grade astrocytomas that could not be explained by partial volume effects. O-2A progenitors which contain NAA (143) are primitive bipotential cells which can give rise to oligodendrocytes or type-2

astrocytes, and some low grade astrocytomas express antigens consistent with type-2 astrocytic lineage (144).

Myo-inositol has been found to correlate positively and Gly negatively with neoplastic glial elements. This is as expected as mIns is known to be relatively high in glial tumours (astrocyte 'marker' (91)) and glycine is known to be higher in high grade tumours (75). In our study, the glial tumours were mainly low grade. This also explains the negative correlation between glycine and GFAP staining. mIns was not found to correlate with GFAP, although they are both considered to be gliosis markers, and this agrees with the results of another study by Oz et al. (145), who studied GFAP levels in CSF of patients with spinocerebellar ataxia type 1 and their relationship to metabolites from different brain locations (TE=5ms, 4T). However, they found that the patients with the highest GFAP level had the highest mIns level in the vermis, which we did not observe in our results.

6.5. CONCLUSION

In summary, we have addressed all the principal histological features routinely assessed by histopathologists in the diagnostic process and found spectroscopic correlates for most, providing additional evidence for the use of in vivo ^{1}H MRS as a non-invasive characterization tool in paediatric brain tumours.

CHAPTER 7

PRELIMINARY STUDY OF IN VITRO NMR SPECTROSCOPY OF PAEDIATRIC PILOCYTIC ASTROCYTOMA CELL LINES

CHAPTER 7

PRELIMINARY STUDY OF IN VITRO NMR SPECTROSCOPY OF PAEDIATRIC PILOCYTIC ASTROCYTOMA CELL LINES

7.1. INTRODUCTION

Data presented earlier on suggests the presence of NAA in low grade gliomas, not explained by partial volume effects. This is in agreement with the observations of Lazareff et al.(67), and combined with the controversy in the literature surrounding the origins and functions of this amino acid, a preliminary study to investigate this was designed. This pilocytic astrocytoma cell line study also aims at describing the ^{1}H MR spectroscopic profile of the cells lines at a high magnetic field, and investigating the ability to detect subtle differences in tumour cells originating from histologically identical samples.

N-acetyl-L-aspartate (NAA) is an amino acid that is present in the vertebrate brain (146). It is synthesized and stored primarily in neurons, but cannot be hydrolysed in these cells. Neuronal NAA is dynamic with a turnover of more than once per day, via extracellular fluids between neurons (anabolic compartment) and oligodendrocytes (catabolic compartment) (146). Oligodendrocyte amidohydrolase II hydrolyzes NAA liberated from neurons into aspartate and acetate (amidohydrolase I activity in astrocytes also has a minor role) (146). Aspartate gets recycled back to form new NAA, and most of the acetate gets taken up and

metabolised by oligodendrocytes and astrocytes and lost from the NAA cycle(146). Other sources of brain NAA are mast cells, astrocytes, microglia, CSF, and the intravascular compartment, all of which (including ECF and oligodendrocytes) comprise a negligible component of NAA under normal conditions (146). It is a major brain metabolite which is being increasingly used in clinical and experimental MRS studies as a putative neuronal/axonal marker (132, 147).

Abnormalities of NAA resonance intensity have been found in various cerebral disorders, from brain tumours to stroke, inborn genetic abnormalities and neurodegenerative disorders including multiple sclerosis (143, 147). However, to interpret the changes in NAA seen in vivo, its cell type specific localization and function need to be known (132, 143). A lot of work has been done on this metabolite, and it has been suggested that it may be a specific constituent of neurons in the mammalian brain (132, 143) and is synthesized by mitochondria (132). Experiments have involved causing damage to neurons and observing the decrease in NAA (143), immunocytochemical studies using antibodies to NAA showing that it was discretely localized in a substantial number of neurons throughout the rat CNS (although many neurons remained unstained (148, 149))(132, 143). Additional evidence to support the neuronal localization of NAA has come from its absence in cultured cortical astrocytes (143), its undetectable or very low levels in meningiomas and astroglial tumours and its relative abundance in medulloblastomas (132, 143). NAA has therefore been thought of as a marker of neuronal loss or viability (132, 143).

However, NAA has been reported to decrease reversibly in various disorders, suggesting that the initial decrease was not due to neuronal or axonal loss. Examples of spontaneous or treatment-related reversibility in NAA decrease include multiple sclerosis, mitochondrial diseases, acquired immunodeficiency syndrome, temporal lobe epilepsy and amyotrophic lateral sclerosis (147). Temporal studies of multiple sclerosis and mitochondrial encephalopathy with lactic acidosis and stroke like episodes and hypothyroidism have shown reversible changes in NAA in vivo (132). These changes are related with an underlying pathology which involved a dysfunction of myelination. It is therefore paradoxical to consider NAA to be neuron-specific whilst in the early stages of disease there is preservation of relatively normal grey matter but degeneration of myelin (132). Thus, the possibility of a contribution to the NAA signal by oligodendrocytes is raised (responsible for myelination of neurons in the CNS) (132). Other explanations have been proposed in conditions where there is reversible loss of NAA, including axonal recovery after an insult to the neuron which does not destroy it completely, consolidation of surviving brain tissue after neuronal death in cortical atrophy, presence of other metabolites with spectra resonances in the same region, fluctuations due to osmolarity since NAA is a reversible cerebral osmolyte, and slow NAA resynthesis (91).

In addition, although NAA is accepted as a marker of neuronal viability, its presence in other major cell types in not completely unexpected. It has been shown in rat brain extracts to increase rapidly to adult levels from day 10 to 20 of

life, which is the time of active myelination in this animal (132). Human foetal and child brains also show an increase in NAA at a time when myelination is at its maximum. The neuronal cell density in the cerebral cortex decreases with dendritic maturation, therefore an increase in NAA with age may reflect a contribution from cells other than neurones (132). Furthermore, experimental work using isolated nonsynaptic brain mitochondria has shown that partial inhibition of the mitochondrial respiratory chain results in partial decrease in NAA synthesis, meaning that an impairment of mitochondrial function may contribute to a decrease in NAA without cell death (132).

Urenjak et al. found NAA in cultures of purified neurons, O-2A progenitors (higher than in cerebellar granule neurons) and immature oligodendrocytes, but not mature oligodendrocytes, purified meningeal cells or purified cortical astrocytes (from neonatal rats) (143). Therefore, at least in the developing brain, there is a possibility that a major contribution of NAA comes from oligodendrocyte precursors rather than being solely due to neuronal populations (143). However, it would seem paradoxical that immature oligodendrocytes have less NAA and mature oligodendrocytes none compared to O-2A progenitors, if NAA is involved in myelination. An explanation for this by Urenjak et al. is that lipid synthesis is so extensive that it depletes newly produced NAA in oligodendrocytes (143).However, more recently, studies on oligodendrocyte biology revealed the requirement for ciliary neurotrophic factor (CNTF) to promote the generation, maturation and survival of oligodendrocytes in vitro. Bhakoo and Pearce used this new cell

cultivation procedure (cells from 7-day old rats) and found that mature oligodendrocytes actually do express NAA in vitro (132). Bhakko and Pearce (132) found NAA in the O-2A progenitors although less than previously published data, and in immature (similar levels) and mature olidendrocytes (both in CNTF-treated and untreated cells, higher in treated). The levels of NAA in mature oligodendrocytes were comparable to those seen in various neuronal cultures (cerebellar granule neurons, cortical neurons, dorsal root ganglion neurons). However, it is uncertain whether these NAA levels are the same in the individual cell types in vivo. The number of live oligodendrocytes was significantly lower in the untreated culture, but this does not account for the absence of NAA in the study by Urenjak et al (143), although NAA in untreated cultures was less.

The function(s) of NAA remain unclear and there have been many proposed roles for it (132). The possibility that it donates acetyl groups for lipid synthesis and especially myelination is interesting when combined with the results from studies showing NAA in oligodendrocyte precursors and oligodendrocytes (132, 143). Other proposed roles range from the metabolism of specific brain fatty acids to ion balance and neuromodulation, regulator of protein synthesis, and storage from of acetyl-CoA or aspartate (132, 147). Baslow suggests that NAA may have several functions in the CNS, but of particular importance is its osmoregulatory role, and in this it may be the primary mechanism for the removal if intracellular water from myelinated neurons, against a water gradient (146). An interesting finding is that the NAA metabolic system may not be required for brain function at all, and

neurons can form synaptic connections without it and oligodendrocytes can still produce myelin and form a sheath around axons in its absence (146). The macroscopic concentration of NAA depends on the fluxes of synthetic and degradation pathways, cellular density and brain water content and distribution (147). A decrease in NAA could be due to an increase in extracellular water or CSF content in the voxel (can be corrected during analysis). Even when tissue NAA content is reduced and is attributed to neuronal or axonal dysfunction or loss, it is not known whether this is due to an irreversible loss of cells or a potentially reversible metabolic process (147).

Care is needed when extrapolating in vitro cellular data to in vivo and to human brains, as many factors such as cell-cell interactions cannot be mimicked in culture (132). Also, quantitative conclusions about NAA in the intact brain are difficult to draw from the work of Urenjak et al. (143) as the cerebellar granule cells were cultured from 7-dat old rats (prior to the rapid increase in NAA), and also the proportions of the various cell types in vivo are unknown. If the proportion of O-2A progenitors and immature oligodendrocytes is very small, then NAA may be a useful neuronal marker as that would be the major source of it. In addition, there are many similarities between O-2A progenitors and neurons, although they are two functionally very distinct cell types (143).

Additional evidence for the presence of NAA in non-neuronal cells comes from the study of Canavan's syndrome, a rare autosomal recessive leukodystrophy that

affects newborn infant and young children (132). There is a deficiency of N-acetylaspartoacylase, which cleaves NAA to acetate and aspartate and is therefore the only disease where NAA increases. This disease involved spongy degeneration of white matter due to vacuolation and demyelination, but no abnormality of neurons (132). The increase in NAA is clearly not due to an increase in neuronal density (147).

This study aims to investigate whether ^{1}H NMR of three paediatric pilocytic astrocytoma cell lines, one from a 'typical' tumour, one from a metastatic tumour at presentation and one from a recurrence, can detect differences between them, even though the tumours are histologically identical. Furthermore, the presence or absence of NAA in these cell line spectra will be investigated, to provide some preliminary evidence as to its origins in in vivo ^{1}H MRS of paediatric pilocytic astrocytomas.

7.2. METHODS

7.2.1. Cell Culture

Three cell lines were used in this work, namely PA1, PA3R and PA7. PA1 was derived from a paediatric pilocytic astrocytoma which was metastatic at presentation (age=2 yrs, cerebellar), PA3R from a recurrence of a paediatric pilocytic astrocytoma (age=2yrs, cerebellar), and PA7 from a 'typical' paediatric pilocytic astrocytoma (age=7 yrs, thalamic). The cells were cultured using standard

protocol in Dulbecco's Modified Eagle Medium (D-MEM) (low glucose), which contained 1000 mg/L glucose, 4mM L-glutamine and 110 mg/L sodium pyruvate and 15% FBS (PAA, UK).

7.2.2. Cell harvest

The cells were harvested at a confluence of about 90% and 24 hours after a final medium change. The flask to be harvested was washed 3x with cold PBS and the cells scraped off into a cryovial. This was centrifuged at 250g for 6min+brake, the supernatant was discarded and the cryovial dropped in liquid Nitrogen prior to storage at -80°C. The time from removing the flask from the incubator and dropping the cryovial into liquid Nitrogen did not exceed 15 min.

7.2.3. Whole cell sample preparation

The cells were thawed, 600µl D2O was added to resuspend the cell pellets, followed by grinding the sample approximately 80 times on ice. This was transferred to an eppendorf and stored at -80°C.

7.2.4. Extraction

20-40 million cells were used for each Nuclear Magnetic Resonance (NMR) spectroscopy sample. The cells were thawed, 85µl of ice cold distilled water and

400µl of ice cold methanol were added. The mixture was grinded approximately 80 times in a glass grinder on ice, transferred into a 1.5ml eppendorf tube and put on ice, then sonicated at a tune value of 8 (power=5W) for 10-15s (Misonix, USA). Following this, 200µl ice cold distilled water and 200µl ice cold distilled chloroform were added and the sample vortexed at high speed for 10-20s. The sample was placed on ice and put on a shaker for 20-30min at 20rpm, then centrifuged in a cold centrifuge at 2000g for 5 min at 4°C (Hettich Zentrifugen, Germany). The upper water phase and the lower chloroform phase were put into new separate eppendorfs (e1, e2), leaving the protein (middle phase) in the original eppendorf (e3). 200µl of ice cold chloroform was added to the upper water phase (e1) and the protein (e3) and these were vortexed for 10-20s and then centrifuged as before. The upper phase of each was transferred to a new eppendorf (e4) and the lower phase of each to e2. The protein was left in e3 and stored at -80°C. The water phase was split into two equal amounts (e4 and e5) and vacuum centrifuged (Eppendorf Concentrator 5301, Germany) to dry, then transferred to -80°C for storage. The organic phase was left in a fume hood overnight to dry and then transferred to -80°C for storage.

7.2.5. NMR sample preparation

7.2.5.1. Whole Cells

5µl of 10mM TMSP was added to the sample which was then vortexed for 10s and transferred to a Norsell s600 NMR tube.

7.2.5.2. Extracts- Water sample

600µl of D_2O was added to the sample (half of sample in eppendorf e4), which was then vortexed for 10s and combined with the sample in e5. 5µl of 10mM TMSP was added as a reference compound and the sample vortexed for 10s, then the sample was transferred to an NMR tube and spun manually.

7.2.6. NMR protocol

There were 4 repeats for PA1 and PA3R and 3 repeats for PA7 extracts. 1 repeat of PA1 was removed from the analysis as it was contaminated. 3 repeats were collected for each cell line for whole cell NMR.

A Varian 600-MHz (14.1 T) vertical bore spectrometer using an HCN probe was used to record the ^1H NMR spectra of cell extracts and whole cells suspended in D_2O. The probe temperature was set to 20°C. Tuning and matching and presaturation pulse frequency were optimized for each sample. A standard pulse and acquire sequence was used, consisting of a single 90° pulse preceded by one second of water presaturation. The acquisition was of 16K complex points at a sampling frequency of 7200Hz. The number of scans used varied according to the signal-to-noise ratio of each sample (256-1024).

Spectral processing and Principal Component Analysis were performed by Dr. Martin Wilson. TARQUIN (150) software was used for processing the in vitro spectra.

7.3. RESULTS

The three paediatric pilocytic astrocytoma cell lines were grown successfully, and microphotographs of cells in culture from each cell line are shown in Fig.1. Whole cell NMR and cell extract NMR of the 3 cell lines showed reproducible results and no NAA in any of the samples. Interestingly, we observed a resonance at 1.9ppm which has been assigned to acetate in all the samples. MAS of pilocytic astrocytomas (performed previously in our lab, results not shown (113, 151)) also showed acetate and very little NAA believed to arise from normal brain in the biopsies. Fig.2 shows spectra obtained with each method (A= 'typical' pilocytic astrocytoma cell extract NMR, B='typical' pilocytic astrocytoma whole cell NMR). In addition, we have shown that 3 cell lines of the same tumour type (1 'typical', 1 recurrence and 1 metastatic at presentation) can be discriminated very well using NMR and principal components analysis. PC2 vs. PC1 plots of the cell extract and whole cell data are shown in Fig.3. The whole cell data was both the easiest to collect and the most reproducible.

A.

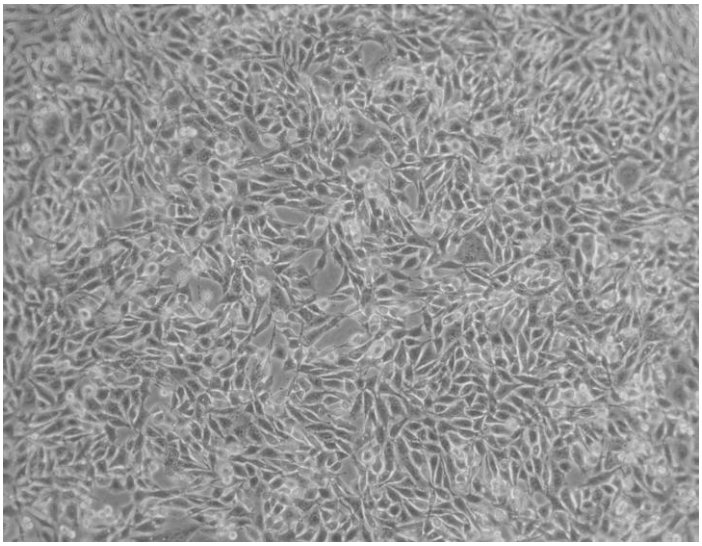

B.

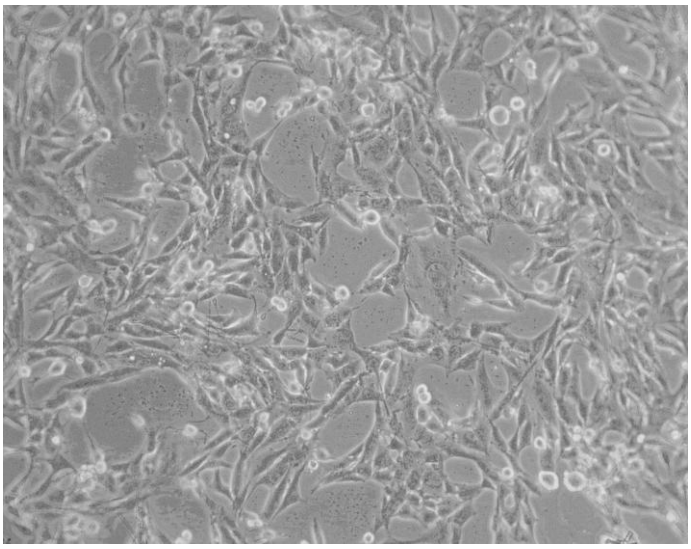

C.

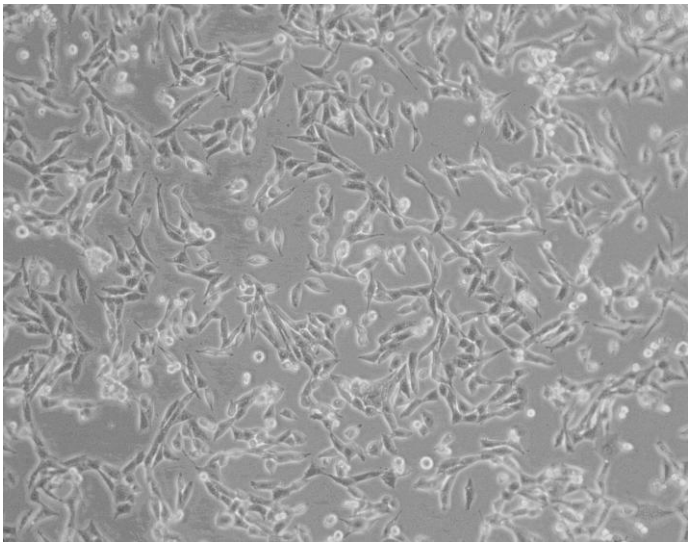

Fig.1 Microphotographs of cells in culture A. PA1, paediatric pilocytic astrocytoma metastatic at presentation cell line, passage 15, magnification x10; B. PA3R, recurrence of a paediatric pilocytic astrocytoma cell line, passage 19, magnification x10; C. PA7, 'typical' paediatric pilocytic astrocytoma cell line, passage 8, magnification x10

A

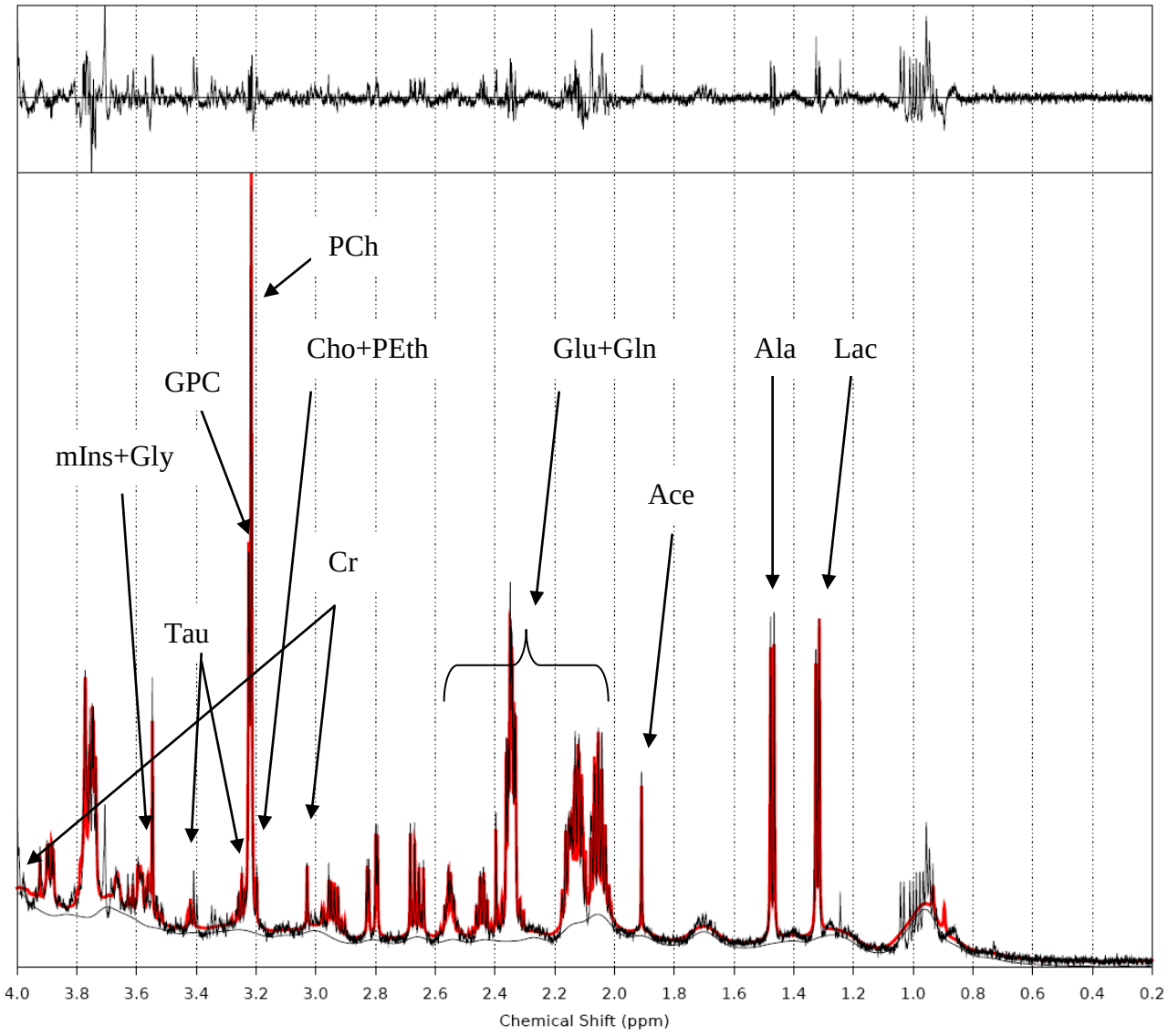
PCh
Cho+PEth
Glu+Gln
Ala
Lac
GPC
mIns+Gly
Ace
Cr
Tau
4.0
3.8
3.6
3.4
3.2
3.0
2.8
2.6
2.4
2.2
2.0
1.8
1.6
1.4
1.2
1.0
0.8
0.6
0.4
0.2
Chemical Shift (ppm)

B

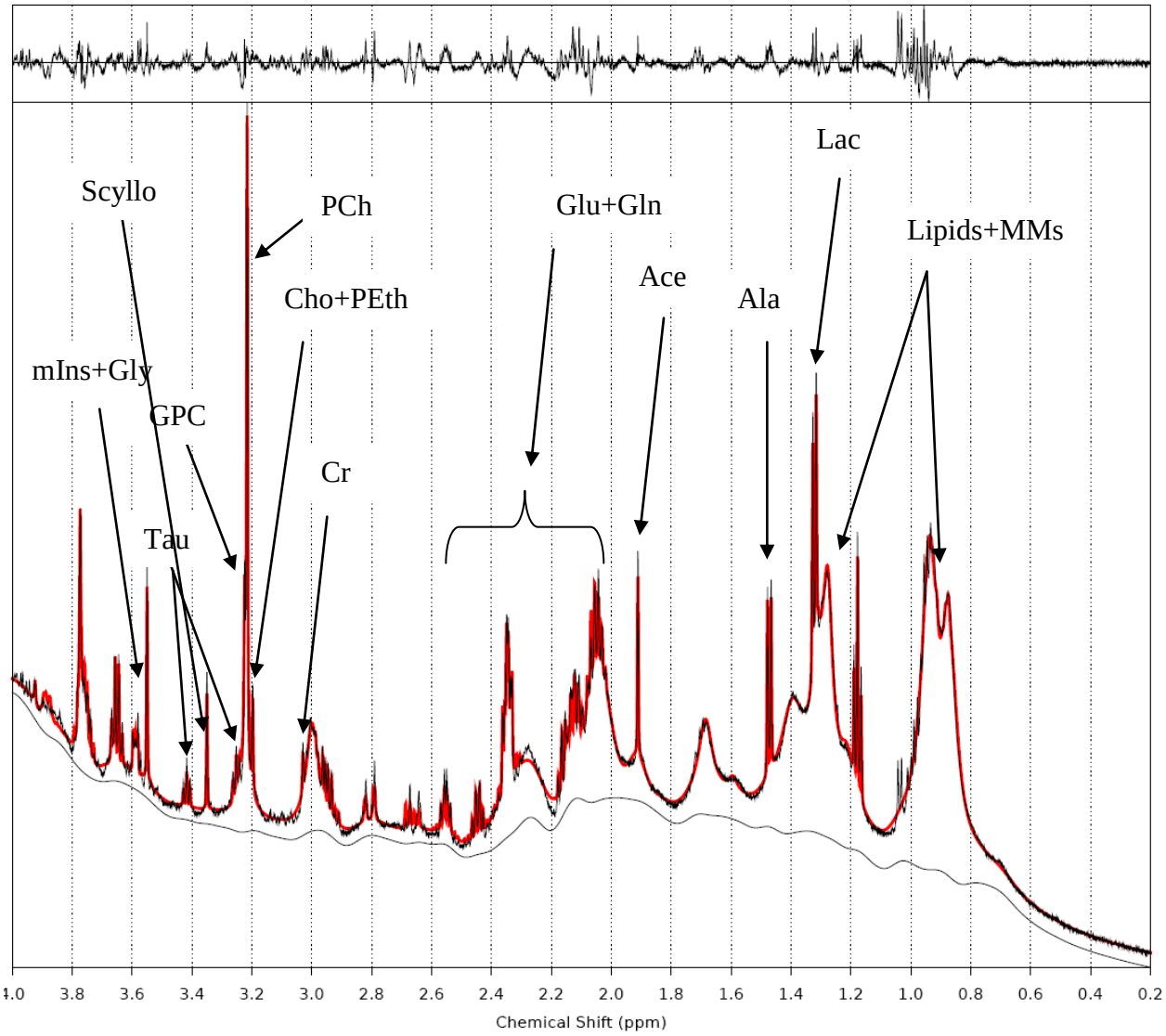

Fig.2 NMR Spectra of 'typical' paediatric pilocytic astrocytoma cell line. A. Water phase extract B. Whole cell sample

Ace= acetate, Ala= alanine, Cho=free choline, Cr= creatine, Gln=glutamine, Glu=glutamate, Gly=glycine, GPC=glycerophosphocholine, Lac=lactate, mIns=myo-inositol, MMs= macromolecules, PCh=phosphocholine, PEth=phosphoehtanolamine, Scyllo= scyllo-inositol, Tau=taurine

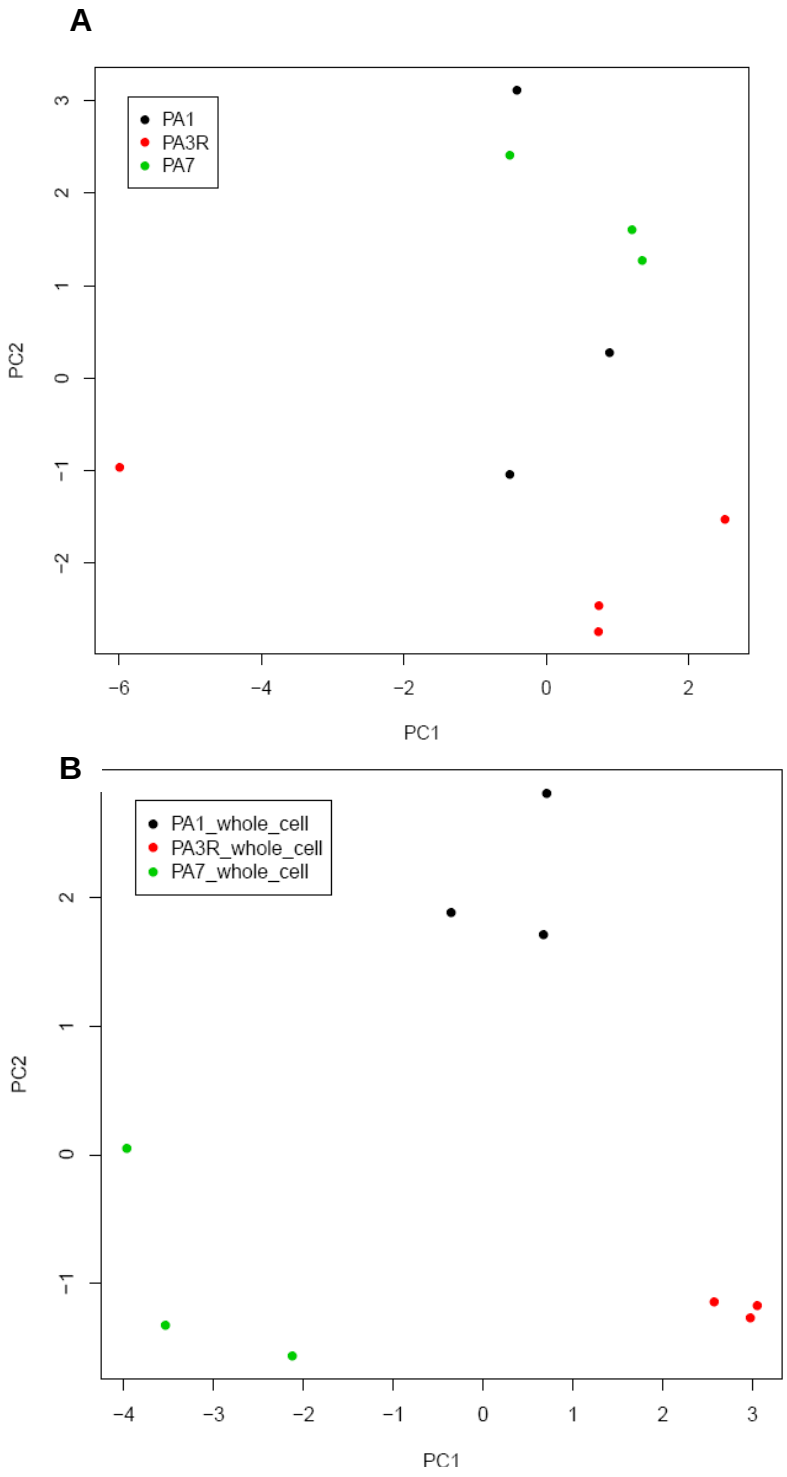

Fig.3 Plots of Principal Component (PC) 2 vs. PC1 from a Principal Component Analysis (PCA) of the NMR spectra from the 3 paediatric astrocytoma cell lines A. Water phase extract spectra B. Whole cell spectra. PA1= paediatric pilocytic astrocytoma metastatic at presentation, PA3R= recurrence of a paediatric pilocytic astrocytoma, PA7= 'typical' paediatric pilocytic astrocytoma

7.4. DISCUSSION

This study demonstrates that ^{1}H NMR has the ability to detect subtle differences and discriminate between three paediatric pilocytic astrocytoma cell lines ('typical', metastatic and recurrence). The in vitro ^{1}H NMR spectra of the pilocytic astrocytoma cell lines demonstrate the characteristic features of pilocytic astrocytomas in vivo. There is a very low Cr, relatively high Cho and myoinositol, and lipids (in whole cells) and lactate can be detected. It is of note that in contrast to pilocytic astrocytomas in vivo, there tends to be more PCh than GPC in the in vitro spectra; this is also the case in metastatic astrocytomas in vivo. Furthermore, we have shown that there is no NAA in these cell lines, which if present, would explain the presence of the NAA seen in vivo in these tumours, thus raising the possibility that the singlet at 2.02ppm in vivo is due to another molecule. However, further work is needed to clarify the origins of NAA seen in vivo in paediatric pilocytic astrocytomas.

The spectra from the cultured cells have shown essentially no NAA in any pilocytic astrocytomas, but significant amounts of acetate (singlet at 1.9ppm). Therefore, our hypothesis is that the resonance around 2.0ppm in pilocytic astrocytomas arises from acetate (or acetate plus NAA when normal brain is contained within the voxel), but it cannot at present be resolved in in vivo MRS at 1.5T. This may provide a better biomarker for pilocytic astrocytomas, but further work is needed. Acetate is a simple molecule with a single CH_3 group which gives a singlet at

1.9ppm (152). It may be an artifact of sample preparation (152), however it was present in the whole cell NMR samples as well, meaning that this is probably not the case in our work. It has been observed to be higher in brain tumours (152). An interesting point is that it gets shifted downfield at lower pH (152), which may make it even more difficult to observe in in vivo MRS as it merges with the resonance from NAA and lipids at around 2.0ppm. This is of particular interest in pilocytic astrocytomas, as they often contain significant amounts of lactate, which may indicate a more acidotic state.

7.5. CONCLUSION

In conclusion, it has been shown that ^{1}H NMR has the ability to detect differences between cells from histologically identical tumours, providing further evidence for its use in characterization and prognostication of paediatric brain tumours, as one of the tumours was metastatic at presentation and the other was a recurrence. Furthermore, from this preliminary work, it is suggested that the resonance assigned to NAA in in vivo ^{1}H MRS in pilocytic astrocytomas may actually correspond to a different molecule, acetate being a possibility. However, the acetate present in the cell lines could be a result of the culturing and harvesting process, and needs further investigation.

CHAPTER 8

MAGNETIC RESONANCE SPECTROSCOPIC IMAGING-CLINICAL CASE STUDIES

CHAPTER 8

MAGNETIC RESONANCE SPECTROSCOPIC IMAGING- CLINICAL CASE STUDIES

8.1. Case Study 1

The following case study demonstrates the value of ^{1}H Magnetic Resonance Spectroscopic Imaging (MRSI) in the assessment of large heterogeneous lesions with areas demonstrating varying aggressiveness and potential for progression.

The patient is a girl who presented at the age of 4 years with a reduced use of the right hand. An MRI in March 2008 revealed a left thalamic lesion going contralateral and extending into deep white matter of the left cerebral hemisphere. After stereotactic biopsy from the middle of the left thalamic lesion (most hyperintense part of lesion on T2-weighted MRI), a diagnosis of diffuse fibrillary astrocytoma WHO grade II was made. Single voxel ^{1}H Magnetic Resonance Spectroscopy (MRS) of the left thalamic lesion pre-treatment, shown in Fig.1, showed decrease N-acetyl-aspartate (NAA) and Creatine (Cr) at 2.02 and 3.0ppm respectively, and increased glycerophosophocholine+phosphocholine (Cho) at 3.2ppm, myo-inositol (mIns) at 3.6ppm and lipids+macromolecules, suggestive of a tumour, although not entirely typical of diffuse astrocytomas on qualitative review (Cho and NAA expected to be higher). However, the possibility of a different histology in the area in the left cerebral hemisphere was raised (MR image in

Fig.2). Short Echo Time (TE, 30ms) MRSI performed in May 2008, showed Cho to be increased more in the area in the left cerebral hemisphere adjacent to the biopsied lesion, rather than at the site of the biopsied lesion, and mIns to be higher in the left thalamic lesion. The Cho and mIns maps, co-registered on the MR images, are shown in Fig.3. Care should always be taken when interpreting chemical shift imaging (CSI) metabolite maps since they are prone to artifacts. One property of the PRESS CSI method, known as the chemical shift artifact, leads to the displacement of the localisation volume for each metabolite depending on their chemical shift. In MRSI, the volume of interest is excited (subject to chemical shift displacement) but then phase encoding is used as a separate means of signal localization (negligible chemical shift displacement). Thus, the voxels around the outer edge of the volume of interest can suffer from chemical shift displacement artifacts (93). At 1.5T the size of the chemical shift artifact is usually small by comparison with the nominal voxel size, and the region of abnormality is sufficiently large in the case presented that the findings should not be greatly affected by this problem (93). Furthermore, the metabolite maps in this case were predictive of disease progression demonstrating their utility. Individual spectra from the MRSI grid, representative of the 2 areas under discussion, are shown in Fig.4. High choline has been shown to be a bad prognostic indicator (78-80). Castillo et al. (57) found a trend toward higher mIns/Cr in low-grade cerebral astrocytomas compared to anaplastic astrocytomas and glioblastoma multiforme in a study of short echo time ^{1}H MRS in children and adults.

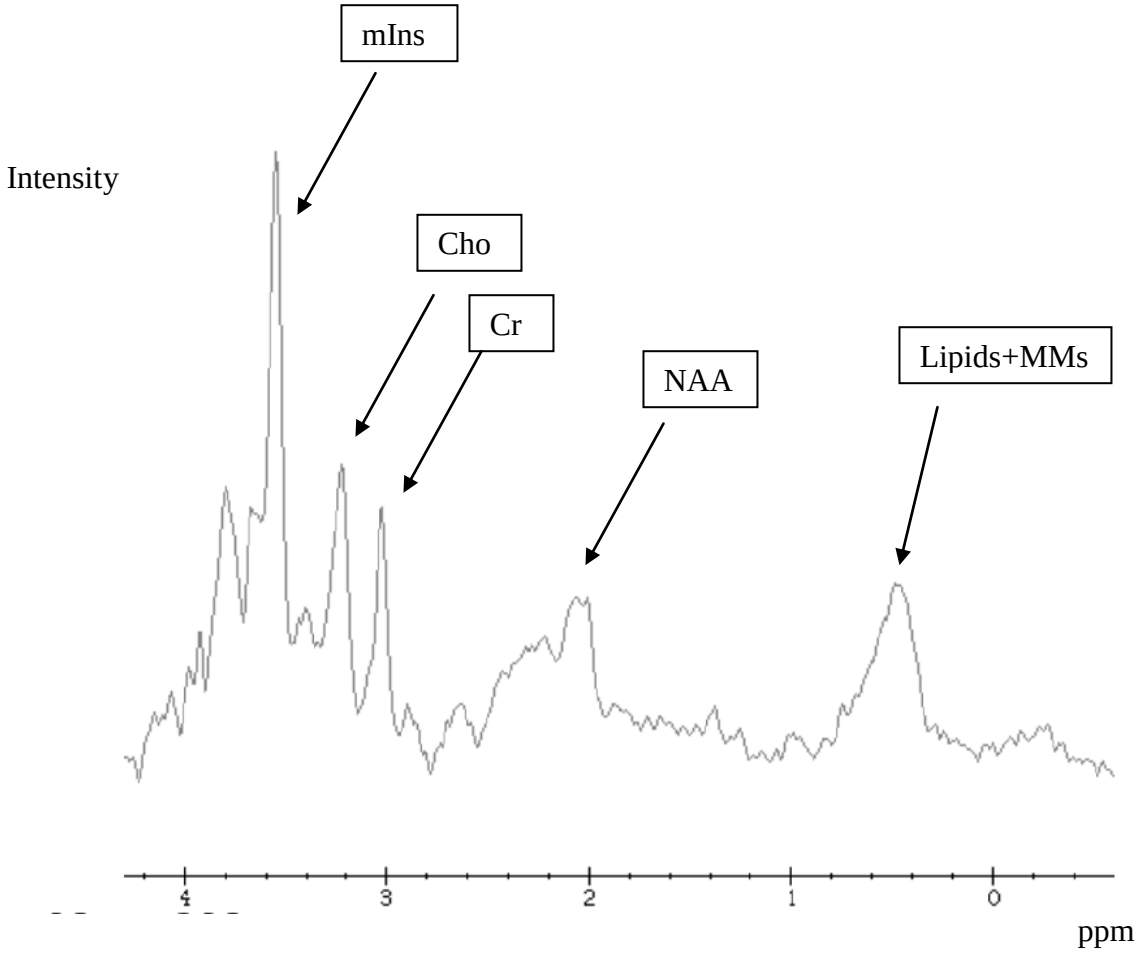

Fig.1 Pre-treatment MRS of left thalamic lesion. NAA= N-acetyl-aspartate, Cr= Creatine, Cho=choline (glycerophosophocholine+phosphocholine), mIns= myo-inositol, MMs= macromolecules

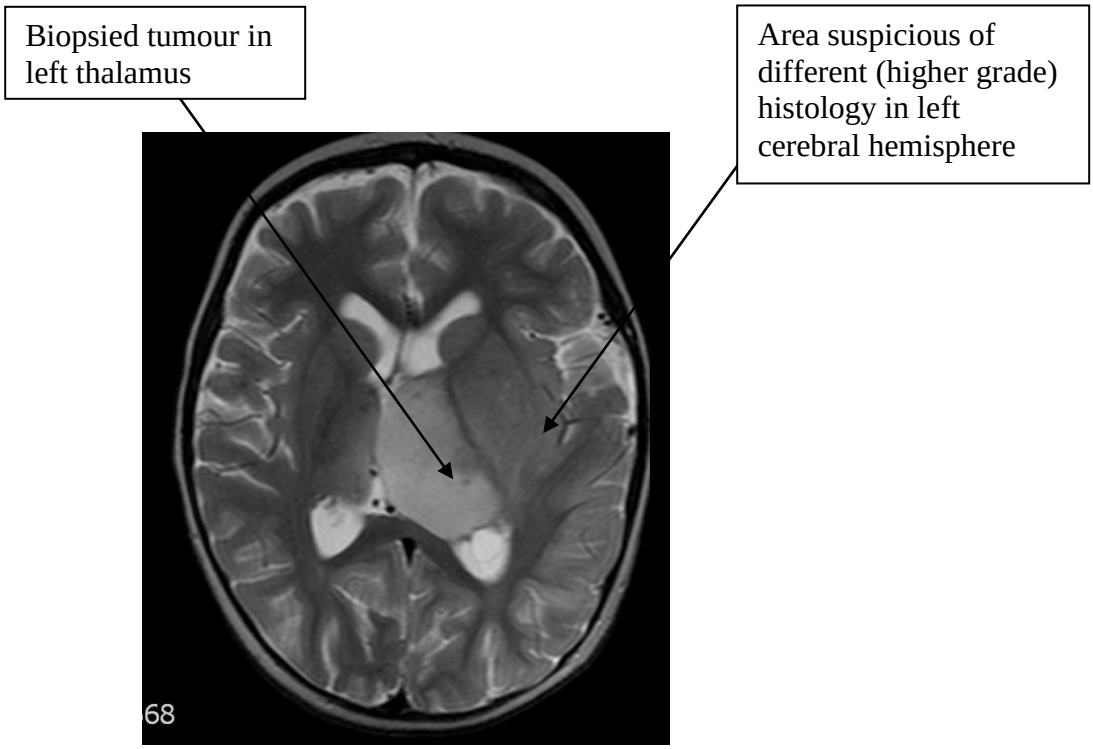

Fig.2 T2-weighted MR image of tumour

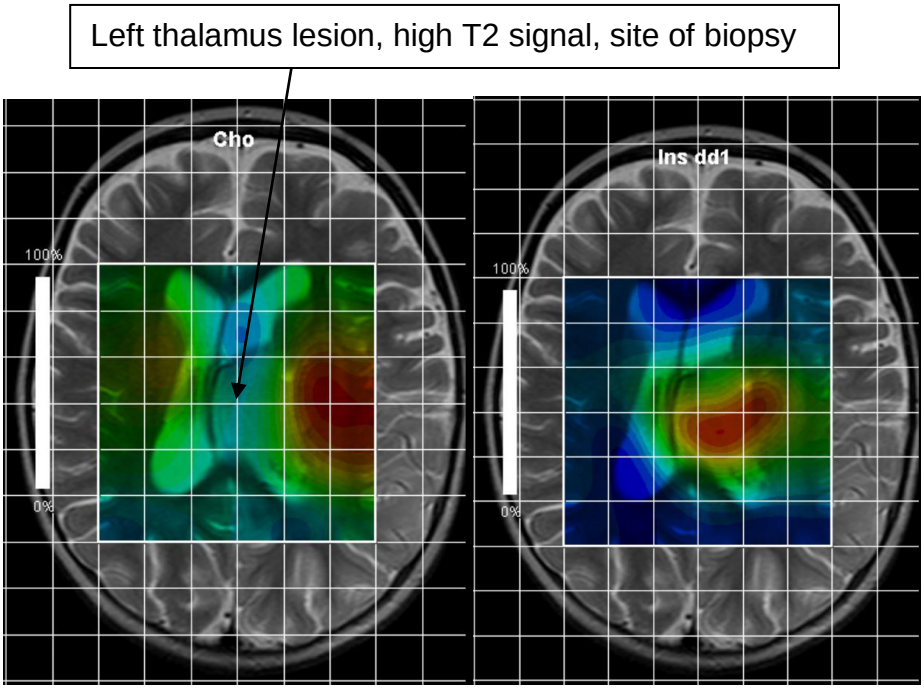

Fig.3 LEFT Choline (Cho) map, showing the highest level of Cho in the left cerebral hemisphere (red). RIGHT Myo-inositol (mIns) map, showing the highest level of mIns in the left thalamus (red).

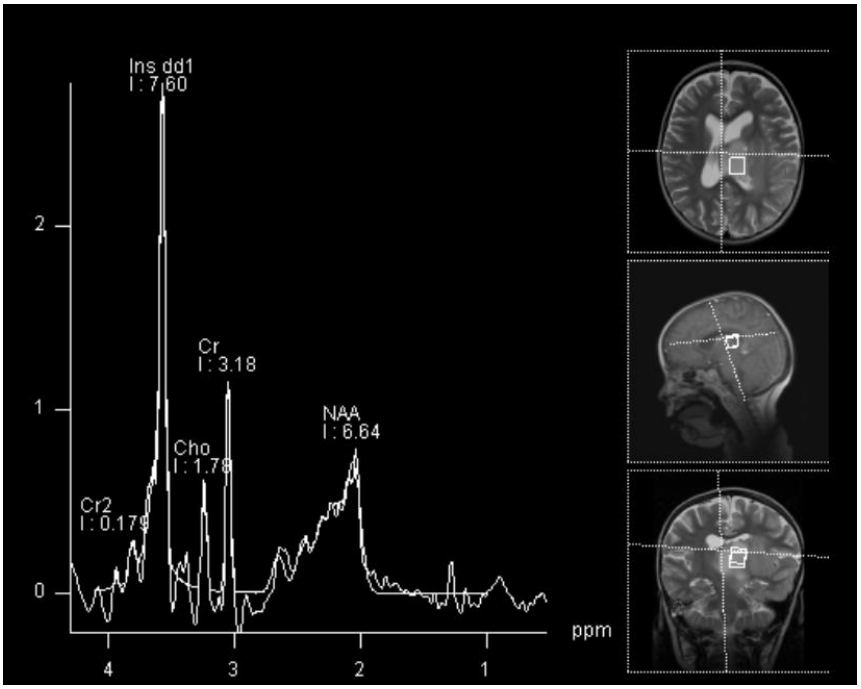

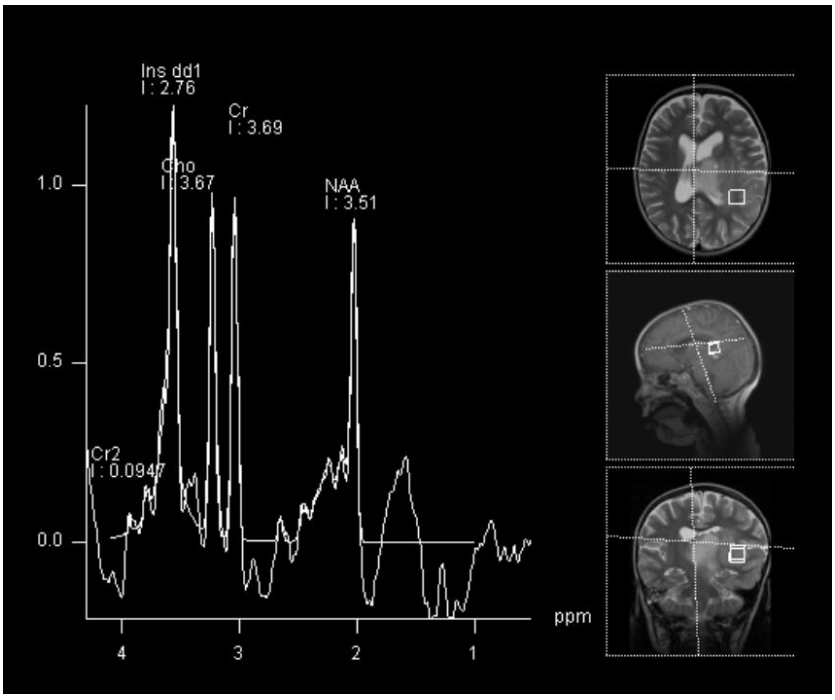

Fig.4 MRSI spectra from the left thalamus (biopsied tumour) (ABOVE) and the adjacent left cerebral area of possible higher grade part of the lesion (BELOW). Ins=myo-inositol, Cho=choline, Cr=creatine, NAA=N-Acetylaspartate

Treatment with chemotherapy as randomised on LGG2 protocol (vincristine and carboplatin) with careful monitoring was started (April 2008). In September 2008, the MRI suggested tumour infiltration of the left hemisphere with possible progression. As there was also significant toxicity from chemotherapy, second line treatment with radiotherapy was undertaken, followed by an increase in tumour size and a subsequent improvement. In October 2009, the MRI showed diffuse disease progression in the left hemisphere, and treatment on oral temozolomide was started. After two courses, there was further disease progression, but as the patient was neurologically stable, treatment was continued. Further disease progression was seen on MRI in April 2010, and oral etoposide was started. Clinical progression was confirmed in June 2010, and end of life palliative care started. The patient died in September 2010.

Although a biopsy of the lesion in the left cerebral hemisphere was not performed, this area behaved in a more aggressive manner compared to the biopsied left thalamic lesion. The MRSI findings in this case were predictive of the worse prognosis of this lesion, as higher choline and lower mIns were found compared to the biopsied diffuse astrocytoma. If this finding is validated in large studies, it could provide tumour biopsy guidance and/or be a predictor of progression.

8.2. Case Study 2

The following case demonstrates the value of MRSI in complex lesions which make single voxel spectroscopy (SVS) difficult, due to for example bleeding as in this case. MRSI can investigate many smaller voxels around the lesion, and still provide useful information, especially when the biopsy sample is small and the diagnosis difficult to make as in this case.

This boy presented at 5 years of age, with a history of Neurofibromatosis type I (NF1) and progressive weakness of the left leg, then arm and face over a few weeks. An MRI showed a right thalamic lesion most consistent with low grade glioma, and an optic chiasm glioma. Single voxel short TE MRS performed at the time was difficult to interpret as there was only a small part of solid tumour in the voxel (Fig.5). However, it is interesting to note that on MRS the tumour looked like a pilocytic astrocytoma but the mIns was low as in patients without NF1 (Cr high as in patients with NF1). Furthermore, high mIns has been shown to be an indicator of good prognosis and this patient did not respond to treatment.

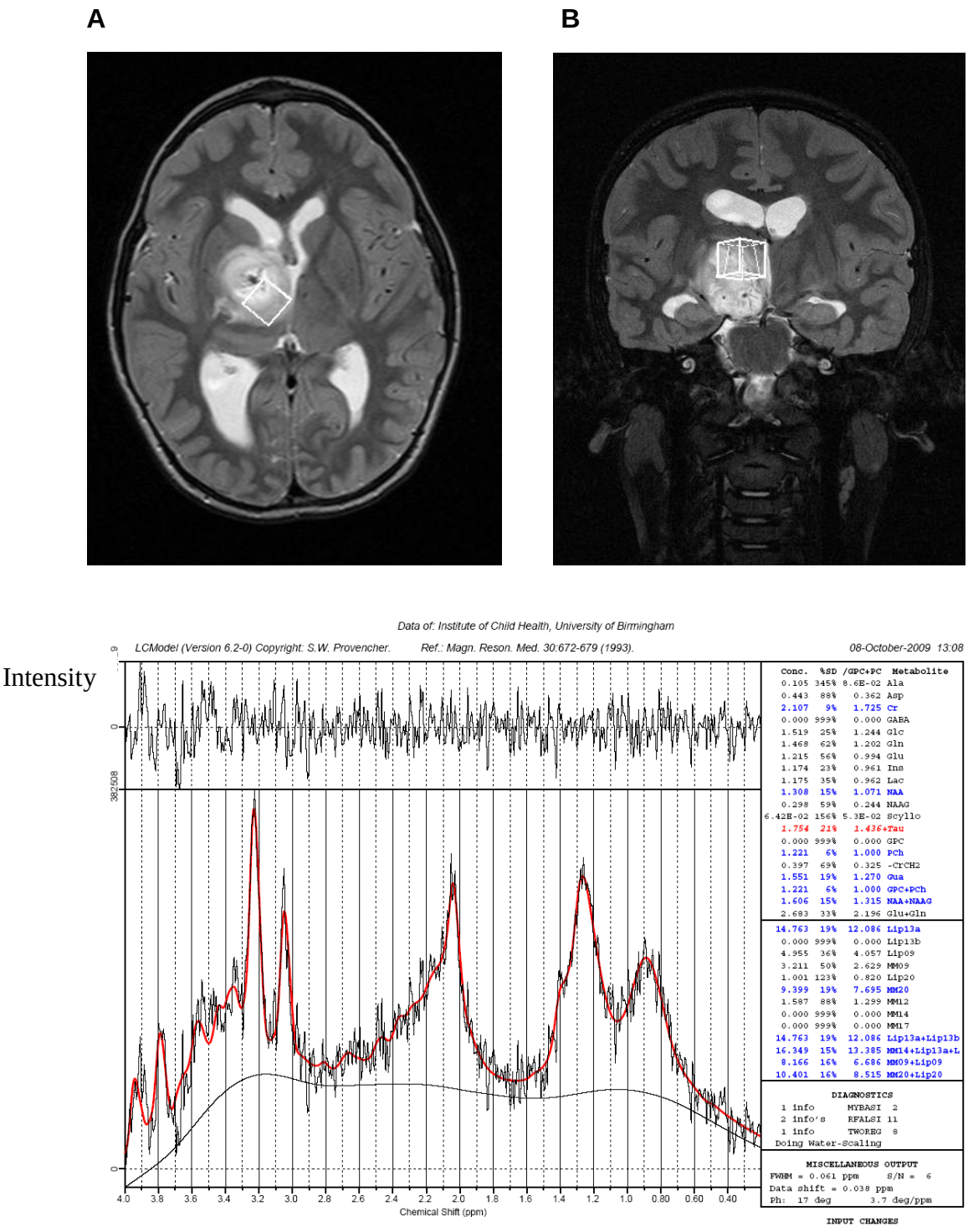

Fig.5 Short TE Single Voxel Spectroscopy of right thalamic Lesion; Voxel placement- A= axial view, B= coronal view. C= Spectrum

After open image guided biopsy in January 2009, the diagnosis of a low grade astrocytoma, likely pilocytic astrocytoma was made. Post-operatively there was an intratumoural bleed. Tissue availability for diagnosis was limited, but the diagnosis of low grade glioma was sufficiently firm, and no further specimens were needed, and resective surgery would present a significant risk. Treatment under the SIOP-LGG2 protocol (9) was started with chemotherapy (carboplatin and vincristine).

In June 2009 there was worsening left sided weakness and an MRI scan was performed. The weakness was attributed mainly to vincristine toxicity. The tumour had decreased in size overall, particularly the cystic element, and was thought indicative of chemotherapy response. The decision to continue on the reduced dose of vincristine he was already on was made. Single voxel MRS (Fig.6) was not helpful due to the bleed and the close proximity of the voxel to bone, which resulted in a bad quality spectrum.

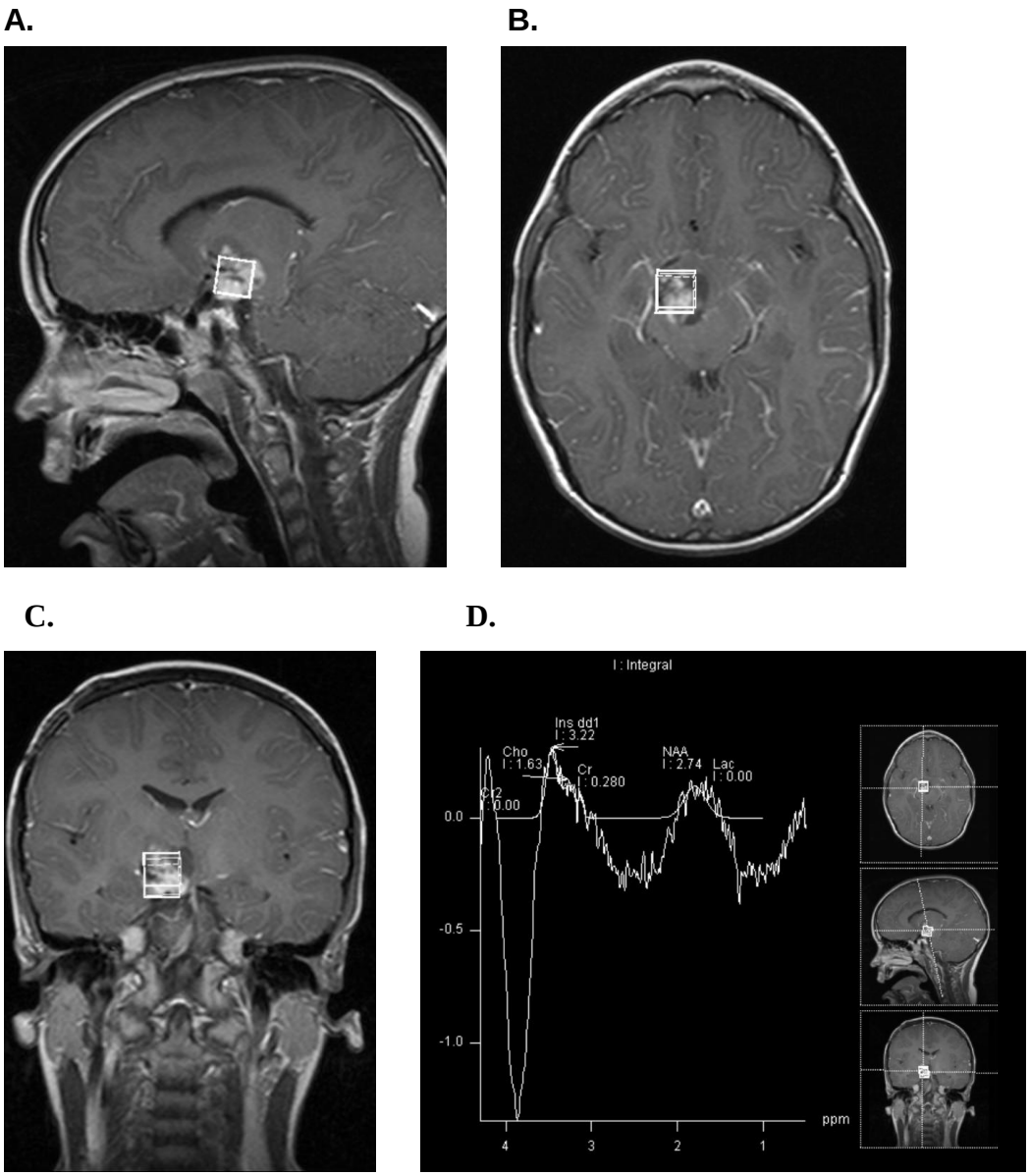

Fig.6 Single voxel MRS June 2009. Voxel placement, A.=sagittal view, B= axial view, C=coronal view. D. Uninterpretable spectrum due to intratumoural bleed and voxel's proximity to bone. Ins=myo-inositol, Cho=choline, Cr=creatine, NAA=N-Acetylaspartate

In August 2009, an MRI scan showed that the residual solid/cystic tumour had increased in size by more than 25% in all planes (mainly but not exclusively the cystic component), and this was considered to represent disease progression. Therapy was changed to vinblastine, and 6 weeks into this treatment the patient developed worsening morning headaches and vomiting. MRI in November 2009 showed marked hydrocephalus related to an increase in size of one of the cystic areas of the tumour (size of solid tumour being stable). The hydrocephalus was drained and a VP shunt inserted, and treatment continued as there was no evidence of failure. MRI in February 2010 showed the cysts to be much smaller and the solid component of the tumour slightly larger on the transverse measurement. This could have been due to the lack of the prior mass effect from the cysts, and the overall size of the solid component was unchanged. Vinblastine was continued. Short echo time CSI (Fig.7) with smaller voxels (10mm grid) was reassuring, because although some spectra were uninterpretable due to the bleed, spectra around the bleed were indicative of pilocytic astrocytoma.

A.

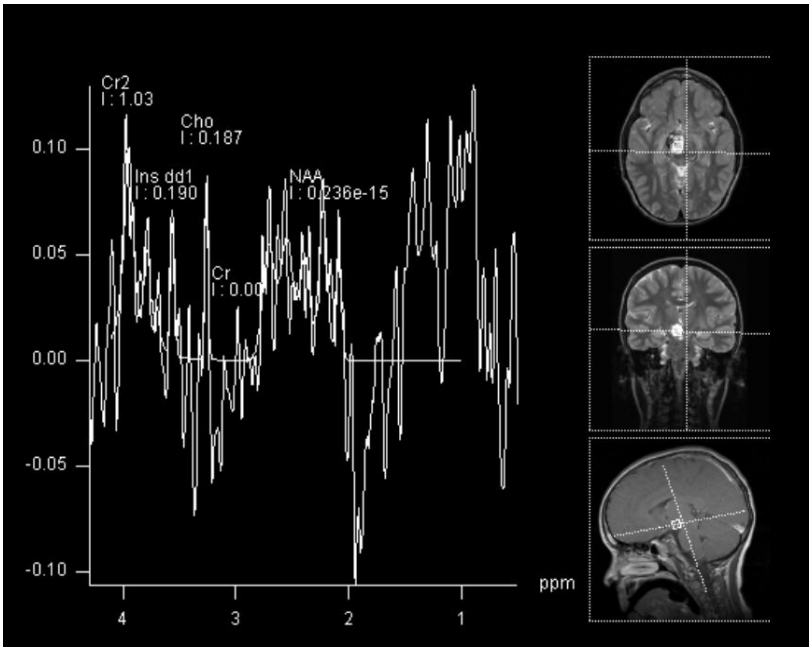

B.

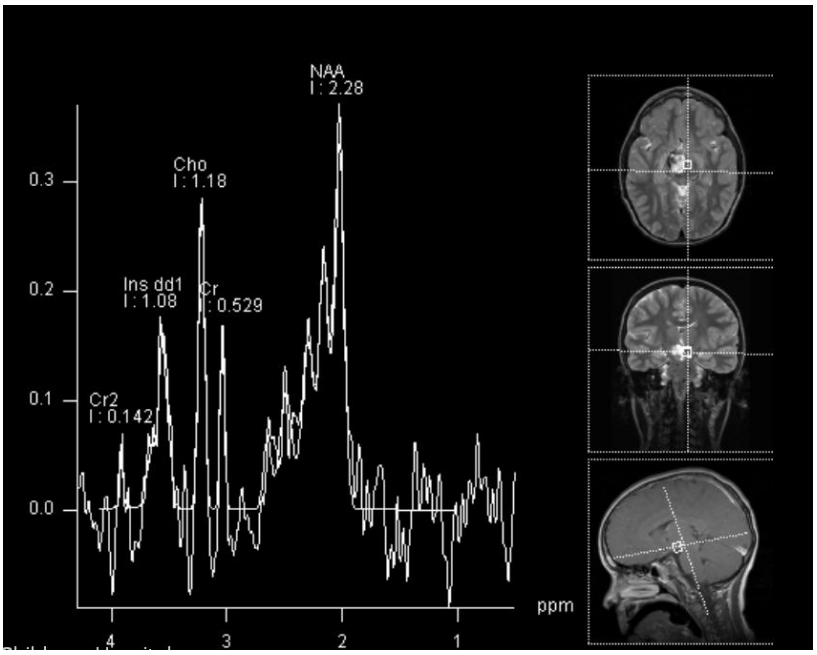

Fig.7 Magnetic Resonance Spectroscopic Imaging Study. A. Bad quality spectrum due to intratumoural bleed/voxel location near bone. B. Better quality spectrum adjacent to the bleed, indicative of a pilocytic astrocytoma.

In July 2010, the patient was stable and well and MRI showed a small (about 2mm) increase in the size of the enhancing solid tumour with no change in the cyst. The decision was to observe and treat when symptoms occur and/or scan appearances dictate, as any other treatment would be third line.

In Nov 2010, there was a small increase in size of enhancing tumour, and the patient was observed. In January 2011 there was subtle worsening of the left sided weakness, and MRI showed a further slight increase in the solid/cystic mass in the right thalamus/midbrain. Treatment with chemotherapy (actinomycin and vincristine) was started.

8.3. CONCLUSION

The first case has demonstrated the use of MRSI in non-invasively assessing large heterogeneous lesions, where areas of different malignancy may be present. The second case demonstrated the value of having smaller voxels in MRSI compared to SVS, which can be used to assess specific tumour areas, such as around a bleed, and aid in the diagnosis of challenging tumours which do not respond to treatment.

CHAPTER 9

TEXTURE ANALYSIS OF T1- AND T2-WEIGHTED MAGNETIC RESONANCE IMAGES AND PROBABILISTIC NEURAL NETWORK TO DISCRIMINATE POSTERIOR FOSSA TUMOURS IN CHILDREN

CHAPTER 9

TEXTURE ANALYSIS OF T1- AND T2-WEIGHTED MAGNETIC RESONANCE IMAGES AND PROBABILISTIC NEURAL NETWORK TO DISCRIMINATE POSTERIOR FOSSA TUMOURS IN CHILDREN

9.1. INTRODUCTION

MRS has been shown to provide additional information for the diagnosis and prognosis of paediatric low grade gliomas, and can be performed at the same time as conventional MR imaging. Conventional MR imaging is collected on all cases of paediatric brain tumours, and is usually assessed qualitatively; quantitative analysis is rarely undertaken. However, there is a potential wealth of information not visible to the human eye which can be extracted from MR images and quantified using texture analysis techniques. This may yield additional information to characterize paediatric brain tumours, provide new insights on the characteristic features, and enable the combination of MRI and MRS data.

In this study, texture analysis for the diagnosis of paediatric posterior fossa tumours has been employed. Posterior fossa tumours are studied here as they are relatively common and usually biopsied, therefore providing a useful test-bed for the technique. The commonest posterior fossa tumours are pilocytic astrocytomas (grade 1), medulloblastomas (grade 4), and ependymomas (grade 2 or 3) (7). Although posterior fossa tumours are generally resected (except those located in

the brainstem) (11), having a means of non-invasive diagnosis is useful in guiding and planning treatment. Conventionally, radiologists use image patterns and associate a diagnosis with these (153). However, it is to be expected that the accuracy of this diagnosis depends on the training, expertise and judgment of the radiologist and invariably carries a degree of variability between (and within) radiologists (153). Furthermore, radiologists can only use information visible to the human eye. Texture analysis can quantify the variation in image patterns, and includes data not visible to the human eye (153). It can be particularly valuable where robustness is important, such as in monitoring disease progression or the longitudinal evaluation of new therapeutic agents (153) and clinical trials (especially multicentre). In addition, using information present on the conventional MR imaging means that no additional infrastructure, expertise or cost is required, and the technique can be widely implemented.

Texture analysis has shown promise in discriminating between lesions on MR images (153) and gives quantitative, reproducible results. It has been used in brain tumours, epilepsy, multiple sclerosis and other disorders (153-155), as wells as for various image types (e.g. MR, X-Ray, camera) (156-163). Texture analysis involves four issues: feature extraction, which refers to using a digital image and computing a feature that can describe the texture numerically; texture discrimination, which involves identifying perceptually homogeneous regions and leads to image segmentation; texture classification, which assigns each

homogeneous texture region to one of the defined classes; shape from texture, which is a reconstruction of 3D surface geometry from texture information (164).

In this study we look at feature extraction and texture classification, to classify paediatric brain tumours of the posterior fossa into pilocytic astrocytomas, medulloblastomas and ependymomas. There are many textural features which can be investigated and various ways of computationally implementing the analysis. One of the methods which has been used in research and is well documented in the literature is the MaZda software, a software package for 2D and 3D image texture analysis (156), and this was used in this study. There are four approaches to texture analysis, namely structural, statistical, model based and transform methods (164). 279 features can be computed in total.

Another issue in texture analysis is ensuring that the features computed characterize the image texture exclusively regardless of the global image characteristics, such as overall brightness, contrast, or other bias (156). This is achieved in MaZda using a normalization procedure, which reduces the dependency of higher-order parameters on first-order gray-level distribution. The two image-histogram normalization options are remapping an image histogram in a range with the mean luminance in the middle and a range of 3 standard deviations onto the white-to-black gray-scale range; or remapping an image histogram in the range between the first and 99^{th} percentile onto the white-to-black range (156, 165). Collewet et al. studied the influence of MRI acquisition protocols (protein-

density and T2-weighted) and four image intensity normalization methods on texture classification of cheese (166). If no normalization or multiplicative normalization was performed, the classification errors depended on the MR acquisition protocols. This was not the case for the '+/-3σ' normalization, where no relationship was found and it provided the best classification results (166). Lerski et al.(167) investigated the discrimination between reticulated foam test objects in a multicentre trial and found that results from different centers did not agree. Although the same MR sequence was used, different scanners (make, model, and field strength) were used and no normalization was applied to the images. Also, only principal component analysis was used to classify the test objects, and this may not have been the most suitable approach (167). Herlidou-Meme et al.(168) used data from 3 scanners (T1 and T2 weighted images) on 10 healthy volunteers and 63 patients with intracranial tumours, to test the robustness of texture analysis. The same statistical textural features were used to segment the tumours, irrespective of the acquisition parameters, scanner, reconstruction or processing. They found highly reproducible results in a comparison of second-order features from T1- and T2-weighted images of gliomas from 3 different MR scanners. Importantly, the imaging was carried out at three hospitals using their own routine acquisition conditions.

9.1.1 Feature Reduction and Classification

The general purpose of feature selection is to find the optimum combination of features which provides the best classification result. Features which are not

relevant to the classification problem should be eliminated. Principal Component Analysis is an unsupervised feature reduction technique which is widely used in pattern recognition studies (114, 151).

Various types of artificial neural networks (ANNs) have found a widespread use in a great number of medical diagnostic decision support system applications because of the belief that they are efficient and reliable algorithms with a great predictive power as compared to other statistical modeling techniques such as statistical regression (169-173). ANNs are highly non-linear computational systems capable of modelling complex systems without requiring an explicit knowledge or formulation of the relationship existing among the variables. They can be a valuable alternative to structured models or empirical correlations between the various independent (explanatory) and dependent (response) variables (170, 172, 174). The most common neural network, which is the multilayer feed-forward network, uses the back-propagation algorithm as a learning rule (171, 173, 175-178). However, a back-propagation neural network has to be trained for a long time to learn the relationship between input and output variables (178). Moreover, a sufficient dataset must be available to divide the data into a training set, a test set and a validation set to avoid overfitting (178). Also, the internal behavior of this kind of network is not fully understood (176). Probabilistic neural networks (PNN) are an alternative method, and they can provide a very general and powerful classification model when there is adequate data of known classification. PNN offers several advantages over back-propagation networks, such as shorter training time (usually

a single pass)(179), effectiveness on small datasets, and easier and better interpretability (169, 178, 180). Moreover, PNN allows true incremental learning where new training data can be added at any time without requiring retraining of the entire network (178, 181-185).

The PNN operates by defining a probability density function (PDF or kernel function) for each data class based on the training set data and an optimized kernel spread parameter (σ)(169). The PDF essentially determines the boundaries for classification (186). The selection of the value of spread parameter is crucial because it determines the width of the basis function that covers the space of the input variables. It is also called the “smoothing parameter” (169, 176, 178). Different types of radial basis functions could be used, but the most common is the multivariate Gaussian function. A large spread has the advantage of producing a smooth shape and exhibits good interpolation properties for predicting new pattern vectors, however, a large kernel width results in a greater possibility of misclassification (169, 176). The optimized kernel width is a compromise between an overly small or large σ. An example of a probabilistic neural network is shown in Fig. 1 (187). It consists of an input layer, a hidden (or pattern) layer, a summation layer and an output layer.

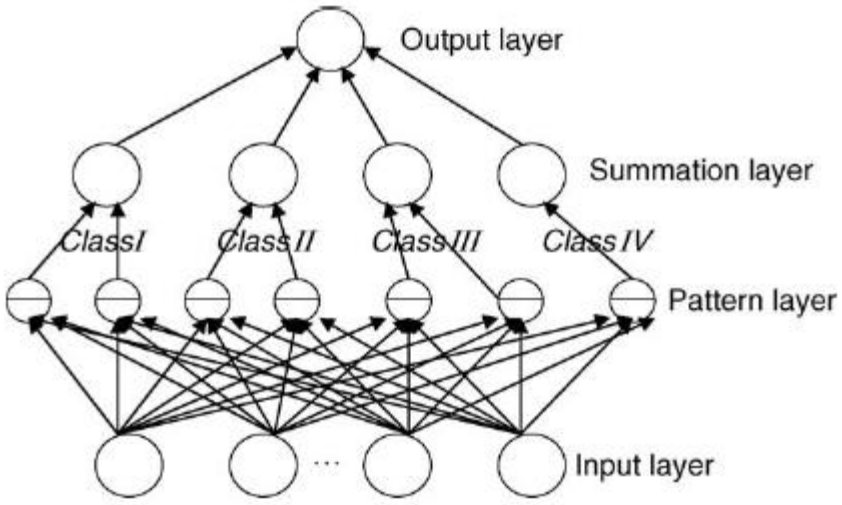

Fig.1 Structure of probabilistic neural networks (187)

The training samples are presented to the input layer. In the second, hidden (or pattern) layer, there are at least as many neurons as there are training samples. The summation layer has as many neurons as classes and there is one output layer neuron.

9.2. METHODS

9.2.1. Magnetic Resonance Imaging

Children with pilocytic astrocytomas, medulloblastomas and ependymomas of the posterior fossa who had MR imaging at Birmingham Children's Hospital prior to treatment (except stereotactic biopsy) have been included in the study.

Acquisition protocol

Images were acquired on a Siemens Symphony MR scanner. T1- weighted (pre-contrast) axial 2D turbo spin echo (TSE) images were acquired using a TR of 700ms and a TE of 10-20ms. T2-weighted axial 2D TSE images were acquired using a TR of 3000ms and a TE of 100ms. The images were anonymized and stored on a research file system at the Institute of Child Health Brain Tumour Research Group in DICOM format.

9.2.2. Texture Analysis

T2 images were analyzed first as tumours were generally easier to detect on these, and three image slices per patient were chosen, where the tumour was most visible/largest and the tumour or region of interest (ROI) was chosen in Image J using thresholding +/- manual outlining. This was saved in .bmp format, opened in MaZda and saved in .roi format. For T1 images the slices most closely matching the T2 slices were used, and the same ROI was used. In MaZda, the image was viewed, normalized (using +/- 3σ), the ROI was loaded over it and texture analysis run.

9.2.3. Feature Reduction

Principal component analysis (PCA) was applied in Minitab 15, a commercially available statistics package, in order to identify the underlying data structure and

achieve dimensionality reduction. The number of principal components to be used in the classifiers was chosen in order to account for 95% of the cumulative variance.

9.2.4. Classification

Classification of the posterior fossa tumours based on the MR image features was performed using the principal component scores as input variables in a PNN in DTREG v.9.6, a commercially available software. Different PNN training schemes can be examined using the commercial software DTREG: (a) a Gaussian kernel or a Reciprocal kernel and (b) one smoothing parameter σ for all input random variables or a different σ for each input random variable or a separate σ for each input random variable and class. A Gaussian kernel and a separate σ for each input random variable and class were used as the training scheme, as these gave the best results. Also, as the target variable is categorical it is expected that a separate σ for each input random variable and class would give better results.

Smoothing parameters may take values of different orders of magnitude. As these parameters have a great effect on the classification performances of PNN, it is necessary to automatically assess their optimal values. DTREG uses a conjugate gradient method for automatic calculation of the smoothing parameter. To obtain the optimal σ, the neural networks with different smoothing parameters were trained, the spread varying from 0.0001 to 10 (multiple steps used to find the optimal σ, which gives a value for each PC for each class). The PNN had 55 and

37 hidden neurons in the second layer for T1 and T2 respectively; these were determined using the minimum error criterion, which is one of three criteria which can be selected to guide the removal of neurons in DTREG software. There were three summation layer neurons; each corresponds to one of three classes and one output layer neuron to make a three-class Bayesian decision. Classification errors were determined using the known class labels from histopathology. Due to the quite small number of data (120 images, 40 patients), the classifier was validated using leave-one-out (LOO) cross-validation (leaving one image slice out at a time).

9.3. RESULTS

MR images from 21 patients with medulloblastomas, 14 patients with pilocytic astrocytomas and 5 patients with ependymomas were investigated using texture analysis. Principal Component Analysis of texture features from T1-weighted images yielded 13 principal components (PC) to explain >95% of the variance. The first PC (PC1) mostly represents Co-occurence matrix-derived parameters (Sum Entropy) S(1,0)SumEntrp, S(0,1)SumEntrp. PC2 mostly represents Co-occurence matrix-derived parameters (Correlation), S(4,0)Correlat, S(3,-3)Correlat, S(2,-2)Correlat.

These PCs were then used as input to the Probabilistic Neural Network to classify the tumours into the three categories (Pilocytic Astrocytoma, Ependymoma, Medulloblastoma). The classifier achieved 100% accuracy on training the data and

93.3% on leave-one-out cross validation (validation data accuracy: Medulloblastoma: 98.4%, Ependymoma: 80%, Pilocytic Astrocytoma: 100%).

Principal Component Analysis of texture features from T2-weighted images also yielded 13 principal components (PC) to explain >95% of the variance. The first PC (PC1) mostly represents Co-occurrence matrix-derived parameters (Difference entropy), S(1,-1)DifEntrp, S(2,-2)DifEntrp, S(0,2)DifEntrp. PC2 mostly represents Co-occurrence matrix-derived parameters (Sum variance), S(0,2)SumVarnc, S(0,1)SumVarnc, S(1,-1)SumVarnc**.**

These PCs were then used as input to the Probabilistic Neural Network to classify the tumours into the three categories (Pilocytic Astrocytoma, Ependymoma, Medulloblastoma). The classifier achieved 100% accuracy on training the data and 95% on leave-one-out cross validation (Validation data accuracy: Medulloblastoma: 100%, Ependymoma: 73.3%, Pilocytic Astrocytoma: 93.2%).

9.4. DISCUSSION

This study shows that texture analysis can be implemented easily on standard T1- and T2-weighted images routinely acquired when children present with suspected brain tumours of the posterior fossa. The analysis can be done with commercially available software, which has extensive manuals to support its use, and therefore does not require highly specialized computing knowledge. In addition, it is possible to distinguish between the three commonest paediatric posterior fossa tumours

with high accuracy (93.3 and 95% for T1- and T2-weighted images respectively), making it a valuable tool to aid diagnosis by contributing information not visible to the radiologist on inspection, and also providing a robust method of quantifying the images, which can be used where consistency is particularly important.

The features found to hold the highest discriminating potential are all co-occurrence matrix derived. The co-occurrence matrix is a second-order histogram, computed from the intenisites of pairs of pixels. The spatial relationship of the pixels in a pair is defined. When divided by the total number of neighboring pixels in the region of interest, this matrix becomes the estimate of the joint probability of two pixels, a distance d apart along a given direction θ having particular co-occurring values i and j. The result is a square matrix with dimensions equal to the number of intensity levels in the image, for each distance d and orientation θ (156, 165).

It is worth noting the classification method used here (PNN), as most of the previous studies used some form of linear discriminant analysis (LDA) (153). Although this is a reasonable approach and a more straight-forward and perhaps more intuitive method, it is important to incorporate and test more advanced methods, which may substantially improve classification, as in this study (LDA results not shown).

Although radiologists are often able to distinguish the type of tumour from inspection of the images, this usually includes a degree of uncertainty, and all 3 tumour types may appear in the differential diagnosis in the radiologists' report. This is because some features can overlap between tumours, and each type of tumour can also have variable appearances within the group. For example, ependymomas appear isointense to gray matter on T2-weighted images, like medulloblastomas. Cerebellar astrocytomas can be low-signal intesnisity on T1-weighted images, as can ependymomas and medulloblastomas (34, 188). Arle et al.(72) studied 33 children with primitive neuroectodermal tumours, astrocytomas and ependymomas/other tumours of the posterior fossa with long TE SVS. Cr/NAA, NAA/Cho and Cr/Cho, 10 MR imaging tumour characteristics, tumour size, patient's age and sex were used in a neural network and compared to predictions made by a neuroradiologist blind to the MRS and histopathology results. The neuroradiologist predicted the tumour type with 73% accuracy, and neural networks with different data combinations as inputs achieved accuracies of 58-95%. The neural network which included all data achieved a prediction accuracy of 94.6%.

A similar study of paediatric cerebellar tumours by Davies et al.(114) used magnetic resonance spectroscopy in the same 3 categories of patients (most patients the same as in the study here as performed at BCH) and found an accuracy of 94.7% in the glial-cell (astrocytoma+ependymoma) versus non-glial-cell (medulloblastoma) classifier, 93.1% for astrocytoma vs. medulloblastoma and

92.8% for astrocytoma vs. medulloblastomas vs. ependymoma. Principal component analysis was used for dimension reduction, and linear discriminant analysis for variable selection and classification, with a bootstrap cross-validation method (114). It is clearly more difficult to classify 3 groups, but in this study comparable accuracies were achieved. It would be interesting to combine the data sets to investigate whether there can be any further improvement in classification. Posterior fossa tumours are a good test-bed for the technique as they are easier to identify on imaging, and they usually belong to one of the 3 categories mentioned. Texture analysis and classification could also be applied on other brain tumours, such as low grade gliomas, using the analysis scheme described in this paper, and the results combined with MRS in the same cohort. In addition, texture analysis can be used in prognostication and treatment monitoring to provide additional, robust and reproducible information. An important advantage of quantitative analysis such as the one presented here, is the ability to combine the results with other quantitative techniques such as MRS and diffusion imaging.

9.5. CONCLUSION

This study shows that texture analysis can be implemented easily on standard T1- and T2-weighted images routinely acquired when children present with suspected brain tumours of the posterior fossa. Discriminatory features do not correspond to those used in clinical interpretation of the images and therefore provide novel tumour characteristics. This methodology can be extended to other paediatric brain

tumours, such as low grade gliomas, and combined with MRS metabolite values in a pattern recognition method. Information from the two techniques is likely to be independent and the combination could provide improved characterization. The analysis can be done with commercially available software, which have extensive manuals to support their use, and therefore does not require highly specialized computing knowledge. Texture analysis can produce a quantitative analysis of MR images which is robust and reproducible, and could play an important role in the radiological investigation of patients with brain tumours.

CHAPTER 10

CONCLUSIONS AND FUTURE WORK

CHAPTER 10

CONCLUSIONS AND FUTURE WORK

Multiple aspects of advanced paediatric tumour imaging and biology have been studied in this work. Paediatric low grade gliomas present a clinical management challenge, but also the need to apply functional imaging techniques to non-invasively assess them. ^{1}H MRS has been shown to provide diagnostic and prognostic information in paediatric brain tumours, but as these are relatively rare, there is a need for multicentre studies. Furthermore, most studies have investigated various groups of paediatric brain tumours together. Low grade gliomas often have a complex clinical course, with multiple recurrences or progression, and there is therefore a need for studies to focus on this specific group of tumours exclusively.

In this work, the use of ^{1}H MRS in the diagnosis, characterization and prognostication of paediatric low grade gliomas is demonstrated; histological correlates for metabolites detected by MRS are identified; the ability of in vitro NMR to distinguish between cell lines originating from tumours of the same histology presenting in different ways is portrayed; applications of chemical shift imaging in answering specific clinical questions are demonstrated through case studies; and finally another quantitative MR technique, texture analysis, is applied to paediatric posterior fossa tumours. This is the first study to the best of our

knowledge which investigates an extensive cohort of paediatric low grade gliomas with MRS, collecting clinical, imaging and histopathological data from 2 centers and 5 scanners, in a robust and reliable manner.

Many important conclusions have been drawn from this work. MRS has been shown to detect differences between subgroups of low grade brain tumours in children, making MRS a valuable aid to non-invasive diagnosis. Metabolite differences between tumours of the same histology have been detected, emphasizing the potential for metabolite profiles to improve the characterization of these tumours. Investigation of the value of ^{1}H MRS in the prognostication of paediatric low grade gliomas revealed high mIns and GPC and low PCh as being markers of good prognosis. Furthermore, comparison between sequential MRS studies showed that patients with stable disease had lower concentrations of metabolites associated with more aggressive tumours in the second MRS (compared to the pre-treatment MRS), although this depends on the specific group of patients being investigated. Having detected important metabolites in the diagnosis and prognostication of paediatric low-grade gliomas, the next step was to investigate their correlation to routinely assessed histopathological features. Many significant correlations were found, mainly involving choline-containing compounds, lipids, taurine, NAA, mIns and Gly. Having investigated in vivo ^{1}H MR spectra and detected metabolites of diagnostic and prognostic importance, and also found histopathological correlates for many of these, in vitro ^{1}H NMR of different cell lines was performed. This demonstrated that ^{1}H NMR has the ability to detect subtle

differences and discriminate between three paediatric pilocytic astrocytoma cell lines ('typical', metastatic and recurrence), and the in vitro spectra demonstrated the characteristic features of pilocytic astrocytomas in vivo. Furthermore, no NAA was detected in these cell lines in this preliminary work, suggesting that the resonance assigned to NAA in in vivo ^{1}H MRS in pilocytic astrocytomas may actually correspond to a different molecule, acetate being a possibility. However, further work is needed to clarify the origins of NAA seen in vivo in paediatric pilocytic astrocytomas. The majority of this work focused on single voxel spectroscopy; however, magnetic resonance spectroscopic imaging can also be used in the assessment of paediatric brain tumours, and has value in answering specific clinical questions, which has been demonstrated through the case studies described. Finally, another quantitative technique, texture analysis of MR images, has been used to diagnose posterior fossa paediatric brain tumours with high accuracy, showing that this can be easily implemented on standard T1- and T2-weighted images, routinely acquired on all children with a brain tumour.

Although a direct comparison with conventional radiology was not possible in the time-frame of this work, the inclusion of MRS in routine MR imaging protocols for paediatric brain tumours would enable the collection of larger datasets on these relatively rare tumours, thus facilitating future work on the clinical application and reliability of the technique. The results presented in this thesis need to be validated on larger multicentre datasets, and then prospectively tested in order to provide robust evidence for the specific use of MRS in clinical paediatric oncology practice.

In addition to the need for validation and testing of the methods and results in this work, other questions on MRS in paediatric low grade gliomas have been raised, which need to be further explored. In the work on histological correlates of MRS metabolites, a larger study using quantitative markers of histological features is needed. Conventional MR imaging characteristics could also be tested for their histological correlates; for example, T2 intensity can be tested against microcystic elements or cell density, and T1 contrast enhancement against vascularity. The origins of NAA in paediatric brain tumours in vivo needs to be studied further, as no clear answer is available as yet; it is detected reliably in these tumours, cannot be attributed to partial volume effects or normal brain infiltration, yet in vitro NMR on pilocytic astrocytoma cell lines does not detect any NAA. Cell lines from other low grade gliomas need to be grown and tested with in-vitro NMR, to provide better characterization of the tumours, or alternatively magic angle spinning on a large number of tissue samples performed. Texture analysis needs to be applied on the cohort of low grade gliomas presented here and the results combined with metabolite values from MRS, to test whether more accurate diagnostic and prognostic information can be obtained. Texture analysis can also be used for treatment monitoring in low grade gliomas, as T2 intensity is often seen to decrease after treatment. The texture analysis features which are significant discriminators between tumours, such as co-occurrence matrix parameters, need to be investigated further as to what specifically they represent. A starting point

would be to test against the number of blood vessels per image, using CD 34 staining.

Paediatric low grade gliomas are a challenging condition, both due to their complex clinical course and their relatively small numbers which make any clinical study difficult to perform. However, they form a very important disease entity, which has significant effect on children's and families' lives, and continuing efforts to collect information on large patient cohorts from multiple centers is crucial. Promising results have been reported by our group and others in the field, and advanced magnetic resonance imaging techniques now have a significant role in the study of these tumours.

10.1. Summary of the Main Conclusions

- MRS can detect differences between subgroups of low grade brain tumours in children.
- The main differences can be readily identified on visual inspection of the spectra and quantitative analysis can aid the process of interpretation, making MRS a valuable aid to non-invasive diagnosis.
- The detection of metabolite differences between tumours of the same histology emphasizes the potential for metabolite profiles to improve the characterization of these tumours and its combination with emerging molecular genetic biomarkers should improve the assessment of these tumours.
- High mIns and GPC and low PCh are markers of good prognosis in paediatric low grade gliomas.
- mIns and PCh are significant predictors of survival in a Cox regression model.
- Patients with stable disease show lower metabolite concentrations of lipids+ macromolecules, PCh and Ala on their second MRS compared to the pre-treatment MRS, or no change in metabolites, depending on the treatment group.
- Patients who progressed had higher Gln in their second MRS study.
- Ki67 has a significant positive correlation with PCh and GPC+PCh detected in paediatric brain tumours.

- Apoptosis has a significant positive correlation with lipids+macromolecules and taurine.
- Long TE lipids+macromolecules have a significant positive correlation with necrosis.
- Atypia correlates positively with PCh, GPC+PCh and lipids+macromolecules.
- Mitosis correlates positively with PCh and lipids+macromolecules.
- Lesional neuronal elements correlate negatively with NAA and NAA+NAAG.
- Neoplastic glial elements correlate positively with mIns, NAA, NAA+NAAG and negatively with Gly.
- GFAP staining correlates negatively with Gly.
- ^{1}H NMR has the ability to detect subtle differences and discriminate between three paediatric pilocytic astrocytoma cell lines ('typical', metastatic and recurrence).
- The in vitro ^{1}H NMR spectra of the pilocytic astrocytoma cell lines demonstrate the characteristic features of pilocytic astrocytomas in vivo.
- No NAA is detected in these cell lines in this preliminary work, and it is suggested that the resonance assigned to NAA in in vivo ^{1}H MRS in pilocytic astrocytomas may actually correspond to a different molecule, acetate being a possibility. However, further work is needed to clarify the origins of NAA seen in vivo in paediatric pilocytic astrocytomas.

- MRSI is useful in non-invasively assessing large heterogeneous lesions, where areas of different grade may be present.
- MRSI can be used to assess specific tumour areas, such as around a bleed, and aid in the diagnosis of challenging tumours which do not respond to treatment.
- Texture analysis can be implemented easily on standard T1- and T2-weighted images routinely acquired when children present with suspected brain tumours of the posterior fossa and achieves high classification accuracies using a PNN.
- Discriminatory features do not correspond to those used in clinical interpretation of the images and therefore provide novel tumour characteristics.

Some of the work presented in this thesis has been published in conference papers, listed at the beginning of the thesis.

APPENDIX 1 DATABASE DESIGN

REGISTRATION
Hospital number_Hospital
Name
DOB
Gender
Hospital
Ethnicity
NF1
Tuberous Sclerosis
Date of diagnosis
Progressed
Date of progression
Progression comments
Date of last known clinical contact
Date data collected
Comments
Alive
Date of death
Cause of death
Cause of death comments

DIAGNOSIS
Hospital number_Hospital
Histological diagnosis performed
Date of histology
Consencus diagnosis
Consencus grade
Diagnosis comments
Unusual features
Final diagnosis to use
Episode
Diagnosis id

OBSERVATION
Hospital number_Hospital
Observation
Date observation started
Date observation stopped
Reason for stopping observation
Observation comments
Episode
Observation id

SURGERY
Hospital number_Hospital
Surgery
Date of surgery
Type of surgery
Post-operative stage- surgical assessment
Post-operative stage-Radiological assessment
Surgery comments
Surgical report needed
Surgical report read
Episode
Surgery id

TREATMENT
Hospital number_Hospital
Treatment trial
Observation
Surgery
Chemotherapy
Radiotherapy
Diencephalic syndrome
Focal neurological deficit
Seizures
Increased ICP
Definite history of visual deterioration
Borderline vision (threat to vision)
Nystagmus due to visual impairement in infants
Symptomatic metastases
Manifestation of new neurologic symptoms secondary to tumour growth
Increase in severity of existing neurologic symptoms
Any loss of vision in 2nd eye if the other eye is blind
Increase in tumour size >25%
Increase in tumour size
Increase in cystic part of tumour
New lesions
Indication comments
Episode
Date of episode
Treatment id

CHEMOTHERAPY
Hospital number_Hospital
Chemotherapy
Date chemotherapy started
Date chemotherapy completed
Name of protocol
Drugs
Drugs free text
Chemotherapy comments
Reason for ending treatment
Episode
Chemotherapy id

RADIOTHERAPY
Hospital number_Hospital
Radiotherapy
Date radiotherapy started
Date radiotherapy completed
Comments
Total dose delivered
Fraction dose
Interruptions
Number of days of interruption
Reason for ending treatment
Episode
Radiotherapy id

MRI
Hospital number_Hospital
MRI date
followup
Is there an MRS
Site of tumour
Side of tumour
Site of tumour comments
Disease outside primary
Number of sites affected
Which sites
Stage
Recurrance outside primary site
Stage at recurrence
Recurrence comments
CSF result checked
MRI id

MRS
ID
Hospital number_Hospital
Date of MRS
Time of MRS
Pre-treatment
Scanner
TE
Field strength
Type of MRS
RDA file
Processed with LCModel
Comments for CSI
Data Missing
Data missing_comments
Voxel location
Voxel location comments
Quality of MRS_ICH WATER
Quality of MRS_ICH WEDDY_tick if need to use WEDDY
Quality of MRS comments
Possibility of MRS on NBO

All tables are connected by a one-to-many relationship from the Registration table, using Hospital number_Hospital

APPENDIX 2 MATLAB CODES

MATLAB CODE 1

```
%%%%%%%%%%%%%%%%%%%%%%%%%%%%%%%%%%%%%%%%%%%%%
%Description: Find file structure paths using excel file as input   %
%and load csv files to get metabolite values/CRLBs                  %
%BCH & QMC                                                           %
%%%%%%%%%%%%%%%%%%%%%%%%%%%%%%%%%%%%%%%%%%%%%

clear
clc


%%% Temp
addpath('C:\Documents and Settings\eorph\Desktop')
[num,text]=xlsread('C:\Documents and Settings\eorph\Desktop\To get
metabolites_followup.xls');


str_path = '';
PSDIR = '\ICH_PS';
LCMODEL_DIR = '\LCM_6_2_0';
LCMODEL_TYPE = '\WATER';
TE =num(:,5);
METABOLITES = [3:3:99];
CRLB = [4:3:100];

names = text(:,1);
names=deblank(names);              %% Delete whitespaces from names
names=char(names);                 %% to make string
ID= num(:,1);
DOB=datestr(datenum((text(:,3)),'dd/mm/yyyy'),'yyyymmdd');
DOS=datestr(datenum((text(:,4)),'dd/mm/yyyy'),'yyyymmdd');

for k=1:length(ID)
   if strcmp((text(k,5)), 'QMC')        %%choose directory based on hospital
      str_path(k,:) = 'Y:\test-sy\DATA\QMC';

   else str_path(k,:)= 'Y:\test-sy\DATA\BCH';

   end

end


for q=1:length(ID)

   if strcmp((text(q,7)), 'WATER')
      LCMODEL_TYPE(q,:)='\WATER';
   else LCMODEL_TYPE(q,:)='\WEDDY';

  end
end
```

```
%%
str_names = strcat(names(:,:),'-*',num2str(ID(:,:)),'-',num2str(DOB(:,:)),'\',
num2str(DOS(:,:)));

str_2= cellstr(strcat(str_path,'\', char(strrep(cellstr(str_names),' ','')) ,
'\SVS_TE',num2str(TE(:,:)),'*\**', PSDIR, LCMODEL_DIR, LCMODEL_TYPE,
'\*.csv'));

 % combines common path with above, *s mean anything in between and
goes to csv files

 %%
for i = 1:length(str_2)
   str_files = rdir(char(str_2(i))) ;
   c = 0;
   str_files_cell{i} = '';
   for j=3:length(str_files)
      if ~str_files(j).isdir
         if strfind(str_files(j).name,'SVS_TE') & strfind(str_files(j).name,'.csv')
         c = c+1;
         if c==1
            str_files_cell{i} = str_files(j).name;
            disp(str_files(j).name)
         else
            warning('More than one SVS found with correct TE for %s \n',
char(str_2(i)))
         end
         end
      end
   end
   if ~isempty(str_files_cell{i})
   data_patient{i} = importdata(str_files_cell{i});
   lcm_data.conc(i,:) = data_patient{i}.data(METABOLITES);
   lcm_data.CRLB(i,:) = data_patient{i}.data(CRLB);

temp_metab_str=strrep(strrep(strrep(strrep(data_patient{i}.colheaders(META
BOLITES),'',''),'Cre','Cr'),'Ins','ml'),
   'Cho','GPC+P  Ch');
   [lcm_data.metab_str_sorted{i}, sorted_idx] = sort(temp_metab_str);
   lcm_data.metab_str{i} = temp_metab_str;
   lcm_data.sorted_idx{i} = sorted_idx;
   lcm_data.conc_sorted(i,:) = lcm_data.conc(i,sorted_idx);
   lcm_data.CRLB_sorted(i,:) = lcm_data.CRLB(i,sorted_idx);
   else
      fprintf('File not found for %s \n',char(str_2(i)));
      %error('Error in finding file...')
   end
end
```

MATLAB CODE 2

```
%%%%%%%%%%%%%%%%%%%%%%%%%%%%%%%%%%%%%%%%%%%%%%%%%%%%%%%%%%%
%Description: Output mean spectra line by inputting excel file data,      %
%extracting data from NAS for each patient, subtracting baseline from %
%individual spectra, finding mean spectra, plotting mean spectra          %
%%%%%%%%%%%%%%%%%%%%%%%%%%%%%%%%%%%%%%%%%%%%%%%%%%%%%%%%%%%

Clear
clc



%%% Primer file location
addpath('C:\Documents and Settings\eorph\Desktop\Print spectra_mean
spectra')
[num,text]=xlsread('C:\Documents and Settings\eorph\Desktop\PF_PA.xls');

%Prime NAS location (and establish matrix for metabolites and CRLB)


%From excel priming file load names, ID, DOB, DOS
names = text(:,1);
names=deblank(names);                        %% Delete whitespaces from names
names=char(names);                           %% to make string
ID= num(:,1);
DOB=datestr(datenum((text(:,3)),'dd/mm/yyyy'),'yyyymmdd');
DOS=datestr(datenum((text(:,4)),'dd/mm/yyyy'),'yyyymmdd');


PSDIR = '\ICH_PS';
LCMODEL_DIR = '\LCM_6_2_0';
%LCMODEL_TYPE = '\WATER';
TE =num(:,5);
METABOLITES = [3:3:99];
CRLB = [4:3:100];
SUB_BASELINE_FLAG = 'Y';
ERROR_TYPE_FLAG = 'se';
str_path='';



for k=1:length(ID)                          %%choose directory based on hospital
   if strcmp((text(k,5)), 'QMC')
       str_path(k,:) = 'Y:\test-sy\DATA\QMC';

   else str_path(k,:)= 'Y:\test-sy\DATA\BCH';

   end
end
```

```
for q=1:length(ID)

   if strcmp((text(q,7)), 'WATER')
      LCMODEL_TYPE(q,:)='\WATER';
   else LCMODEL_TYPE(q,:)='\WEDDY';

  end
end

%% Create direction to results.txt file for each patient by concatenating
%% all components needed

str_names = strcat(names(:,:),'-*',num2str(ID(:,:)),'-',num2str(DOB(:,:)),'\',
num2str(DOS(:,:)));
str_2= cellstr(strcat(str_path,'\', char(strrep(cellstr(str_names),' ','')) ,
'\SVS_TE',num2str(TE(:,:)),'*\**', PSDIR, LCMODEL_DIR, LCMODEL_TYPE,
'\*results.txt'));

 % combines common path with above, *s mean anything in between and
goes to csv files

%%
for i = 1:length(str_2)
   str_files = rdir(char(str_2(i))) ;
   c = 0;
   str_files_cell{i} = '';
   for j=3:length(str_files)
      if ~str_files(j).isdir
         if strfind(str_files(j).name,'SVS_TE') &
strfind(str_files(j).name,'results.txt')
            c = c+1;
            if c==1
               str_files_cell{i} = str_files(j).name;
               disp(str_files(j).name)
            else
               warning('More than one SVS found with correct TE for %s \n',
char(str_2(i)))
            end
         end
      end
   end


   if ~isempty(str_files_cell{i})

   else
      fprintf('File not found for %s \n',char(str_2(i)));
      %error('Error in finding file...')
   end
end
```

```
for j=1:length(str_files_cell)
   a{j}= str_files_cell{j};
   fid{j}=fopen(a{j});
   if fid{j} == -1
      disp ('File open not successful')
      %continue
 % continues to the next patient in the loop even if one is not successful
   else
      %Skip introductory lines (47 lines)
      InputText=textscan(fid{j},'%s',46,'delimiter','\n');

% Read strings delimited by a carriage return
      InputText=textscan(fid{j},'%s',1,'delimiter','\n');
      temp_str = char(InputText{1});
      Npoints = str2num(temp_str(1:3));

      %This gets to x-axis values and reads x values
      ppm_orig=textscan(fid{j},'%.6f',Npoints);

      if Npoints ~= 496
         ppm_axis_GE=resample(ppm_orig{:},496,Npoints);
      else
         ppm_axis_Siemens=ppm_orig{:};
      end

      %Skip to y-axis values for phased data points & read raw y values
      InputText=textscan(fid{j},'%s',2,'delimiter','\n');
      InputText{:};

      orig_phased_data=textscan(fid{j},'%.6f',Npoints);
      if Npoints ~= 496
% this resamples anything to 496 points so does not matter how many points
initially_number points depends on bandwidth not scanner, on GE cannot
change bandwidth but on Siemens and Philips can
         phased_data(j,:)=resample(orig_phased_data{:},496,Npoints);
      else
         phased_data(j,:)=orig_phased_data{:};
      end

      %Skip to y-axis values for fit data points and read fit y values
      InputText=textscan(fid{j},'%s',2,'delimiter','\n');
      InputText=textscan(fid{j},'%.6f',Npoints);
      if Npoints ~= 496
         Fityval(j,:)=resample(InputText{:},496,Npoints);
      else
         Fityval(j,:)=InputText{:};
      end

      %Skip to y-axis values for baseline points and read baseline values
      InputText=textscan(fid{j},'%s',2,'delimiter','\n');
```

```
        InputText=textscan(fid{j},'%.6f',Npoints);

        if Npoints ~= 496
            baselineyval(j,:)=resample(InputText{:},496,Npoints);
        else
            baselineyval(j,:)=InputText{:};
        end
    end

    closeresult{j}=fclose(fid{j});
    if closeresult{j}==0
        disp ('File close successful')
    else
        disp ('File close not successful')
    end

end

% Subtract baseline for each case
switch SUB_BASELINE_FLAG
    case 'Y'

 % can change this to N or anything else at the top of script if don't want to
subtract
        y = phased_data - baselineyval;
% can change phased_data to Fityval if prefer
    otherwise
        y = phased_data;
end

ymean = mean(y);
y_sdev = std(y);
y_se = y_sdev/sqrt(length(str_files_cell));

switch ERROR_TYPE_FLAG
% can change this according to what error you want to plot
    case 'sd'
        y_err = y_sdev;
    case 'se'
        y_err = y_se;
    case 'CI'
        y_err = y_se * 1.96;
    otherwise
        error('Unrecognised error type!\n');
end

%Plot figure
figure
upper = area(ppm_axis_Siemens,ymean + y_err);
% plots using Siemens axis to avoid rounding error due to resampling
```

```
set(upper,'FaceColor',[0.5 0.5 0.5],'EdgeColor','w');
hold on
lower = area(ppm_axis_Siemens,ymean - y_err);
set(lower,'FaceColor','w','EdgeColor','w');
plot(ppm_axis_Siemens,ymean)
set(gca,'XDir','reverse')
```

LIST OF REFERENCES

1. Peet AC, Leach MO, Pinkerton CR, Price P, Williams SR, Grundy RG. Proceedings of the Engineering and Physical Sciences Research Council Workshop - the development of functional imaging in the diagnosis, management and understanding of childhood brain tumours. Pediatr Blood Cancer. 2005;44(2):103-13.

2. Levy AS. Brain Tumors in Children: Evaluation and Management. Curr Probl Pediatr Adolesc Health Care. 2005;35(6):230-45.

3. Stevens MCG, Cameron AH, Muir KR, Parkes SE, Reid H, Whitwell H. Descriptive Epidemiology of Primary Central Nervous System Tumours in Children: A Population-based Study. Clin Oncol. 1991;3:323-9.

4. Stiller CA, Nectoux J. International Incidence of Childhood Brain and Spinal Tumours. Int J Epidemiol. 1994 June 1, 1994;23(3):458-64.

5. Rickert C, Paulus W. Epidemiology of central nervous system tumors in childhood and adolescence based on the new WHO classification. Childs Nerv Syst. 2001;17(9):503-11.

6. Cohen KJ, Broniscer A, Glod J. Pediatric Glial Tumors. Curr Treat Options Oncol. 2001;2:529-36.

7. Panigrahy A, Bluml S. Neuroimaging of Pediatric Brain Tumors: From Basic to Advanced Magnetic Resonance Imaging (MRI). J Child Neurol. 2009 November 1, 2009;24(11):1343-65.

8. Blaney SM, Kun LE, Hunter J, Rorke-Adams LB, Lau C, Strother D, et al. Tumors of the Central Nervous System In: Pizzo PA, Poplack DG, editors. Principles and Practice of Pediatric Oncology
5th edition ed. Philadelphia: Lippincott Williams & Wilkins; 2006. p. 786-864.

9. ICLGG/SIOP. Protocol SIOP-LGG 2004 (UKCCSG CNS 2004 03) Version 2 Cooperative multicentre Study for Children and Adolescents With Low Grade Glioma. 2006.

10. Qaddoumi I, Sultan I, Broniscer A. Pediatric low-grade gliomas and the need for new options for therapy: Why and how? Cancer Biol Ther. 2009;8(1):1-7.

11. Sievert AJ, Fisher MJ. Pediatric Low-Grade Gliomas J Child Neurol. 2009;24(11):1397-408.

12. Smoots DW, Geyer JR, Lieberman DM, Berger MS. Predicting disease progression in childhood cerebellar astrocytoma. Childs Nerv Syst. 1998;14(11):636-48.

13. Opocher E, Kremer LCM, Dalt LD, Van de Wetering MD, Viscardi E, Caron HN, et al. Prognostic factors for progression of childhood optic pathway glioma: A systematic review. Eur J Cancer. 2006;42(12):1807-16.

14. Listernick R, Charrow J, Gutmann DH. Intracranial gliomas in neurofibromatosis type 1. Am J Med Genet. 1999;89(1):38-44.

15. Fisher PG, Tihan T, Goldthwaite PT, Wharam MD, Carson BS, Weingart JD, et al. Outcome analysis of childhood low-grade astrocytomas. Pediatr Blood Cancer. 2008;51(2):245-50.

16. Tzika AA, Astrakas LG, Zarifi MK, Petridou N, Young-Poussaint T, Goumnerova L, et al. Multiparametric MR assessment of pediatric brain tumors. Neuroradiology. 2003;45(1):1-10.

17. Soo TM, Bernstein M, Provias J, Tasker R, Lozano A, Guha A. Failed Stereotactic Biopsy in a Series of 518 Cases. Stereotact Funct Neurosurg 1995;64(4):183-96.

18. Eisenhauer EA, Therasse P, Bogaerts J, Schwartz LH, Sargent D, Ford R, et al. New response evaluation criteria in solid tumours: Revised RECIST guideline (version 1.1). Eur J Cancer. 2009;45(2):228-47.

19. Verweij J, Therasse P, Eisenhauer E. Cancer clinical trial outcomes: Any progress in tumour-size assessment? Eur J Cancer. 2009;45(2):225-7.

20. Galanis Evanthia, Buckner Jan C, Maurer Matthew J, Sykora Rene, Castillo Rene, Ballman Karla V, et al. Validation of neuroradiologic response assessment in gliomas: Measurement by RECIST, two-dimensional, computer-assisted tumor area, and computer-assisted tumor volume methods. Neuro-Oncol. 2006;8(2):156-65.

21. Wen PY, Macdonald DR, Reardon DA, Cloughesy TF, Sorensen AG, Galanis E, et al. Updated Response Assessment Criteria for High-Grade Gliomas: Response Assessment in Neuro-Oncology Working Group. J Clin Oncol. 2010 April 10, 2010;28(11):1963-72.

22. Macdonald DR, Cascino TL, Schold SC, Cairncross JG. Response criteria for phase II studies of supratentorial malignant glioma. J Clin Oncol. 1990;8(7):1277-80.

23. van den Bent MJ, Wefel JS, Schiff D, Taphoorn MJB, Jaeckle K, Junck L, et al. Response assessment in neuro-oncology (a report of the RANO group): assessment of outcome in trials of diffuse low-grade gliomas. Lancet Oncol. 2011;12(6):583-93.

24. European Medicines Agency, Science Medicines Health. Meeting report on the paediatric high-grade glioma medicines expert workshop. Development of high quality medicines to treat children with high-grade glioma. London: European Medicines Agency 2011. Report No.: EMA/289125/2011.

25. Vaidya SJ, Payne GS, Leach MO, Pinkerton CR. Potential role of magnetic resonance spectroscopy in assessment of tumour response in childhood cancer. Eur J Cancer. 2003;39(6):728-35.

26. Sargent DJ, Rubinstein L, Schwartz L, Dancey JE, Gatsonis C, Dodd LE, et al. Validation of novel imaging methodologies for use as cancer clinical trial end-points. Eur J Cancer. 2009;45(2):290-9.

27. Peet AC, Lateef S, MacPherson L, Natarajan K, Sgouros S, Grundy RG. Short echo time 1 H magnetic resonance spectroscopy of childhood brain tumours Childs Nerv Syst. 2007;23:163-9.

28. Tzika AA, Zarifi MK, Goumnerova L, Astrakas LG, Zurakowski D, Young-Poussaint T, et al. Neuroimaging in Pediatric Brain Tumors: Gd-DTPA-enhanced, Hemodynamic, and Diffusion MR Imaging Compared with MR Spectroscopic Imaging. AJNR Am J Neuroradiol. 2002 February 1, 2002;23(2):322-33.

29. Preul MC, Caramanos Z, Collins DL, Villemure J-G, Leblanc R, Olivier A, et al. Accurate, noninvasive diagnosis of human brain tumors by using proton magnetic resonance spectroscopy Nat Med. 1996;2(3):323-5.

30. Peet AC, Arvanitis TN, Auer DP, Davies NP, Hargrave D, Howe FA, et al. The value of magnetic resonance spectroscopy in tumour imaging. Arch Dis Child. 2008;93(9):725-7.

31. Wang Z, Sutton LN, Cnaan A, Haselgrove JC, Rorke LB, Zhao H, et al. Proton MR spectroscopy of pediatric cerebellar tumors. AJNR Am J Neuroradiol. 1995;16(9):1821-33.

32. Cousin-Lafay L, Sung L, Carret A, Hukin J, Wilson B, Johnston DL, et al. Carboplatin Hypersensitivity Reaction in Pediatric Patients with Low-grade Glioma. A Canadian Pediatric Brain Tumor Consortium Experience. Cancer. 2008;112(4):892-9.

33. Vezina LG. Neuroradiology of childhood brain tumors: new challenges. J Neurooncol. 2005;75(3):243-52.

34. Intracranial, Orbital, and Neck Masses of Childhood. In: A.J.Barkovich, , editors. Pediatric Neuroimaging 4th ed. Philadelphia Lippincott Williams & Wilkins

35. Koeller KK, Henry JM. Superficial gliomas: radiologic-pathologic correlation. Radiographics. 2001;21:1533-56.

36. Kwock L, Smith JK, Castillo M, Ewend MG, Collichio F, Morris DE, et al. Clinical role of proton magnetic resonance spectroscopy in oncology: brain, breast, and prostate cancer. Lancet Oncol. 2006;7(10):859-68.

37. Cookson M.S., Fleshner N.E., Soloway S.M., Fair WR. Correlation between Gleason score of needle biopsy and radical prostatectomy specimen: accuracy and clinical implications. J Urol. 1997;157(2):559-62.

38. Scheidler J, Hricak H, Vigneron DB, Yu KK, Sokolov DL, Huang R, et al. Prostate Cancer: Localization with three-dimensional Proton MR spectroscopic Imaging- Clinicopathologic Study. Radiology. 1999;213:473-80.

39. Zakian KL, Sircar K, Hricak H, Chen H, Shukla-Dave A, Eberhardt S, et al. Correlation of Proton MR Spectroscopic Imaging with Gleason Score Based on Step-Section Pathologic Analysis after Radical Prostatectomy Radiology. 2005;234:804-14.

40. Swanson MG, Vigneron DB, Tabatabai ZL, Males RG, Schmitt L, Carroll PR, et al. Proton HR-MAS spectroscopy and quantitative pathologic analysis of MRI/3D-MRSI-targeted postsurgical prostate tissues. Magn Reson Med. 2003;50:944-54.

41. Menard C, Smith ICP, Somorjai RL, Leboldus L, Patel R, Littman C, et al. Magnetic Resonance Spectroscopy of the malignant prostate gland after radiotherapy: a histopathologic study of diagnostic validity. Int J Radiat Oncol Biol Phys. 2001;50:317-23.

42. Coakley FV, Teh HS, Qayyum A, Swanson MG, Lu Y, Roach III M, et al. Endorectal MR Imaging and MR Spectrosocpic imaging for locally recurrent prostate cancer after external beam radiation therapy: preliminary experience Radiology. 2004;233:441-8.

43. Roebuck JR, Cecil KM, Schnall MD, Lenkinski RE. Human breast lesions: characterization with proton MR spectrosocpy Radiology. 1998;209:269-75.

44. Kvistad KA, Bakken IJ, Gribbestad IS, Ehrnholm B, Lundgren S, Fjosne HE, et al. Characterization of neoplastic and normal human breast tissues with in vivo (1)H MR spectroscopy. J Magn Reson Imaging 1999;10:159-64.

45. Huang W, Fisher P, Dulaimy K, Tudorica LA, O'Hea B, Button T. Detection of Brest Malignancy: Diagnostic MR Protocol for Improved Specificity. Radiology. 2004;232:585-91.

46. Meisamy S, Bolan PJ, Baker EH, Pollema MG, Le CT, Kelcz F, et al. Adding in Vivo Quantitative 1H MR Spectroscopy to Improve Diagnostic Accuracy of Breast MR Imaging: Preliminary Results of Observer Performance Study at 4.0T. Radiology. 2005;236:465-75.

47. Jagannathan NR, Kumar M, Seenu V, Coshic O, Dwivedi SN, Julka PK, et al. Evaluation of total choline from in-vivo volume localized proton MR spectroscopy and its response to neoadjuvant chemotherapy in locally advanced breast cancer Br J Cancer 2001;84:1016-22.

48. Meisamy S, Bolan PJ, Baker EH, Bliss RL, Gulbahce E, Everson LI, et al. Neoadjuvant Chemotherapy of Locally Advanced Brest Cancer: Predicting Response with in Vivo 1H MR spectroscopy- A Pilot Study at 4T Radiology. 2004;233:424-31.

49. Burtscher I.M., Holtas S. Proton MR Spectroscopy in Clinical Routine. J Magn Reson Imaging 2001;13:560-7.

50. Stanley JA. In vivo magnetic resonance spectroscopy and its application to neuropsychiatric disorders. Can J Psychiatry. 2002;47(4):315-26.

51. Moller HE, Vermathen P, Rummeny E, Wortler K, Wuisman P, Rossner A, et al. *In vivo* ^{31}P NMR Spectroscopy of Human Musculoskeletal Tumors as a Measure of Response to Chemotherapy. NMR Biomed. 1996;9:347-58.

52. Smith S.R., Martin P.A., Davies J.M., Edwards R.H.T., Stevens A.N. The assessment of treatment response in non-Hodgkin's lymphoma by image guided ^{31}P magnetic resonance spectroscopy. Br J Cancer. 1990;61:485-90.

53. Tate A.R., Underwood J., Acosta D.M., Julia-Sape M., Majos C., Moreno-Torres A., et al. Development of a decision support system for diagnosis and grading of brain tumours using *in vivo* magnetic resonance single voxel spectra. NMR Biomed. 2006;19:411-34.

54. Gonzalez-Velez H, Mier M, Julia-Sape M, Arvanitis T.N., Garcia-Gomez J.M., Robles M, et al. HealthAgents: Distributed Multi-Agent Brain Tumour Diagnosis and Prognosis. Applied Intelligence.

55. Garcia-Gomez J.M., Luts J, Julia-Sape M, Krooshof P, Tortajada S, Robledo JV, et al. Multiproject-multicenter evaluation of automatic brain tumor classification by magnetic resonance spectroscopy. Magn Reson Mater Phy. 2009;22:5-18.

56. Martin AJ, Liu H, Hall WA, truwit CL. Preliminary Assessment of Turbo Spectroscopic Imaging for Targeting in Brain Biopsy AJNR Am J Neuroradiol. 2001;22:959-68.

57. Castillo M, Smith JK, Kwock L. Correlation of Myo-inositol Levels and Grading of Cerebral Astrocytomas. AJNR Am J Neuroradiol. 2000;21(9):1645-9.

58. Shimizu H, Kumabe T, Shirane R, Yoshimoto T. Correlation between Choline Level Measured by Proton MR Spectroscopy and Ki-67 Labeling Index in Gliomas. AJNR Am J Neuroradiol. 2000 April 1, 2000;21(4):659-65.

59. Graves EE, Nelson SJ, Vigneron DB, Verhey L, McDermott M, Larson D, et al. Serial Proton MR Spectroscopic Imaging of Recurrent Malignant Gliomas after Gamma Knife Radiosurgery AJNR Am J Neuroradiol. 2001;22:613-24.

60. Nelson SJ, Vigneron DB, Dillon WP. Serial Evaluation of patients with brain tumors using volume MRI and 3D ^{1}H MRSI. NMR Biomed. 1999;12:123-8.

61. Tzika AA, Vajapeyam S, Barnes PD. Multivoxel proton MR spectroscopy and hemodynamic MR imaging of childhood brain tumors: preliminary observations. AJNR Am J Neuroradiol. 1997 February 1, 1997;18(2):203-18.

62. Tzika AA, Zurakowski D, Poussaint TY, Goumnerova L, Astrakas LG, Barnes PD, et al. Proton magnetic spectroscopic imaging of the child's brain: the response of tumors to treatment. Neuroradiology. 2001;43(2):169-77.

63. Panigrahy A, Krieger MD, Gonzalez-Gomez I, Liu X, McComb JG, Finlay JL, et al. Quantitative Short Echo Time 1H-MR Spectroscopy of Untreated Pediatric Brain Tumors: Preoperative Diagnosis and Characterization. AJNR Am J Neuroradiol. 2006;27(3):560-72.

64. Gibb A, Easton J, Davies N, Sun Y, MacPherson L, Natarajan K, et al. The development of a graphical user interface, functional elements and classifiers for the non-invasive characterization of childhood brain tumours using magnetic resonance spectroscopy. The Knowledge Engineering Review. 2011;26:353-63.

65. Peet A, Davies N, Ridley L, Brundler M, Kombogiorgas D, Lateef S, et al. Magnetic resonance spectroscopy suggests key differences in the metastatic behaviour of medulloblastoma. Eur J Cancer. 2007;43(6):1037-44.

66. Harris LM, Davies NP, MacPherson L, Lateef S, Natarajan K, Brundler MA, et al. Magnetic resonance spectroscopy in the assessment of pilocytic astrocytomas. Eur J Cancer. 2008;44(17):2640-7.

67. Lazareff JA, Olmstead C, Bockhorst KH, Alger JR. Proton magnetic resonance spectroscopic imaging of pediatric low-grade astrocytomas. Childs Nerv Syst. 1996 Mar;12(3):130-5.

68. Wilkinson ID, Griffiths PD, Wales JK. Proton magnetic resonance spectroscopy of brain lesions in children with neurofibromatosis type 1. Magn Reson Imaging. 2001;19(8):1081-9.

69. Gonen O, Wang Z. J., Viswanathan A.K., Molloy P.T., Zimmerman R.A. Three-Dimensional Multivoxel Proton MR Spectrosocpy of the Brain in Children with Neurofibromatosis Type 1. AJNR Am J Neuroradiol. 1999;20:1333-41.

70. Castillo M, Green C, Kwock L, Smith K, Wilson D, Schiro S, et al. Proton MR Spectroscopy in Patients with Neurofribromatosis Type 1: Evaluation of Hamartomas and Clinical Correlation. AJNR Am J Neuroradiol. 1995;16:141-7.

71. Schneider JF, Confort-Gouny S, Viola A, Le Fur Y, Viout P, Bennathan M, et al. Multiparametric differentiation of posterior fossa tumors in children using diffusion-weighted imaging and short echo-time 1H-MR spectroscopy. J Magn Reson Imaging. 2007 Dec;26(6):1390-8.

72. Arle JE, Morriss C, Wang ZJ, Zimmerman RA, Phillips PG, Sutton LN. Prediction of posterior fossa tumor type in children by means of magnetic resonance image properties, spectroscopy, and neural networks. Neurosurg Focus. 1997;2(3):E2.

73. Peet A., Garala P., MacPherson L., Natarajan K., Sgouros S., grundy R. Mobile lipids detected by short echo time 1H magnetic resonance spectroscopy correlate with malignancy in childhood brain tumors. Neuro-oncol. 2004;6:471.

74. Astrakas LG, Zurakowski D, Tzika AA, Zarifi MK, Anthony DC, De Girolami U, et al. Noninvasive Magnetic Resonance Spectroscopic Imaging Biomarkers to Predict the Clinical Grade of Pediatric Brain Tumors. Clin Cancer Res. 2004 December 15, 2004;10(24):8220-8.

75. Davies NP, Wilson M, Natarajan K, Sun Y, MacPherson L, Brundler MA, et al. Non-invasive detection of glycine as a biomarker of malignancy in childhood brain tumours using *in-vivo* ^{1}H MRS at 1.5 Tesla confirmed by *ex-vivo* high-resolution magic-angle spinning NMR. NMR Biomed.2010; 23(1):80-7.

76. Bluml S, Panigrahy A, Laskov M, Dhall G, Krieger MD, Nelson MD, et al. Elevated citrate in pediatric astrocytomas with malignant progression Neuro-oncol. 2011;13(10):1107-17.

77. Girard N., Wang Z.J., Erbetta A., Sutton L.N., Philips P.C., Rorke L.B., et al. Prognostic value of proton MR spectroscopy of cerebral hemisphere tumors in children. Neuroradiology. 1998;40:121-5.

78. Lazareff JA, Bockhorst KHJ, Curran J, Olmstead C, Alger J. Pediatric Low-grade Gliomas: Prognosis with Proton Magnetic Resonance Spectroscopic Imaging Neurosurgery. 1998;43(4):809-17.

79. Tzika AA, Astrakas LG, Zarifi MK, Zurakowski D, Poussaint TY, Goumnerova L, et al. Spectroscopic and Perfusion Magnetic Resonance Imaging Predictors of Progression in Pediatric Brain Tumors. Cancer. 2004;100(6):1246-56.

80. Warren KE, Frank JA, Black JL, Hill RS, Duyn JH, Aikin AA, et al. Proton Magnetic Resonance Spectroscopic Imaging in Children With Recurrent Primary Brain Tumors. J Clin Oncol. 2000 March 1, 2000;18(5):1020-6.

81. Marcus KJ, Astrakas LG, Zurakowski D, Zarifi MK, Mintzopoulos D, Poussaint TY, et al. Predicting survival of children with CNS tumors using proton magnetic resonance spectroscopic imaging biomarkers. Int J Oncol. 2007;30(3):651-7.

82. Lazareff J.A., Gupta R.K., Alger J. Variation of post-treatment H-MRSI choline signal intensity in pediatric gliomas J Neurooncol. 1999;41:291-8.

83. Steffen-Smith EA, Shih JH, Hipp SJ, Bent R, Warren KE. Proton magnetic resonance spectroscopy predicts survival in children with diffuse intrinsic pontine glioma J Neurooncol. 2011;105(2):365-73.

84. Hipp SJ, Steffen-Smith EA, Hammoud D, Shih JH, Bent R, Warren KE. Predicting outcome of children with diffuse intrinsic pontine gliomas using multiparametric imaging Neuro-oncol. 2011;13(8):904-9.

85. Yamasaki F, Kurisu K, Kajiwara Y, Watanabe Y, Takayasu T, Akiyama Y, et al. Magnetic resonance spectroscopic detection of lactate is predictive of a poor prognosis in patients with diffuse intrinsic pontine glioma Neuro-oncol. 2011;13(7):791-801.

86. A.C.Peet, S.Lateef, L.MacPherson, K.Natarajan, S.Sgouros, R.G.Grundy. Short echo time 1 H magnetic resonance spectroscopy of childhood brain tumours Childs Nerv Syst. 2007;23:163-9.

87. Hwang JH, Egnaczyk GF, Ballard E, Dunn RS, Holland SK, Ball WS, Jr. Proton MR spectroscopic characteristics of pediatric pilocytic astrocytomas. AJNR Am J Neuroradiol. 1998 March 1, 1998;19(3):535-40.

88. Warren KE. NMR Spectroscopy and Pediatric Brain Tumors. Oncologist. 2004;9:312-8.

89. Bluml S., Ross B. Magnetic Resonance Spectroscopy of the Human Brain In: Windhorst U, Johansson H, editors. Modern Techniques in Neuroscience Research Berlin-Heidelberg: Springer 1999.

90. Jiru F. Introduction to post-processing techniques. Eur J Radiol. 2008;67:202-17.

91. Ross B., Bluml S. Magnetic Resonance Spectroscopy of the Human Brain. Anat Rec. 2001;265:54-84.

92. Jansen JFA, Backers WH, Nicolay K, Kooi ME. 1H MR Spectroscopy of the Brain: Absolute Quantification of Metabolites. Radiology. 2006;240:318-32.

93. Van der Graaf M. In vivo magnetic resonance spectroscopy: basic methodology and clinical applications Eur Biophys J. 2010;39:527-40.

94. Andronesi OC, Ramadan S, Ratai E, Jennings D, Mountford CE, Sorensen G. Spectroscopic Imaging with Improved Gradient Modulated Constant Adiabadicity Pulses on High-Field Clinical Scanners. J Magn Reson. 2010;203(2):283-93.

95. Provencher S.W. Automatic quantitation of localized *in vivo* ^{1}H spectra with LCModel. NMR Biomed. 2001;14:260-4.

96. Provencher SW. Estimation of metabolite concentrations from localized in vivo proton NMR spectra. Magn Reson Med. 1993 Dec;30(6):672-9.

97. Provencher S. LCModel & LCMgui User's Manual. 2008.

98. Davies NP. An Example of Quality Control for a Multicentre Trial- 1H MRS. Personal Communication2011.

99. SPSS Statistics 17.0 Manuals.

100. Kirkwood B.R, Sterne J.A.C. Essential Medical Statistics. 2nd ed. Oxford: Blackwell Publishing Ltd.; 2003.

101. IST-1999-10310 INTERPRET International network for Pattern Recognition of Tumours Using Magnetic Resonance. 2009 05/01/2007

102. Devos A, Lukas L, Suykens JAK, Vanhamme L, Tate AR, Howe FA, et al. Classification of brain tumours using short echo time 1H MR spectra. J Magn Reson. 2004;170(1):164-75.

103. Davies NP. , Arvanitis TN. , Auer D. , French A. , Grazier R. , Grundy R., et al. Multicentre prospective classification of childhood brain tumours based on 1H MRS metabolite profiles. Neuro-oncol. 2010;12(6):ii32.

104. Louis DN, Ohgaki H, Wiestler OD, Cavenee WK, editors. WHO Classification of Tumours of the Central Nervous System
4th ed. Lyon: International Agency for Research on Cancer 2007.

105. Listernick R, Ferner RE, Liu Grant T, Gutmann DH. Optic pathway gliomas in neurofibromatosis-1: Controversies and recommendations. Ann Neurol. 2007;61(3):189-98.

106. Peduzzi P, Concato J, Kemper E, Holford TH, Feinstein AR. A simulation study of the number of events per variable in logistic regression analysis. J Clin Epidemiol. 1996;49(12):1373-9.

107. DeBella K, Poskitt K, Szudek J, Friedman JM. Use of "unidentified bright objects" on MRI for diagnosis of neurofibromatosis 1 in children. Neurology. 2000 April 25, 2000;54(8):1646-51.

108. Barbier C, Chabernaud C, Barantin L, Bertrand P, Sembely C, Sirinelli D, et al. Proton MR spectroscopic imaging of basal ganglia and thalamus in neurofibromatosis type 1: correlation with T2 hyperintensitites. Neuroradiology. 2011;53:141-8.

109. Urenjak J, Williams SR, Gadian DG, Noble M. Proton nuclear magnetic resonance spectroscopy unambiguously identifies different neural cell types. J Neurosci. 1993 March 1, 1993;13(3):981-9.

110. Ternier J, Wray A, Puget S, Bodaert N, Zerah M, Sainte-Rose C. Tectal plate lesions in children. J Neurosurg. 2006;104(6):369-76.

111. Lázaro BCR, Landeiro JA. Tectal plate tumors. Arq Neuropsiquiatr. 2006;64:432-6.

112. Tamiya T, Kinoshita K, Ono Y, Matsumoto K, Furuta T, Ohmoto T. Proton magnetic resonance spectroscopy reflects cellular proliferative activity in astrocytomas. Neuroradiology. [Research Support, Non-U.S. Gov't]. 2000 May;42(5):333-8.

113. Wilson M, Davies NP, Grundy RG, Peet AC. A quantitative comparison of metabolite signals as detected by in vivo MRS with ex vivo ^{1}H HR-MAS for childhood brain tumours. NMR Biomed. 2009;22:213-9.

114. Davies NP, Wilson M, Harris LM, Natarajan K, Lateef S, MacPherson L, et al. Identification and characterisation of childhood cerebellar tumours by <I>in vivo</I> proton MRS. NMR Biomed. 2008;21(8):908-18.

115. Griffin JL, Kauppinen RA. A metabolomics perspective of human brain tumours. FEBS J. 2007;274:1132-9.

116. Mirbahai L, Wilson M, Shaw CS, MCConville C, Malcomson RDG, Griffin JL, et al. ^{1}H Magnetic resonance spectroscopy metabolites as biomarkers of cell cycle arrest and cell death in rat glioma cells. Int J Biochem Cell Biol. 2011;43(990-1001).

117. Schubert F, Gallinat J, Seifert F, Rinneberg H. Glutamate concentrations in human brain using single voxel proton magnetic resonance spectroscopy at 3 Tesla Neuroimage. 2004;21(4):1762-71.

118. Brindle KM. Detection of apoptosis in tumors using magnetic resonance imaging and spectroscopy Adv Enzyme Regul. 2002;42:101-12.

119. Nafe Reinhold, Herminghaus Sebastian, Raab Peter, Wagner Sabine, Pilatus Ulrich, Schneider Berthold, et al. Preoperative proton-MR spectroscopy of gliomas-correlation with quantitative nuclear morphology in surgical specimen. J Neurooncol. 2003;63(3):233-45.

120. Nafe Reinhold, Herminghaus Sebastian, Pilatus Ulrich, Hattingen Elke, Marquardt Gerhard, Schlote Wolfgang, et al. Morphology of proliferating and non-proliferating tumor cell nuclei in glioblastomas correlates with preoperative data from proton-MR-spectroscopy. Neuropathology. 2004;24(3):172-82.

121. Hakumaki JM, Poptani H, Sandmair AM, Yla-Herttuala S, Kauppinen RA. 1H MRS detects polyunsaturated fatty acid accumulation during gene therapy of glioma: implications for the in vivo detection of apoptosis. Nat Med. [Research Support, Non-U.S. Gov't]. 1999 Nov;5(11):1323-7.

122. Blankenberg FG, Katsikis PD, Storrs RW, Beaulieu C, Spielman D, Chen JY, et al. Quantitative analysis of apoptotic cell death using proton nuclear magnetic resonance spectroscopy. Blood. 1997;89(10):3778-86.

123. Tzika AA. Proton magnetic resonance spectroscopic imaging as a cancer biomarker for pediatric brain tumors (Review). Int J Oncol. 2008 Mar;32(3):517-26.

124. Moran J, Hernandez-Pech X, Merchant-Larios H, Pasantes-Morales H. Release of taurine in apoptotic cerebellar granule neurons in culture. Pflugers Arch. 2000;439(3):271-7.

125. Lang F, Madlung J, Uhlemann AC, Risler T, Gulbins E. Cellular taurine release triggered by stimulation of the Fas(CD95) receptor in Jurkat lymphocytes. Pflugers Arch. 1998;436(3):377-83.

126. Plathow C, Weber WA. Tumor Cell Metabolism Imaging The Journal of Nuclear Medicine. 2008;49(6 (Suppl)):43S-63S.

127. Golman K, Zandt R, Lerche M, Pehrson R, Ardenkjaer-Larsen JH. Metabolic Imaging by Hyperpolarized ^{13}C Magnetic Resonance Imaging for *In vivo* Tumor Diagnosis. Cancer Res. 2006;66(22):10855-60.

128. Terpstra M, High WB, Luo Y, de Graaf RA, Merkle , Garwood M. Relationships Among Lactate Concentration, Blood Flow and Histopathologic Profiles in Rat C6 Glioma NMR Biomed. 1996;9:185-94.

129. Kugel H, Heindel W, Ernestus RI, Bunke J, du Mesnil R, Friedmann G. Human brain tumors: spectral patterns detected with localized H-1 MR spectroscopy Radiology. 1992;183:701-9.

130. Chang K, Song IC, KimSH, Han MH, KimHD, Seong SO, et al. In Vivo Single-Voxel Proton MR Spectroscopy in Intracranial Cystic Masses. AJNR Am J Neuroradiol. 1998;19:401-5.

131. Ramaekers F.C.S., Puts J.J.G., Moesker O., Kant A., Huysmans A., Haag D., et al. Antibodies to intermediate filament proteins in the immunohistochemical identification of human tumours: an overview. Histochem J. 1983;15:691-713.

132. Bhakoo Kishore K, Pearce D. In Vitro Expression of N-Acetyl Aspartate by Oligodendrocytes. J Neurochem. 2000;74(1):254-62.

133. Takei H., Bhattacharjee M.B., Rivera A., Dancer Y., Powell S.Z. New Immunohistochemical Markers in the Evaluation of Central Nervous System Tumors. A Review of 7 Selected Adult and Pediatric Brain Tumors. Arch Pathol Lab Med. 2007;131:234-41.

134. Chen J, Huang S-L, Li T, Chen X-L. In vivo research in astrocytoma cell proliferation with 1H-magnetic resonance spectroscopy: correlation with histopathology and immunohistochemistry. Neuroradiology. 2006 May;48(5):312-8.

135. Gupta RK, Cloughesy TF, Sinba U, Garakian J, Lazareff J, Rubino G, et al. Relationships between choline magnetic resonance spectroscopy, apparent diffusion coefficient, and quantitative histopathology in human glioma J Neurooncol. 2000;50(3):215-26.

136. Hakumaki JM, Brindle KM. Techniques:Visualizing apoptosis using nuclear magnetic resonance Trends Pharmacol Sci. 2003;24(3):146-9.

137. Opstad KS, Bell BA, Griffiths JR, Howe FA. Taurine: a potential marker of apoptosis in gliomas. Br J Cancer. [Evaluation Studies
Research Support, Non-U.S. Gov't]. 2009 Mar 10;100(5):789-94.

138. Opstad Kirstie S, Bell B. Anthony, Griffiths John R, A. HF. An investigation of human brain tumour lipids by high-resolution magic angle spinning ^{1}H MRS and histological analysis. NMR Biomed. 2008;21(7):677-85.

139. Zoula S, Herigault G, Ziegler A, Farion R, Decorps M, Remy C, et al. Correlation between the occurrence of 1H-MRS lipid signal, necrosis and lipid droplets during C6 rat glioma development. NMR Biomed. [Research Support, Non-U.S. Gov't]. 2003 Jun;16(4):199-212.

140. Kuesel AC, Sutherland GR, Halliday W, Smith ICP. 1H MRS of high grade astrocytomas: Mobile lipid accumulation in necrotic tissue. NMR Biomed. 1994;7(3):149-55.

141. Negendank W, Sauter R, Brown TR, Evelhoch JL, Falini A, Gotsis ED, et al. Proton magnetic resonance spectroscopy in patients with glial tumors: a multicenter study. J Neurosurg. 1996;84(3):449-58.

142. Sappey-Marinier D, Calabrese G, Hetherington HP, Fisher SNG, Deicken R, Van Dyke C, et al. Proton magnetic resonance spectroscopy of human brain: Applications to normal white matter, chronic infarction, and MRI white matter signal hyperintensities. Magn Reson Med. 1992;26(2):313-27.

143. Urenjak J, Williams SR, Gadian DG, M N. Specific Expression of *N*-Acetylaspartate in Neurons, Oligodendrocyte-Type-2 Astrocyte Progenitors, and Immature Oligodendrocytes In Vitro. J Neurochem. 1992;59(1):55-61.

144. Piepmeier J, Fried I, Makuch R. Low-Grade Astrocytomas may arise from different astrocyte lineages Neurosurgery 1993;33:627-32.

145. Oz G., Hutter D., Tkac I., Clark H.B., Gross M.D., Jiang H., et al. Neurochemical Alterations in Spinocerebellar Ataxia Type 1 and their Correlations with Clinical Status Mov Disord. 2010;25(9):1253-61.

146. Baslow MH. N-acetylaspartate in the vertebrate brain: metabolism and function. Neurochem Res. 2003 Jun;28(6):941-53.

147. Barker PB. N-Acetyl Aspartate - A Neuronal Marker? Ann Neurol. 2001;49(4):423-4.

148. Moffett JR, Aryan Namboodiri MA, Cangro CB, Neale JH. Immunohistochemical localization of N-acetylaspartate in rat brain. Neuroreport. 1991;2(3):131-4.

149. Simmons ML, Frondoza CG, Coyle JT. Immunocytochemical localization of N-acetyl-aspartate with monoclonal antibodies. Neuroscience. 1991;45(1):37-45.

150. Reynolds GM, Wilson MP, Peet AC, Arvanitis TN. An algorithm for the automated quantitation of metabolites in in vitro NMR signals Magn Reson Med. 2006;56:1211-99.

151. Wilson M, Davies NP, Brundler M, McConville C, Grundy RG, Peet AC. High resolution magic angle spinning 1H NMR of childhood brain and nervous system tumours. Mol Cancer. 2009;8(6).

152. Govindaraju V, Young K, Maudsley AA. Proton NMR chemical shifts and coupling constants for brain metabolites. NMR Biomed. [Research Support, U.S. Gov't, P.H.S.]. 2000 May;13(3):129-53.

153. Kassner A, Thornhill RE. Texture Analysis: A Review of Neurologic MR Imaging Applications. AJNR Am J Neuroradiol. 2010 May 1, 2010;31(5):809-16.

154. Drabycz S, Roldán G, de Robles P, Adler D, McIntyre JB, Magliocco AM, et al. An analysis of image texture, tumor location, and MGMT promoter methylation in glioblastoma using magnetic resonance imaging. Neuroimage.49(2):1398-405.

155. Brown R, Zlatescu M, Sijben A, Roldan G, Easaw J, Forsyth P, et al. The Use of Magnetic Resonance Imaging to Noninvasively Detect Genetic Signatures in Oligodendroglioma. Clin Cancer Res. 2008 April 15, 2008;14(8):2357-62.

156. Szczypinski Piotr M, Strzelecki Michal, Materka Andrzej, Klepaczko Artur. MaZda--A software package for image texture analysis. Comput Methods Programs Biomed. 2009;94(1):66-76.

157. Yu O, Parizel N, Pain L, Guignard B, Eclancher B, Mauss Y, et al. Texture analysis of brain MRI evidences the amygdala activation by nociceptive stimuli under deep anesthesia in the propofol-formalin rat model. Magn Reson Imaging. 2007;25(1):144-6.

158. Bonilha Leonardo, Kobayashi Eliane, Castellano Gabriela, Coelho Giselle, Tinois Eduardo, Cendes Fernando, et al. Texture Analysis of Hippocampal Sclerosis. Epilepsia. 2003;44(12):1546-50.

159. Chen G, Jespersen S, Pedersen M, Pang QI, Horsman MR, JÃˆRgensen HSD. Evaluation of Anti-vascular Therapy with Texture Analysis. Anticancer Res. 2005 September 2005;25(5):3399-405.

160. Jirák Daniel, Dezortová Monika, Taimr Pavel, Hájek Milan. Texture analysis of human liver. J Magn Reson Imaging. 2002;15(1):68-74.

161. Harrison L, Dastidar P, Eskola H, Järvenpää R, Pertovaara H, Luukkaala T, et al. Texture analysis on MRI images of non-Hodgkin lymphoma. Comput Biol Med. 2008;38(4):519-24.

162. Mayerhoefer Marius E, Breitenseher Martin J, Kramer Josef , Aigner Nicolas, Hofmann Siegfried, Materka Andrzej. Texture analysis for tissue discrimination on T1-weighted MR images of the knee joint in a multicenter study: Transferability of texture features and comparison of feature selection methods and classifiers. J Magn Reson Imaging. 2005;22(5):674-80.

163. Blouin S, Moreau MF, Basl`e MF, Chappard D. Relations between Radiograph Texture Analysis and Microcomputed Tomography in Two Rat Models of Bone Metastases. Cells Tissues Organs. 2006;182(3-4):182-92.

164. Materka A, Strzelecki M. Texture Analysis Methods - A Review. Technical University of Lodz, COST B11 Report. 1998.

165. Materka A, Strzelecki M, Szczypinski P. MaZda Manual [online]. 2006; [cited 2008 Nov 12]. Available from: URL: http://www.eletel.p.lodz.pl/mazda/download/mazda_manual.pdf].

166. Collewet G, Strzelecki M, Mariette F. Influence of MRI acquisition protocols and image intensity normalization methods on texture classification. Magn Reson Imaging. 2004;22(1):81-91.

167. Lerski RA, Schad LR, Luypaert R, Amorison A, Muller RN, Mascaro L, et al. Multicentre magnetic resonance texture analysis trial using reticulated foam test objects. Magn Reson Imaging. 1999;17(7):1025-31.

168. Herlidou-Même S, Constans JM, Carsin B, Olivie D, Eliat PA, Nadal-Desbarats L, et al. MRI texture analysis on texture test objects, normal brain and intracranial tumors. Magn Reson Imaging. 2003;21(9):989-93.

169. Behzadi SS, Prakasvudhisarn C, Klocker J, Wolschann P, Viernstein H. Comparison between two types of Artificial Neural Networks used for validation of pharmaceutical processes. Powder Technology. 2009;195(2):150-7.

170. Hajmeer M, Basheer I. A probabilistic neural network approach for modeling and classification of bacterial growth/no-growth data. J Microbiol Methods. 2002;51(2):217-26.

171. Hajmeer MN, Basheer IA, Marsden JL, Fung DYC. New approach for modeling generalized microbial growth curves using artificial neural networks. Journal of Rapid Methods and Automation in Microbiology. 2000;8(4):265-83.

172. Übeyli ED, Übeyli M. Estimation of radiation damage at the structural materials of a hybrid reactor by probabilistic neural networks. Expert Systems with Applications. 2009;36(3, Part 1):5184-9.

173. Übeyli ED. Implementing automated diagnostic systems for breast cancer detection. Expert Systems with Applications. 2007;33(4):1054-62.

174. Thibault J, Grandjean BPA. A neural network methodology for heat transfer data analysis. International Journal of Heat and Mass Transfer. 1991;34(8):2063-70.

175. Chaudhuri BB, Bhattacharya U. Efficient training and improved performance of multilayer perceptron in pattern classification. Neurocomputing. 2000;34(1-4):11-27.

176. Chtioui Y, Bertrand D, Barba D. Reduction of the size of the learning data in a probabilistic neural network by hierarchical clustering. Application to the discrimination of seeds by artificial vision. Chemometrics and Intelligent Laboratory Systems. 1996;35(2):175-86.

177. Haykin S. Neural networks: a comprehensive foundation. New York: Macmillan; 1994.

178. Shan Y, Zhao R, Xu G, Liebich HM, Zhang Y. Application of probabilistic neural network in the clinical diagnosis of cancers based on clinical chemistry data. Anal Chim Acta. 2002;471(1):77-86.

179. Wasserman PD. Advanced Methods in Neural Computing (Vnr Computer Library). New York: Van Nostrand Reinhold 1993.

180. Tsai C-Y. An iterative feature reduction algorithm for probabilistic neural networks. Omega. 2000;28(5):513-24.

181. Specht DF. Probabilistic neural networks and polynomial Adaline as complementary
techniques for classification. IEEE Trans Neural Netw. 1990;1(1):111-21.

182. Specht DF. Probabilistic neural networks. Neural Netw. 1990;3(1):109-18.

183. Musavi MT, Chan KH, Hummels DM, Kalantri K, Ahmed W. A probabilistic model for evaluation of neural network classifiers. Pattern Recognition. 1992;25(10):1241-51.

184. Masters T. Advanced Algorithms for Neural Networks: A C++ Sourcebook New York: John Wiley & Sons Inc 1995.

185. Masters T. Practical Neural Network Recipes. New York: Wiley; 1993.

186. Muniz AM, Liu H, Lyons KE, Pahwa R, Liu W, Nobre FF, et al. Comparison among probabilistic neural network, support vector machine and logistic regression for evaluating the effect of subthalamic stimulation in Parkinson disease on ground reaction force during gait. J Biomech. [Comparative Study
Evaluation Studies
Research Support, Non-U.S. Gov't]. Mar 3;43(4):720-6.

187. Xue CX, Zhang XY, Liu MC, Hu ZD, Fan BT. Study of probabilistic neural networks to classify the active compounds in medicinal plants. J Pharm Biomed Anal 2005;38(3):497-507.

188. Koeller KK, Rushing EJ. Medulloblastoma: A Comprehensive Review with Radiologic-Pathologic Correlation. Radiographics. 2003;23(6):1613-37.